

Thesis
2928

UNIVERSITY OF NEVADA
RENO
MACKAY SCHOOL OF MINES

✓
"The Geology and Mineralization of the Grayback Mountains,
Yavapai County, Arizona"

A thesis submitted in partial fulfillment of the
requirements for the degree of Master of Science
in Geology

By

Michael Robert Kotraba

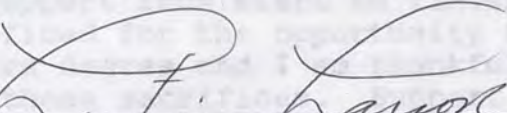
April 1992

Signature Page

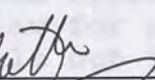
Many things go into the completion of a Masters Degree. Once you are given the opportunity to pursue the degree you need to find a thesis project and the support to complete the project.

Without a doubt the most important support needed in this sort of endeavor comes from home. I would like to

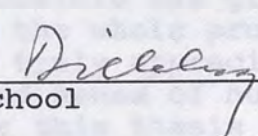
The thesis of Michael R. Kotraba is approved:



Dr. L.T. Larson - Thesis Advisor



Dr. Robert Watters - Department Chair



Dean, Graduate School

The idea for this thesis grew out of conversations with the staff geologist at Cyprus Sagdud, Dr. Phil Black. I would like to thank Dr. Black for taking the time to get the project started and providing some of the initial geologic data.

Funding for the project was provided by a variety of sources. Scholarship money was provided by the Department of Geological Sciences at the University of Nevada, Reno. Additional support was provided by the Department of Geological Sciences at the University of Nevada, Reno.

Special thanks go to the geologists at Cyprus Sagdud for their support and cooperation with this thesis project, specifically Dr. John Sawyer and Dr. Phil Black.

University of Nevada,
Reno
Mackay School of Mines

April 1992

Acknowledgements

Many things go into the completion of a Masters Degree. Once you are given the opportunity to pursue the degree you need to find a thesis project and the support to complete the project.

Without a doubt the most important support needed in this sort of endeavor comes from home. I would like to thank my wife, Julie and daughter, Kellie for their patience and support from start to finish. Many things were sacrificed for the opportunity to return to school for a Masters degree and I am thankful for their willingness to make those sacrifices. Support from other family members was also appreciated. Thanks goes to my dad for being a faithful field assistant and camp cook, and to my sister and brother-in-law for providing a place to stay and a vehicle to drive while out in the field.

The opportunity and funding to make my pursuit of a Masters degree possible was given by Dr. L.T. Larson. Not only did he make the whole process possible but he also made it enjoyable. I truly appreciated his guidance, expertise, encouragement, and sense of humor. Thanks L.T.!

The idea for this thesis grew out of conversations with the staff geologist at Cyprus Bagdad, Dr. Phil Blacet. I would like to thank Dr. Blacet for taking the time to get the project started and providing some of the initial geologic data.

Funding for the project came from a variety of sources. Scholarship monies were provided by WAAIME. Research money was provided by MMRI, and teaching assistant support was provided by the Department of Geological Sciences at UNR. Geochemical support was provided by Cyprus Bagdad.

Special thanks goes to the geologists at Cyprus Bagdad for their support and cooperation with this thesis project, specifically Mr. John Hawley and Dr. Phil Blacet.

Abstract

Extrusive and intrusive rocks exposed in the Grayback Mountain thesis area document magmatic activity and evolution from the late Cretaceous through the early Tertiary. Compaction foliation orientations and a thick (+1500 feet) accumulation of tuff indicate that the Grayback Mountain rhyolite tuff erupted from a vent within the thesis area along a major northeast trending shear zone. The tuffaceous vent was then intruded and mineralized by granodiorite to quartz monzonite stocks, with mineralization dominated by a Cu-Fe-S system. High-level magmatic activity continued with the intrusion of rhyolite and diorite porphyry dikes, extrusion of the Copper Ridge tuff, and intrusion of the late quartz monzonite dikes. Precious-metal mineralization appears spatially and temporally related to the late stage dike intrusions.

Several lines of geologic evidence suggest a close space-time relationship between the rocks in the thesis area and the porphyry at Bagdad.

Chapter Four: Space-time Relationships to the Bagdad Porphyry Deposit

General Description of the Bagdad Porphyry
 Relations of the Bagdad Porphyry to the
 Grayback Mountain Thesis Area

Chapter Five: Conclusions

Contents

	Page #	
Signature Page	i	
Acknowledgements	ii	
Abstract	iii	
Contents	iv	
List of Figures	v	
List of Tables	vii	
 Chapter One: Background Information		
Introduction	1	
Geologic Approach and Project Goals	1	
Previous Work	2	
Location	4	
Physiography, Topography, Climate, and Vegetation	4	
Exploration and Mining History	6	
Regional Geology of the Bagdad Area	8	
 Chapter Two: The Geology of the Grayback Mountains		
Geologic History	15	
Geologic Maps and Cross sections	15	
Age Dates and Petrography	17	
Alteration	29	
Mineralization	32	
Structure and Genesis of the Grayback Mountain Rhyolite	54	
 Chapter Three: Mineral Exploration		
Previous Exploration	65	
Exploration Program and Data	65	
Correspondence Analysis of Trace Element Geochemistry	67	
Geophysical Data	78	
Drilling Summary	83	
Exploration Summary and Suggestions for Further Exploration	88	
 Chapter Four: Space/Time Relationships to the Bagdad Porphyry Deposit		
General Description of the Bagdad Porphyry	91	
Relations of the Bagdad Porphyry to the Grayback Mountain Thesis Area	93	
 Chapter Five: Conclusions		95

CONTENTS - Continued

	Page #
Bibliography	98
Appendix One - Opaque Mineralogy	102
Appendix Two - Geochemical Data	104
Plate 1 - Geologic Map of the Grayback Mountain Thesis area on a topographic base (1:12,000)	39

List of Figures

Figure #	Page #
Fig. 1 - Arizona Geologic Map - Bagdad Area (Reynolds, 1988)	3
Fig. 2 - Arizona's Physiographic Provinces (Pierce, 1984)	5
Fig. 3 - Structure Map of the Bagdad Area (Anderson, 1956)	11
Fig. 4 - Map showing the intersection of the two postulated shear zones (Anderson et. al., 1956)	14
Fig. 5 - Generalized geologic map of the Grayback Mountain thesis area (1:36,000)	16
Fig. 6 - Geologic map of the Grayback Mountain thesis area (1:24,000)	18
Fig. 7 - Idealized cross section through the Grayback Mountain thesis area Line: A - A'	19
Fig. 8 - Idealized cross section through the Grayback Mountain thesis area Line: B - B'	20
Fig. 9a - Scanning Electron Microscope plot of garnet from the Copper Ridge tuff	28
b - Fresh garnets and weathered garnets in the Copper Ridge tuff	28
Fig. 10 - Generalized alteration map of the Grayback Mountain thesis area	30
Fig. 11a - Disseminated and vein filling pyrite	34
b - Fractured pyrite grain	34
Fig. 12a - Pyrite with inclusions of chalcopyrite, sphalerite, and covellite	35
b - Disseminated and vein filling chalcopyrite	35
Fig. 13a - Chalcopyrite disease in sphalerite	36
b - Chalcopyrite disease in sphalerite	36

List of Figures - Continued

Figure #	Page #
Fig. 14a - Pyrite with inclusions of pyrrhotite and chalcopyrite, and disseminated covellite	38
b - Fracture filling of chalcopyrite, sphalerite, and pyrite	38
Fig. 15a - Replacement of chalcopyrite by covellite	39
b - Replacement of pyrite by covellite, and chalcopyrite inclusions in pyrite	39
Fig. 16a - Disseminated chalcocite/digenite grains	41
b - Chalcocite/digenite replacing chalcopyrite and rimming pyrite	41
Fig. 17a - Chalcopyrite and bornite	42
b - Disseminated molybdenite	42
Fig. 18a - Galena showing triangular pluck marks	43
b - Azurite (crossed nichols)	43
Fig. 19a - Malachite in-filling fracture	44
b - Malachite in-filling fracture (crossed nichols)	44
Fig. 20a - Copper pitch ore - melanochalcite	46
b - Goethite and hematite after pyrite	46
Fig. 21a - Colloidal banding of iron oxides	47
b - Aggregate pseudomorphs of hematite after pyrite with colloiddally banded iron oxides	47
Fig. 22a - Magnetite grain	48
b - Brass (?) with iron oxides and pyrite	48
Fig. 23a - Graphic derivation of the maximum compaction dip that can be formed by static, postemplacement compaction (Chapin and Lowell, 1979)	57
c - Generalized cross section through the Gribbles Run paleovalley (Chapin and Lowell, 1979)	57
Fig. 24 - Cross section through the fissure vent within the Grizzley Peak caldera, Sawatch Range, Colo. (Fridrich et. al., 1991)	58
Fig. 25 - Cross section through the west-central Nevada fissure vent (Ekren and Beyers, 1976)	60
Fig. 26 - Summary of rock chip geochemistry results	68
Fig. 27 - Geochemical contour map of copper in rock chip samples	69
Fig. 28 - Geochemical contour map of molybdenum in rock chip samples	70
Fig. 29 - Geochemical map of gold in rock chip samples (uncontoured)	71
Fig. 30 - Correspondence analysis graphical plot: (factor 1 vs. factor 2)	74

List of Figures - Continued

Figure #		Page #
Fig. 31	- Correspondence analysis graphical plot: (factor 1 vs. factor 3)	75
Fig. 32	- Correspondence analysis graphical plot: (factor 2 vs. factor 3)	76
Fig. 33	- Aeromagnetics survey over the Bagdad area (Dempsey et. al., 1963)	79
Fig. 34	- Regional gravity of the Bagdad area (Lysonski et. al., 1981)	81
Fig. 35	- I.P./Resistivity survey of the Gallagher claim block (CBCC, 1974)	82
Fig. 36	- Drillhole location diagram	84
Fig. 37	- Exploration drillcore log summary	85
Fig. 38	- Exploration drillcore log summary continued	86
Fig. 39	- Stream sediment sample location diagram	105
Fig. 40	- Rock chip sample location diagram	107

List of Tables

Table #		Page #
Table 1	- Rock type mineralization summary	50
Table 2	- Paragenetic sequence for mineralization in the Grayback Mountain thesis area	53
Table 3	- Grayback Mountain thesis area exploration program outline	66
Table 4	- Correspondence analysis eigenvalue summary	72
Table 5	- Correspondence analysis pathfinder Summary	78
Table 6	- Age dating summary	94
Table 7	- Stream sediment sampling data	104
Table 8	- Rock chip sampling data	106

Background Information

Introduction

Lipman and Sawyer (1985) found several late Cretaceous/early Tertiary ash-flow caldera fragments in southeast Arizona which seemed to have a close space-time relationship to a nearby porphyry system.

Initial conversations with Dr. Phil Blacet, Chief Geologist at the Cyprus Bagdad Mine, suggested the possibility of a close space-time relationship between the porphyry ore body and the Grayback Mountain rhyolite tuff. That is, the Grayback Mountain rhyolite tuff may represent the extrusive equivalent of the mineralized intrusives at Bagdad.

At the time of initiation of this study, it was not clear whether the Grayback Mountain rhyolite tuff represented a flat lying or tilted remnant ash-flow sheet filling a paleovalley, a tuff generated by a localized tuffaceous vent eruption, or possibly a deeply eroded caldera.

Geologic Approach and Project Goals

The geologic approach and project goals are outlined below:

Geologic Approach

1. Geologic mapping of the outer contact of the tuffaceous units with the surrounding Precambrian rocks to geographically define the thesis area.
2. Geologic mapping of the defined thesis area including: rock units, structures, and alteration.
3. Petrographic study of the rock units in the project

area.

4. Description and location of mineralization.
5. Geochemical surveys to pinpoint likely targets for further mineral exploration.
6. Evaluation of evidence for the genetic origin of the Grayback Mountain rhyolite tuff.
7. Evaluation of the possible space-time relationship between the thesis area and the Bagdad porphyry.

Project Goals

1. To establish how the thesis area fits within the bounds of the regional geology.
2. To provide a detailed geologic map of the area.
3. To identify structures within the area, establish the origin and/or source for the rhyolite, and examine evidence for the possible existence of a caldera.
4. To petrographically describe the rocks within the thesis area.
5. To guide further mineral exploration in the area.
6. To ascertain the possible space-time relationships between the thesis area and the Bagdad porphyry.

Previous Work

Anderson et al. (1956) mapped approximately one-half square mile along the northeast flank of the thesis area and determined the rocks to be outcrop of late Cretaceous/early Tertiary rhyolite (Grayback Mountain rhyolite tuff) that unconformably overlies Precambrian alaskite porphyry. The Arizona State Geologic Map and Yavapai County Geologic Map both show the rocks of the thesis area as late Cretaceous/early Tertiary volcanic rocks (see Fig. 1 - purple outcrop of Kv). No outcrops of rocks similar in age and composition to those in the thesis area are known in the region and a source for the Grayback Mountain rhyolite tuff has not been delineated. Anderson et al. (1956) postulated that the Grayback Mountain rhyolite tuff was related to volcanism in the Oatman District, 75 miles west-northwest of

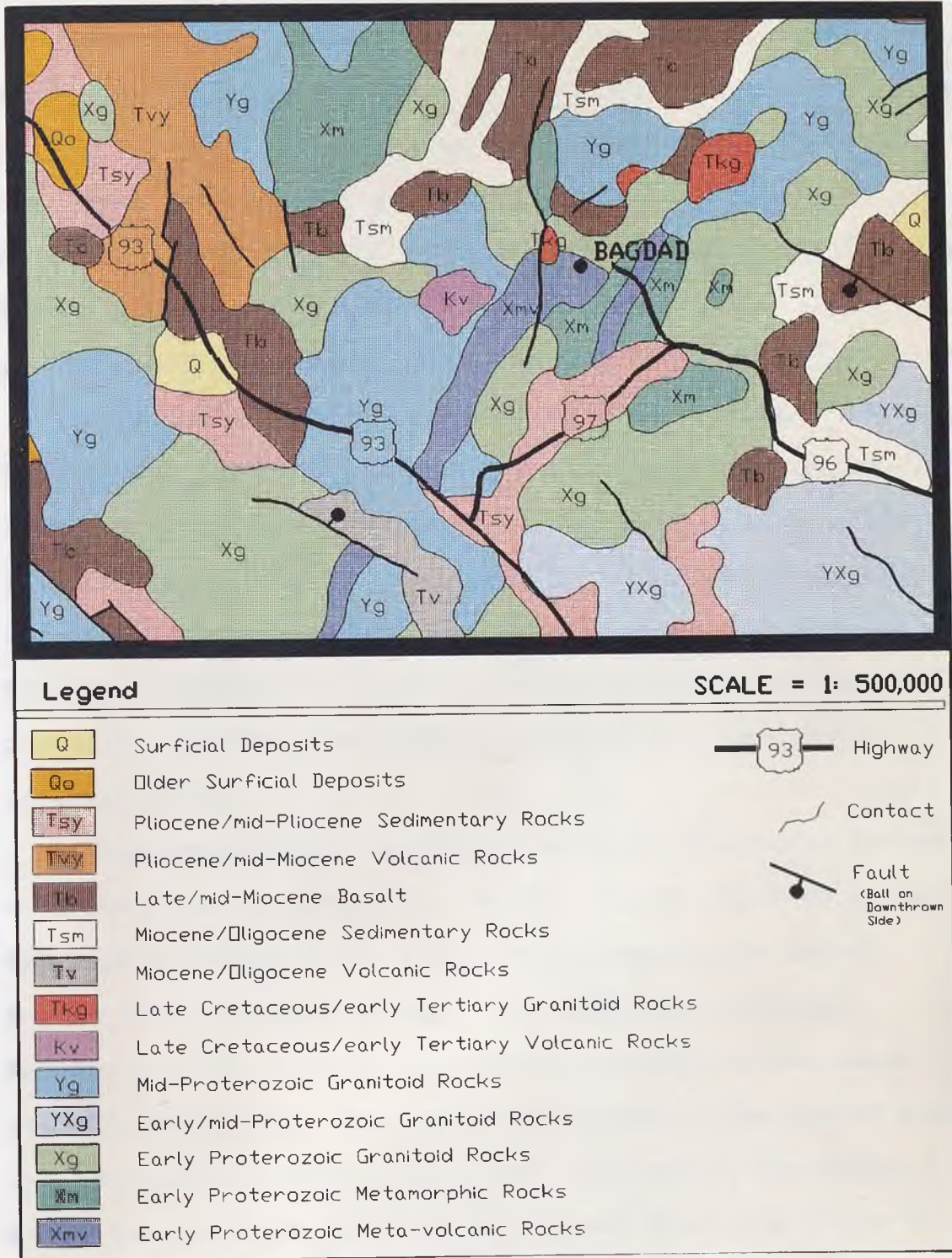


Figure 1. Geologic map of the Bagdad area (Reynolds, 1988).

Bagdad.

Location

The Grayback Mountains are in Yavapai County, approximately five miles WSW of the town of Bagdad, Arizona (Fig. 1). The thesis area is approximately centered about the summit of Grayback Mountain, and includes parts of sections 10-15, 21-28, T. 14N, R. 10W, Grayback Mountain 7½ Minute Quadrangle.

Physiography, Topography, Climate, and Vegetation

Arizona includes three physiographic provinces (Pierce, 1984). The thesis area is within the physiographic province known as the Transition Zone (see Fig. 2). The Transition Zone has been referred to as Arizona's "Backbone" because it separates the relatively undeformed Colorado plateau region from the structurally complex Basin and Range Province and contains extensive exposures of Arizona's oldest rocks (Pierce, 1984).

Topographically, the thesis area consists of a series of ridges nearly enclosing a basin. Basin drainage is to the west and then north where it intersects the Laurel Spring Wash drainage system. The summit of Grayback Mountain is the highest topographic feature in the local area at 5133 feet. The lowest elevation in the thesis area is approximately 3200 feet at the west end of the basin where the drainage joins Laurel Spring Wash (see Plate 1).

Climate in the area is quite variable. Summer

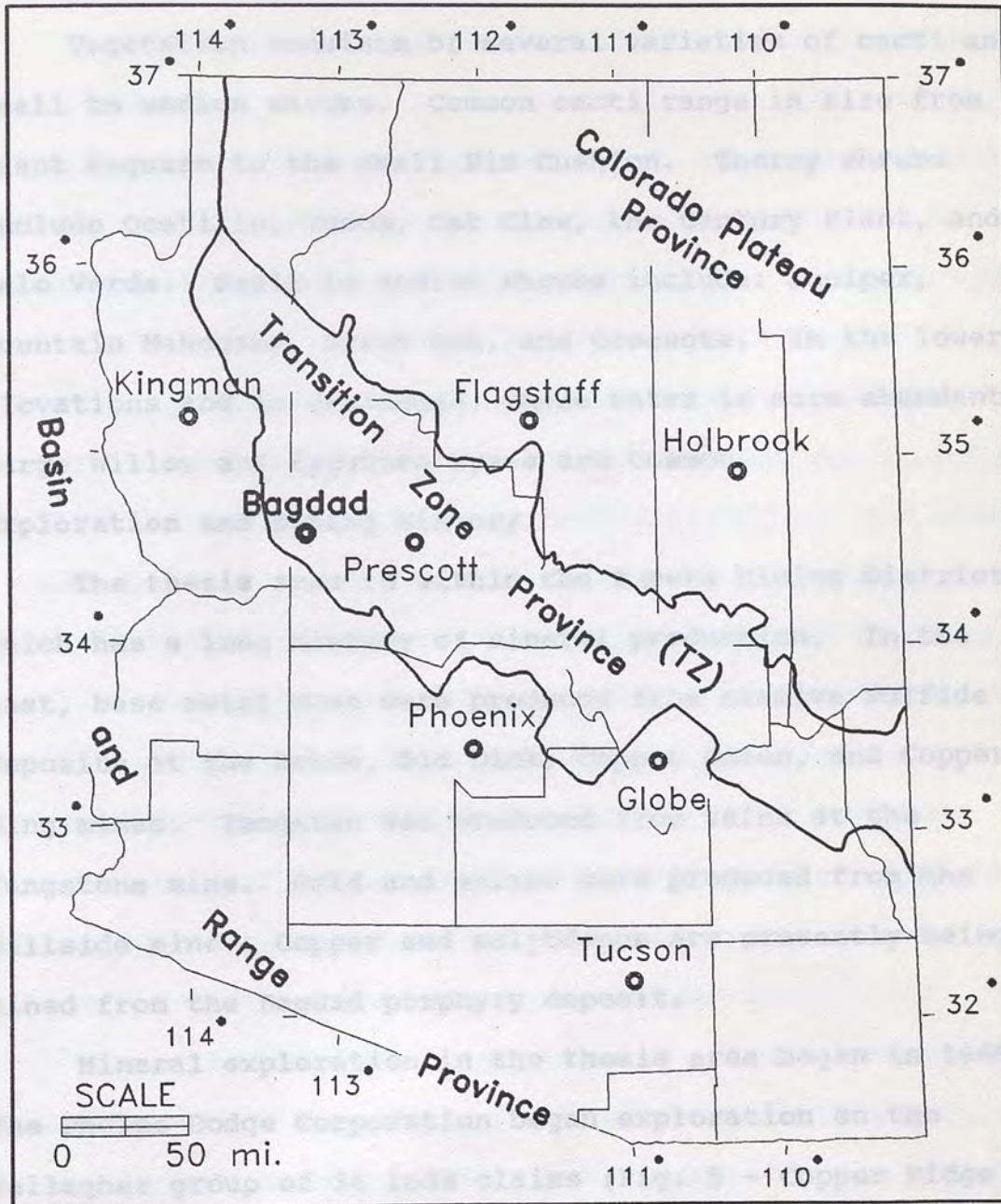


Figure 2. Index map of Arizona, showing physiographic provinces and the location of the Bagdad area (Pierce, 1984 and 1985).

temperatures of over 100° Fahrenheit are common along with monsoon type storms. Winter temperatures as low as 10° Fahrenheit and light to moderate snowfall are common. Snow rarely lasts longer than a few days.

Vegetation consists of several varieties of cacti and small to medium shrubs. Common cacti range in size from the giant Saguaro to the small Pin Cushion. Thorny shrubs include Ocatillo, Yucca, Cat Claw, the Century Plant, and Palo Verde. Small to medium shrubs include: Juniper, Mountain Mahogany, Scrub Oak, and Creosote. In the lower elevations and in drainages, where water is more abundant, large Willow and Sycamore trees are common.

Exploration and Mining History

The thesis area is within the Eureka Mining District, which has a long history of mineral production. In the past, base metal ores were produced from massive sulfide deposits at the Bruce, Old Dick, Copper Queen, and Copper King mines. Tungsten was produced from veins at the Tungstona mine. Gold and silver were produced from the Hillside mine. Copper and molybdenum are presently being mined from the Bagdad porphyry deposit.

Mineral exploration in the thesis area began in 1969. The Phelps Dodge Corporation began exploration on the Gallagher group of 36 lode claims (Fig. 5 - Copper Ridge Claim Block). Four diamond drillholes (Pd-1 to Pd-4, Fig. 36) were completed by 1970 and encountered marginal to

submarginal copper/molybdenum mineralization to depths of 1500 feet. Drillhole logs indicate that hydrothermal alteration and silicification continued to depth (Cyprus Bagdad report, 1974).

Cyprus Minerals acquired the rights to the Gallagher claim block and resumed exploration in 1971. The Copper Ridge property (formerly the Gallagher claims) was selected for exploration based on extensive surficial alteration and mineralization, and the belief of the Cyprus geologic staff that the property had potential for a bulk low-grade copper/molybdenum deposit similar to Bagdad. Geologic mapping and geochemical sampling were carried out from 1971 to 1972. Targets tested by diamond drilling in 1972 showed narrow zones of submarginal copper/molybdenum mineralization with alteration and mineralization increasing with depth. In 1973-1974 Cyprus attempted to outline the possible sulfide occurrence at depth by means of nine Induced Polarization-Resistivity lines. Drillhole CR-1-74 was designed to test an I.P. anomaly at depth and intersected strong to moderate alteration with submarginal amounts of copper and molybdenum, to a depth of 1497 feet.

Since the mid-1970's, exploration efforts have been designed to test the Copper Ridge property for precious metal mineralization, however, no significant precious metal mineralization has been encountered.

Company reports regarding the Copper Ridge property

suggest further exploration be done. To date, efforts to locate ore have yielded marginal results. If an ore body is present, its' discovery will require a much more thorough geologic investigation than those carried out in the past.

Regional Geology of the Bagdad Area

The Arizona State Geologic Map (Reynolds, 1988) shows the thesis area as outcrop of late Cretaceous/early Tertiary volcanics (Fig. 1). Rocks surrounding the thesis area, in the general vicinity of Bagdad, are mapped as early Proterozoic metavolcanics, metamorphic rocks, and granitoid rocks; middle Proterozoic granitoid rocks; late Cretaceous/early Tertiary volcanic and granitoid rocks; and late Tertiary sedimentary and volcanic rocks.

Rock Types

The oldest rocks in the Bagdad area are correlated with the Precambrian Yavapai Series rocks found in the Prescott-Jerome area (Butler and Wilson, 1938) and are radiometrically dated at 1760 Ma (Silver, 1966). They consist of a series of metamorphosed lava flows, tuffs, and sedimentary rocks. The Yavapai Series rocks, in the Bagdad area, have been intruded by later Precambrian plutonic and volcanic rocks. The oldest intrusive is the King Peak rhyolite followed by the Dick rhyolite. Gabbro and related rocks, anorthosite, quartz diorite, and diabase intrude the Yavapai series rocks as well as the King Peak and Dick rhyolites. The gabbro is intruded by alaskite porphyry and

the Lawler Peak granite. The Lawler Peak granite, radiometrically dated at 1411 ± 3 Ma. (Silver et al., 1980), is intruded by the Cheney Gulch granites. The Cheney Gulch granites are in turn intruded by a series of aplite-pegmatite dikes that may represent the waning phase of intrusive activity related to the Lawler Peak granite (Anderson et al., 1956). Igneous activity in the Bagdad area appears to have ceased following the intrusion of the aplite-pegmatite dikes and magmatic/tectonic quiescence appears to have continued well into the Phanerozoic. No Paleozoic to mid-Mesozoic rocks are found in the area and no evidence exists to support sedimentation during this time.

Intrusive and volcanic activity in the Bagdad area resumed in the late Cretaceous/early Tertiary. The Grayback Mountain rhyolite tuff was deposited unconformably over Precambrian rocks. A series of granodiorite to quartz monzonite stocks that trend $N60-70^{\circ}E$ were then emplaced. Flow-banded rhyolite and diorite porphyry dikes intrude the Grayback Mountain rhyolite tuff as well as the older rocks in the area. The rhyolite and diorite porphyry dikes are, in places, cut by later quartz monzonite porphyry dikes.

The late Tertiary Gila (?) conglomerate is essentially a valley-fill deposit composed of nonvolcanic sediment. In places rhyolite (airfall?) tuff is interbedded with the Gila conglomerate. The Wilder formation consists of lava flows, intrusive plugs, pyroclastic cones, and horizontally bedded

tufaceous rocks that overlie, and are intercalated with the Gila conglomerate. The Sanders basalt represents the last magmatic activity in the area and is found capping the mesas. Erosional processes are once again dominant.

Regional Structure and Magmatism

The Precambrian rocks in the Bagdad area are characterized by folds broken by later faults. The faults then provided a conduit along which the younger igneous rocks intruded. Folding is thought to predate faulting, although some evidence exists for the concurrence of folding and faulting. In general, the regional structural trend in the Precambrian rocks of the Bagdad area is northeast-southwest (Fig. 3).

The Matazal Orogeny is the most widespread and intense deformational event visible in the Precambrian rocks of Arizona and probably was responsible for the strong northeast-southwest structural grain observed in the Precambrian rocks of the Bagdad area. Radiometric dating by Williams and Silver (1980) shows the Matazal Orogeny to have occurred between 1660 and 1715 Ma.

From the late Proterozoic through at least the late Mesozoic the region does not appear to have been affected by any major tectonic events. Lack of outcrop of rocks of this age in the region supports a long period of erosion and relative tectonic quiescence.

The most intense orogenic deformation to effect all of

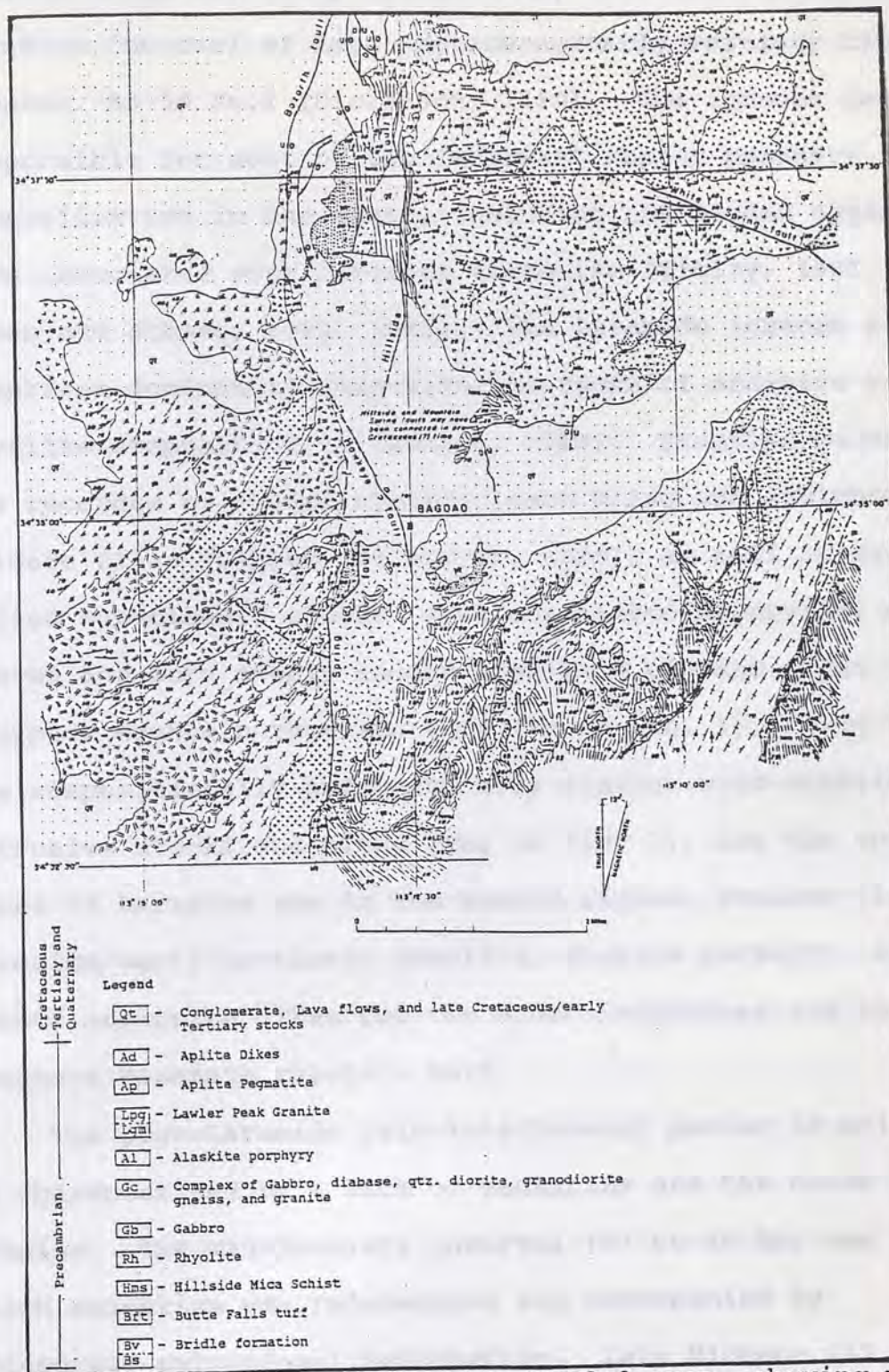


Figure 3. Structure map of the Bagdad area, showing major faults and the strong northeast-southwest structural grain in the Precambrian rocks (Anderson et al., 1956).

Arizona since the early Proterozoic, occurred during the Laramide interval of late Cretaceous/early Tertiary time (approx. 85-55 Ma.) (Dickenson, 1989). The igneous centers responsible for most of the important copper porphyry mineralization in the state, including the Bagdad deposit, were associated with Laramide tectonism (Titley, 1981, 1982; Damon and others, 1981, 1983). The Laramide igneous suite comprises dominantly calc-alkaline rocks of andesite to rhyolite composition (Dickenson, 1989). Eruptive centers are recorded by eroded stratovolcano piles and ignimbrite caldera fills (Lipman and Sawyer, 1985), as well as by varied subvolcanic stocks, with associated hypabyssal dike swarms and more deeply eroded granitoid plutons. The Grayback Mountain rhyolite tuff (Kv in Fig. 1), along with the compositionally and texturally similar calc-alkaline intrusive stocks and plugs (Tkg in Fig. 1), are the only rocks of Laramide age in the Bagdad region. Younger (late Laramide/early Tertiary) rhyolite, diorite porphyry, and quartz monzonite dikes cut the older intrusives and the Grayback Mountain rhyolite tuff.

The post-Laramide (mid-late Eocene) period in Arizona is characterized by a lack of magmatism and the onset of erosion. The mid-Tertiary interval (37 to 15 Ma) was one in which magmatism was rejuvenated and accompanied by widespread extensional deformation. Late Miocene (12 to 5 Ma) volcanic and sedimentary rocks in southern and western

Arizona have been disrupted by Basin and Range Province normal faulting but generally are not tilted (Shafiqullah et al., 1980).

Post Laramide (Tertiary) tectonic activity has been suggested for the Bagdad area, with the northeast uplifted relative to the southwest. Evidence to support post-Laramide tectonism includes: (when moving across the area from northeast to southwest) 1) the surface area of the stocks decreases; 2) the abundance of diking increases; 3) the abundance of complex intrusive breccias increases; and 4) the Grayback Mountain rhyolite tuff is preserved (Hawley and Blacet, 1990).

Figure 3 shows the major faults in the Bagdad area. Anderson (1956) suggested that the northeast and northwest structural trends in the Bagdad area represent conjugate shear zones generated by nearly east-west relative shortening. The intersection of the two shear zones, evidenced by the intersection of the dike swarms (Fig. 4), is believed to be the major factor in emplacement of copper/molybdenum mineralization at Bagdad (Anderson et al., 1956). The northeast trending shear zone, along with its associated dike swarm (Fig. 4), extends into the thesis area and also played an important role in its geologic development.

The Geology of the Grayback Mountain

Geologic History

The Grayback Mountain mylonite zone consists essentially of rocks of Precambrian age. The Precambrian rocks were not mapped in any detail except at the manufacturing mill. A summary of the microscopic and macroscopic characteristics of the Precambrian rocks of the Bagdad area is found in

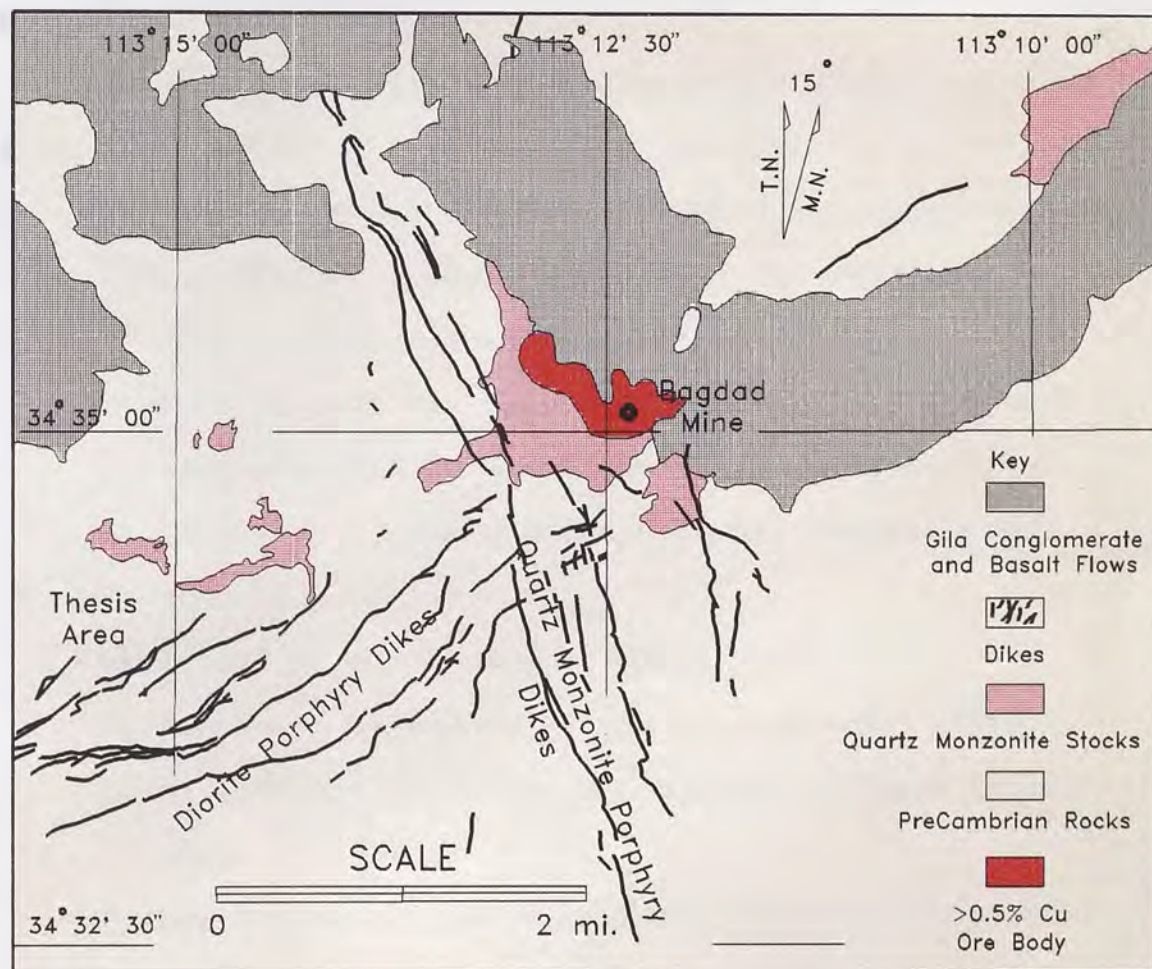


Figure 4. Map showing the intersection of the two postulated shear zones marked by the intrusion of the diorite and quartz monzonite dikes (Anderson et al., 1956). Mining of the porphyry presently shows elongation of the mineralized stock to the northeast (oral comm. J. Hawley, Cyprus Bagdad, 1991).

The Geology of the Grayback Mountains

Geologic History

The Grayback Mountain rhyolite tuff rests unconformably on rocks of Precambrian age. The Precambrian rocks were not mapped in any detail except at the unconformity contact. A discussion of the megascopic and microscopic characteristics of the Precambrian rocks of the Bagdad area is found in Anderson et al., 1956.

The geologic history of the Grayback Mountains drawn from field evidence and available age dates is as follows:

- 1) Venting of the Grayback Mountain rhyolite tuff and deposition, unconformably over the Precambrian rocks of the Bagdad area;
- 2) Intrusion of the Grayback Mountain rhyolite tuff by granodiorite to quartz monzonite stocks;
- 3) Intrusion of dikes of flow-banded rhyolite and diorite porphyry;
- 4) Extrusion of the Copper Ridge tuff;
- 5) Intrusion of the later quartz monzonite dikes;
- 6) Erosion and possible (?) regional tilting of the area;
- 7) Deposition of the rest of the Tertiary section;
- 8) Erosion to present day topography.

Geologic Maps and Cross Sections

Figure 5 shows the general geologic map of the Grayback Mountain thesis area at a scale of 1:36,000. The central

thesis area geology is shown in figure 6 at a scale of 1:24,000. Figures 7 and 8 are idealized cross sections through the Grayback Mountain thesis area along lines A - A' and B - B' respectively (Fig. 6). A detailed geologic map (1:12,000) on a topographic base is found at the end of this thesis (Plate 1).

Age Dates and Petrography

Grayback Mountain Rhyolite Tuff (Kqbrt)

The most extensive unit in the thesis area is the Grayback Mountain rhyolite tuff. The lack of sedimentary, erosional, or other cooling unit breaks in this unit suggest that the Grayback Mountain rhyolite tuff is a single-cooling-unit tuff which resulted from a single climactic eruption. Two fission-track age dates for the Grayback Mountain rhyolite tuff are 71.2 ± 12 Ma. and 84 ± 14 Ma. (oral comm. Bruce Bryant, USGS). Relative age can be determined using field relations. The southeast, east, north, and northeast flanks of Grayback Mountain rhyolite tuff rest unconformably on Precambrian Alaskite Porphyry. The northwest flank rests unconformably over Precambrian schist/diabase. The southern and northwestern flanks display fault/vent margin contact and unconformity relationships with the Precambrian rocks (Fig. 5 and 6). The Precambrian-Grayback Mountain rhyolite tuff contact is obscured by colluvium or covered by the Copper Ridge tuff in some areas. The Grayback Mountain rhyolite tuff is intruded

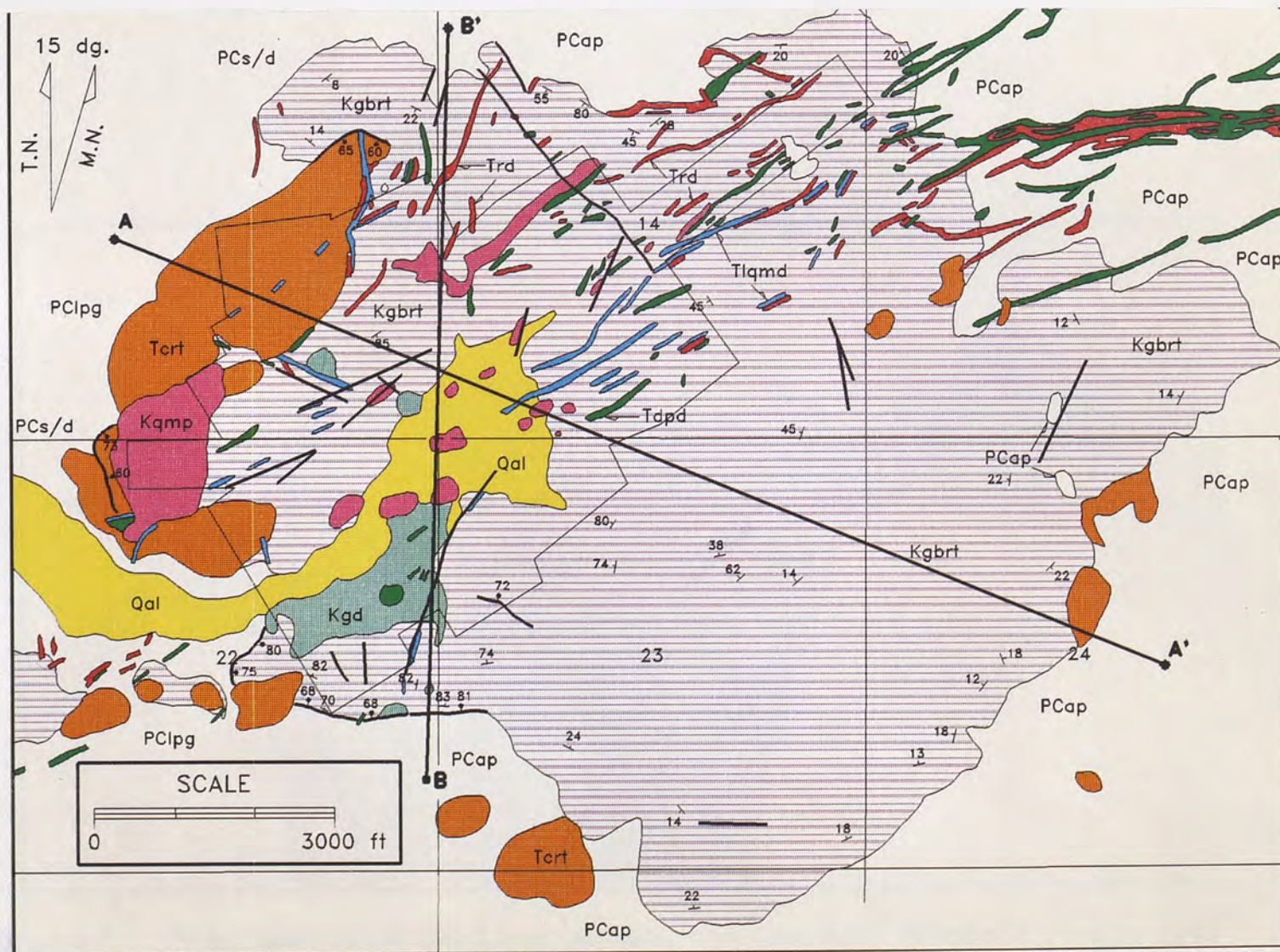


Figure 6. Geologic map of the central thesis area (1:24,000). For legend see Fig. 5.

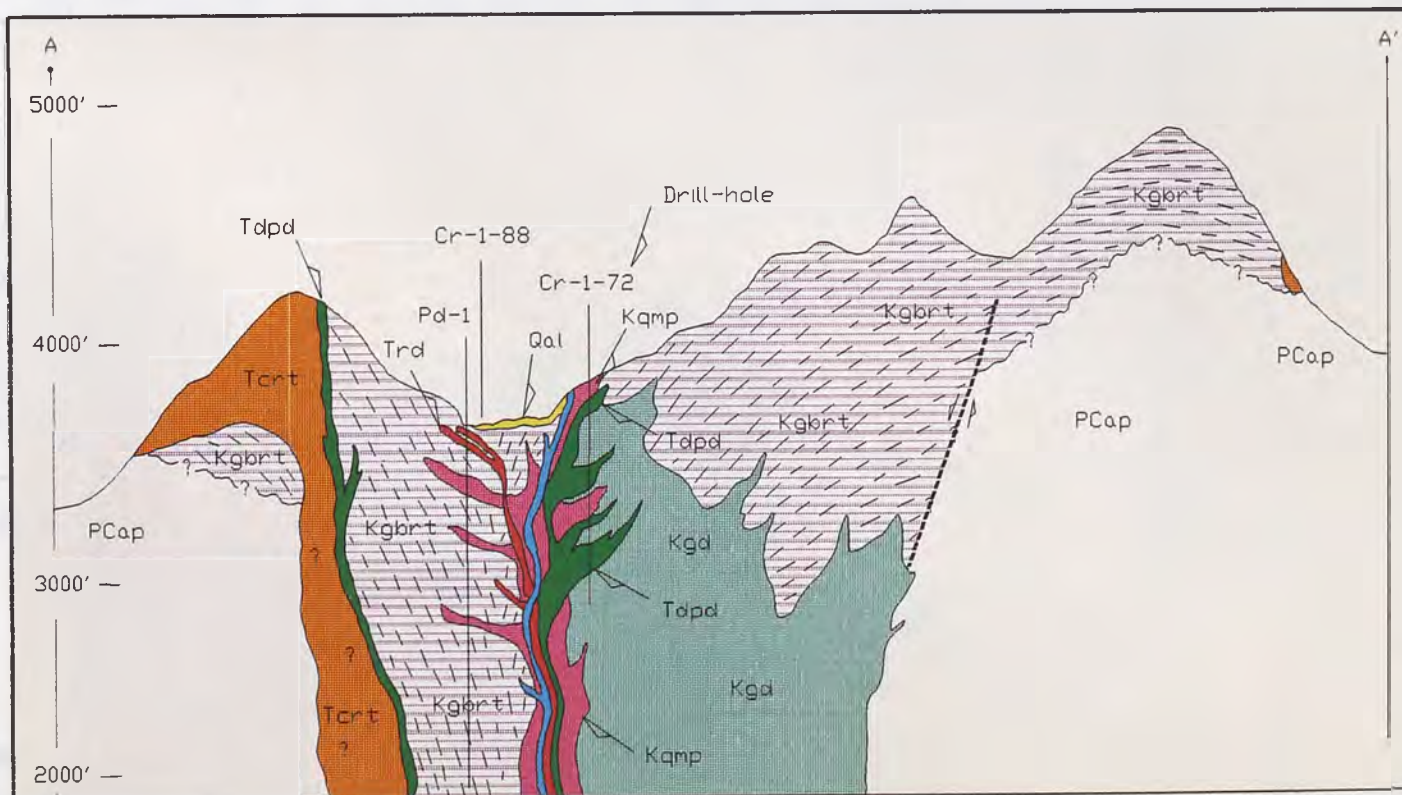


Figure 7. Idealized cross section through the Grayback Mountain thesis area (line: A - A'). For legend see Figure 8.

by granodiorite to quartz monzonite stocks, and by younger dikes of flow-banded rhyolite, diorite porphyry, and late quartz monzonite.

Megascopically, the Grayback Mountain tuff varies from gray to purple or pink on the fresh surface. The weathered surface is commonly bleached white. Pumice content, welding, and compaction are variable within the tuff. The inner-canyon areas (see Plate 1) display moderate to dense welding with abundant compacted pumice. Along the outer ridges, welding remains moderate to dense, however, pumice content decreases. Lithic fragments in the tuff, vary in size from less than one inch to several feet in diameter. Lithic fragments include: Lawler Peak granite, schist, diabase, and alaskite porphyry. The Grayback Mountain rhyolite tuff is relatively apheritic with approximately 10 to 20% phenocrysts. The phenocryst mineralogy in hand specimen includes: quartz, sanidine, plagioclase, and minor biotite.

Microscopically, the Grayback Mountain rhyolite tuff contains hypidiomorphic quartz (0.5-2.0 mm) and plagioclase (0.5-1.0 mm), idio-hypidiomorphic (0.5-1.0 mm) sanidine (adularia, where altered), with minor biotite, zircon, and apatite; set in a groundmass of welded glass shards. Spherulitic and axiolitic aggregates found in pumice cavities and in the ground mass, indicate partial devitrification of the tuff.

Granodiorite Stocks (Kgds)

The Granodiorite stocks have not been radiometrically dated but their relative age is constrained by the geology. They are clearly intrusive into the Grayback Mountain rhyolite tuff (Fig. 6). Crosscutting relationships of both the rhyolite and diorite porphyry dikes with the granodiorite stock can be seen in diamond drillcore (Fig. 37 and 38). The granodiorite is therefore younger than the Grayback Mountain rhyolite tuff and older than the rhyolite and diorite porphyry dikes.

Phenocryst mineralogy in the granodiorite is dominated by the presence of large (up to 5 mm) acicular hornblende phenocrysts and aggregates of biotite. Other phenocrysts include: quartz, plagioclase, and orthoclase. The presence of abundant idiomorphic phenocrysts of hornblende and biotite, a light gray color, and a distinctive rounded morphology, were the main field criteria for distinguishing the granodiorite.

Microscopically, the granodiorite contains idiomorphic to hypidiomorphic phenocrysts of plagioclase (2-3 mm), biotite (1-3 mm), and hornblende (1-5 mm). Quartz (0.5-1 mm) and orthoclase (0.5-1 mm) are hypidiomorphic. Minor phenocrysts include: zircon and apatite. Matrix composition is primarily quartz and feldspars.

Quartz Monzonite Porphyry (Kqmp)

The quartz monzonite porphyry within the thesis area

has not been radiometrically dated. Similar quartz monzonite stocks outside of the thesis area, but within the 12 mile-long intrusive belt, are dated at approximately 77 Ma. (Hawley and Blacet, 1990). This age seems to fit fairly well with the geologic evidence. The quartz monzonite is younger than the Grayback Mountain rhyolite tuff, coeval or just slightly younger than the granodiorite, and older than the rhyolite, diorite porphyry, and later quartz monzonite dikes.

The quartz monzonite porphyry is distinguished from the granodiorite by its lack of mafic minerals (primarily hornblende ± biotite) and abundant porphyritic feldspars in a fine quartz/feldspar matrix. Feldspars are commonly altered to clay giving the rock a speckled appearance.

Microscopically, the quartz monzonite consists of hypidiomorphic quartz (0.5-1 mm) and orthoclase (1-2 mm) phenocrysts, idiomorphic plagioclase (1-3 mm), and book-like (0.5-1 mm) biotite. Minor phenocrysts of zircon and apatite were also noted. The ground mass is a fine grained mixture of quartz and feldspars.

Three bodies of brecciated quartz monzonite porphyry crop out in the central thesis area (see Plate 1). The breccias lie along the N60°E shear zone trend, are clast supported, and healed with fine grained quartz and feldspar. Iron oxides are also common along fractures. The quartz monzonite porphyry clasts are argillically altered,

relatively unmineralized, and sub-angular. The breccia bodies are believed to represent hydrothermal (crackle) breccia pipes related to the intrusion of the quartz monzonite porphyry.

Rhyolite Dikes (Trd)

The flow-banded rhyolite dikes that cut the Grayback Mountain rhyolite tuff and the granodiorite and quartz monzonite stocks have not been dated in the thesis area. A fission track age date (zircon) on a petrographically similar flow-banded rhyolite dike to the southwest of the thesis area yielded an age of 66.7 ± 8.1 Ma. (Bryant, 1988).

Most dikes strike northeast with flowbanding dip varying from 40-90°. Dikes at the Precambrian-Grayback Mountain rhyolite tuff contact are interpreted as in-filling along a crude fracture system related to venting of the Grayback Mountain rhyolite tuff. The flow-banded rhyolite dikes commonly possess a chilled margin along with moderate brecciation.

Megascopically, the dikes contain sparse, large (2-3 mm), idiomorphic to hypidiomorphic phenocrysts of quartz, sanidine, and plagioclase, set in a white sugary groundmass of allotriomorphic quartz and feldspar. The white to cream color, flow-banding, and sparse idio-hypidiomorphic phenocrysts help distinguish the rhyolite dikes in the field.

Microscopically, the rhyolite dikes contain 10 to 15%

phenocrysts. Quartz is hypidiomorphic (0.5-1 mm) and commonly embayed. Sanidine and plagioclase (both 0.5-0.7 mm) are idiomorphic to hypidiomorphic. Minor phenocrysts include: biotite and zircon.

Diorite Porphyry Dikes (Tdpd)

Diorite porphyry dikes crosscut the Grayback Mountain rhyolite tuff, and in places the flow-banded rhyolite dikes. No age dates are available for the diorite porphyry dikes in the thesis area proper. Age dates on dikes petrographically similar to those in the thesis area are a fission-track date of 65.5 ± 11 Ma. (Bryant, 1988) and a K-Ar date of approximately 75 Ma. (Hawley and Blacet, 1990). Both of the dikes dated show similar strike (northeast) to those in the thesis area.

Megascopically, the diorite porphyry dikes are medium to dark green-gray with idiomorphic hornblende, plagioclase, and biotite phenocrysts. Hornblende phenocrysts are locally up to 1 cm. long. On the weathered surface the dikes appear mottled (due to the alteration of the feldspars to clay) and have a rounded morphology.

Phenocrysts in thin section mimic those seen in hand specimen. Plagioclase (1-2 mm) is idiomorphic to hypidiomorphic. Potassium feldspar (0.5-0.7 mm) is hypidiomorphic, and biotite and hornblende (1-5 mm) are idiomorphic. Allotriomorphic quartz was observed in a few sections and is commonly embayed. Groundmass composition is

microlitic feldspars.

Copper Ridge Tuff (Tcrt)

The Copper Ridge Tuff is a poorly to moderately welded, lithic-rich, rhyolite tuffaceous pyroclastic flow and flow breccia with a thin basal unit of airfall tuff, in places. The main outcrop is along the western edge of Copper Ridge in the northwest portion of the thesis area (Figs. 5 and 6). The Copper Ridge tuff is not radiometrically dated but contains lithic fragments of mineralized and unmineralized Grayback Mountain rhyolite tuff and rhyolite dike, and diorite porphyry dike. The Copper Ridge tuff is cut and locally altered by the intrusion of late quartz monzonite dikes. Thus, the Copper Ridge tuff is late in the geologic history of the area; younger than the diorite porphyry dikes and older than the late quartz monzonite dikes. Remnant outcrops of flow breccia mapped throughout the thesis area indicate that the Copper Ridge tuff may, at one time, have completely covered the Grayback Mountain area. A source for the Copper Ridge tuff is not known but Cyprus company reports refer to several "vent" areas along the northern ridge system. This hypothesis seems reasonable, however, field evidence to support the existence of the "vents" is limited.

On a fresh surface the Copper Ridge tuff is creamy white to tan with visible phenocrysts of quartz and feldspars. Vertical jointing, a black "desert varnish"

coating of iron and manganese oxides, and an abundance of lithic fragments of older rocks are distinctive of the Copper Ridge tuff.

Garnet phenocrysts can be found in and around the butte of Copper Ridge tuff at the southwest end of the thesis area. Garnet phenocrysts along fractures and in void spaces clearly are vapor phase in origin (Fig. 9b, left). In other locations the garnets are irregularly distributed within a moderately welded matrix and highly altered suggesting a primary magmatic or hydrothermal alteration origin (Fig. 9b, right). Scanning Electron Microscope analysis indicates the garnets are a compositional mix of almandine and spessartine end members (Fig. 9a). The tuff in the garnet locality, can best be described as having "measles", with the "measles" representing both altered (biotite-chlorite-feldspars \pm quartz) and unaltered garnets (Fig. 9b). Keith and Shanks (1985) found euhedral, deep red, almandine-spessartine garnet phenocrysts in the rhyolitic intrusive and extrusive units associated with the Pine Grove porphyry molybdenum and ash-flow tuff system, southwestern Utah. They found garnet in irregular intergrowths with quartz and feldspar of the matrix (similar to the thesis area garnets) and postulated that garnet development was a late stage magmatic event rather than a product of circulating hydrothermal fluids (Keith and Shanks, 1985).

Microscopically, the Copper Ridge tuff contains

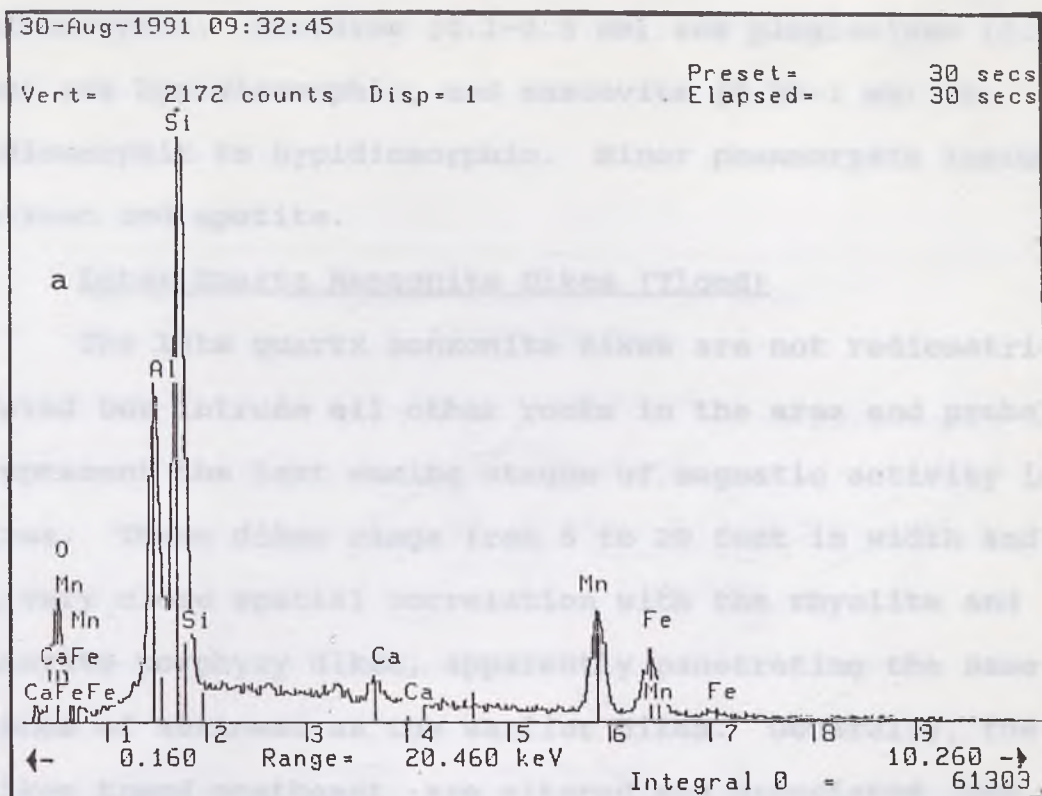


Figure 9. a) Print out of SEM energy dispersive data from garnets of the Copper Ridge tuff; b) Fresh (left) and weathered garnets ("measle rock" - right) from the Copper Ridge tuff (Scale: 1" on photo = 1.74" actual).

allotriomorphic to hypidiomorphic quartz (0.5-1.5 mm) phenocrysts. Sanidine (0.1-0.5 mm) and plagioclase (0.5-2.0 mm) are hypidiomorphic, and muscovite (0.25-1 mm) is idiomorphic to hypidiomorphic. Minor phenocrysts include: zircon and apatite.

Later Quartz Monzonite Dikes (Tlqmd)

The late quartz monzonite dikes are not radiometrically dated but intrude all other rocks in the area and probably represent the last waning stages of magmatic activity in the area. These dikes range from 5 to 20 feet in width and show a very close spatial correlation with the rhyolite and diorite porphyry dikes, apparently penetrating the same zones of weakness as the earlier dikes. Generally, the dikes trend northeast, are altered and brecciated, and possess drusy quartz with iron oxides along fractures.

The appearance of the late quartz monzonite dikes is markedly different from the rhyolite and diorite porphyry dikes, however, alteration and weathering of the late quartz monzonite dikes makes mineralogic determinations difficult. Identifiable minerals include: quartz and altered feldspars. Drusy quartz in-filling along fractures and in brecciated zones, and the iron oxide coating are two of the main diagnostic features of the dikes.

Alteration

Figure 10 is a generalized alteration map (1:24,000) of the Grayback Mountain thesis area. Alteration is spatially

and temporally related to the intrusion of the stocks and dikes. The alteration mineralogy is complex due to successive overprinting of alteration stages and surficial (weathering related) alteration, but in general can be characterized by the mineral assemblage quartz-sericite-pyrite \pm kaolinite. Adularization, silicification, argillization, and propylitization are also present.

Alteration in the Grayback Mountain rhyolite tuff is complex. The outer margins of the tuff are relatively unaltered with localized pyritization and silicification related to dike intrusion. Alteration increases significantly toward the central thesis area (Fig. 10 - near intersection of sections 14, 15, 22, & 23) and is best characterized by the assemblage quartz-adularia-sericite-pyrite \pm kaolinite. Alteration boundaries are not well defined due to transitional and overlapping mineralogic changes.

The granodiorite is characterized by propylitic alteration, with biotite and hornblende altering to chlorite-epidote-sericite \pm calcite. Feldspar is altered, in part, to fine-grained sericite \pm calcite.

The quartz monzonite porphyry is characterized by phyllic and argillic alteration, with feldspars and biotite altered to fine-grained sericite \pm kaolinite.

Alteration in the rhyolite dikes is characterized by the alteration of feldspars to fine-grained sericite.

In the diorite porphyry dikes, feldspars are altered to sericite and carbonate. Hornblende alters to a propylitic assemblage of epidote-chlorite ± calcite. Biotite is altered to chlorite and sericite.

Feldspars in the Copper Ridge tuff weather to clay. Adjacent to intrusions of the late quartz monzonite dikes, the tuff is characterized by the assemblage: quartz-adularia-sericite ± pyrite.

Alteration of the late quartz monzonite dikes is characterized by fracture filling of pyrite with drusy quartz. Pyrite is completely altered to goethite and hematite.

Mineralization

Mineralization is also spatially and temporally related to the intrusion of the stocks and dikes. The nine sulfide minerals identified include: pyrite, chalcopyrite, pyrrhotite, sphalerite, covellite, chalcocite (digenite), bornite, molybdenite, and galena. Gangue minerals are dominantly quartz and feldspars.

Pyrite - FeS₂

The most common sulfide mineral is pyrite. Two contrasting pyrite phases, possibly indicating two distinct mineralization stages, are observed. The dominant phase displays the optical (isotropic) characteristics documented for pyrite and is found in all the rock types. The second pyrite phase appears to be associated with the rhyolite,

diorite porphyry, and late quartz monzonite dikes and displays distinctive brown to green anisotropy, however, SEM analysis does not show it as As-rich or arsenical pyrite. Both pyrite phases occur as disseminated grains, and along fractures with quartz (Fig. 11a). Pyrite is commonly hypidiomorphic, but idiomorphic and allotriomorphic forms are also recognized. The grains are commonly fractured (Fig. 11b) and show varying stages of oxidation to goethite/hematite. Inclusions are common and include: quartz, chalcopyrite, pyrrhotite, sphalerite (Fig. 12a), and possibly covellite (?).

Chalcopyrite - CuFeS_2

Chalcopyrite occurs as disseminated grains and fracture fillings (Fig. 12b), inclusions in pyrite (Fig. 12a, 14a, 15b), and inclusions in sphalerite (Fig. 13a, 13b). The most common occurrence is as inclusions in pyrite. Disseminated chalcopyrite is allotriomorphic with a few hypidiomorphic grains observed (fig 15a). Textural studies do not definitively establish a mode of formation for the chalcopyrite. Irregular distribution of chalcopyrite blebs in sphalerite (Fig. 13b) suggests exsolution and chalcopyrite rims on sphalerite (Fig. 13a) suggests replacement. It is not inconceivable that both exsolution and replacement processes were operative.

Pyrrhotite - $\text{Fe}_{(1-x)}\text{S}$

Pyrrhotite occurs as small inclusions in pyrite

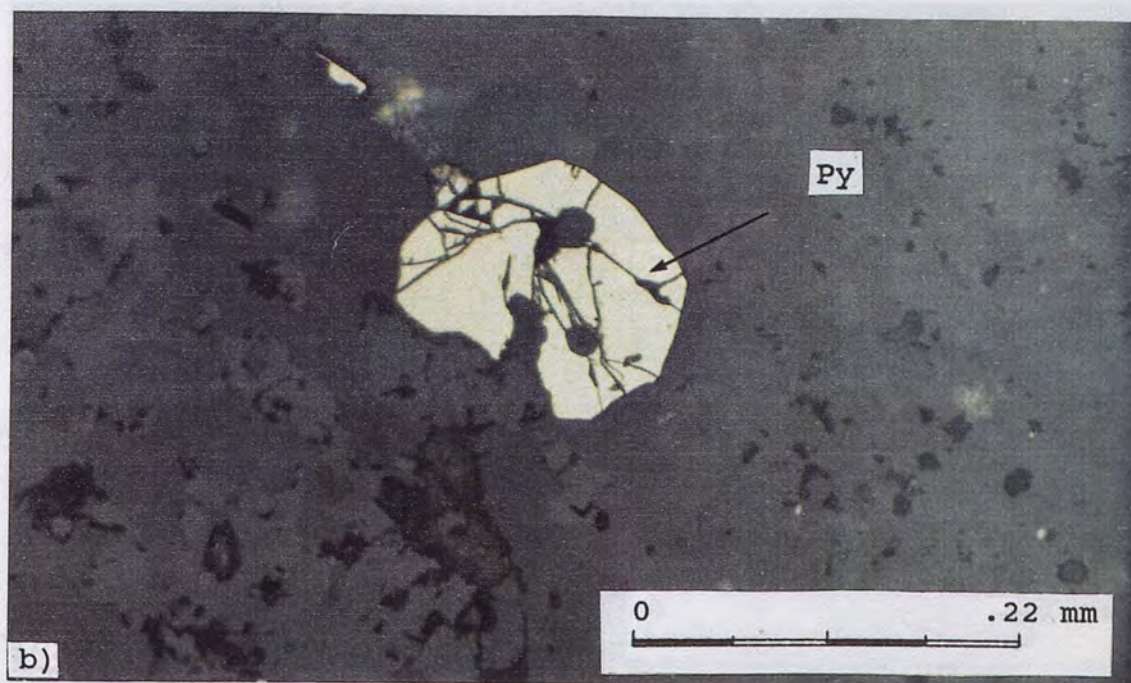
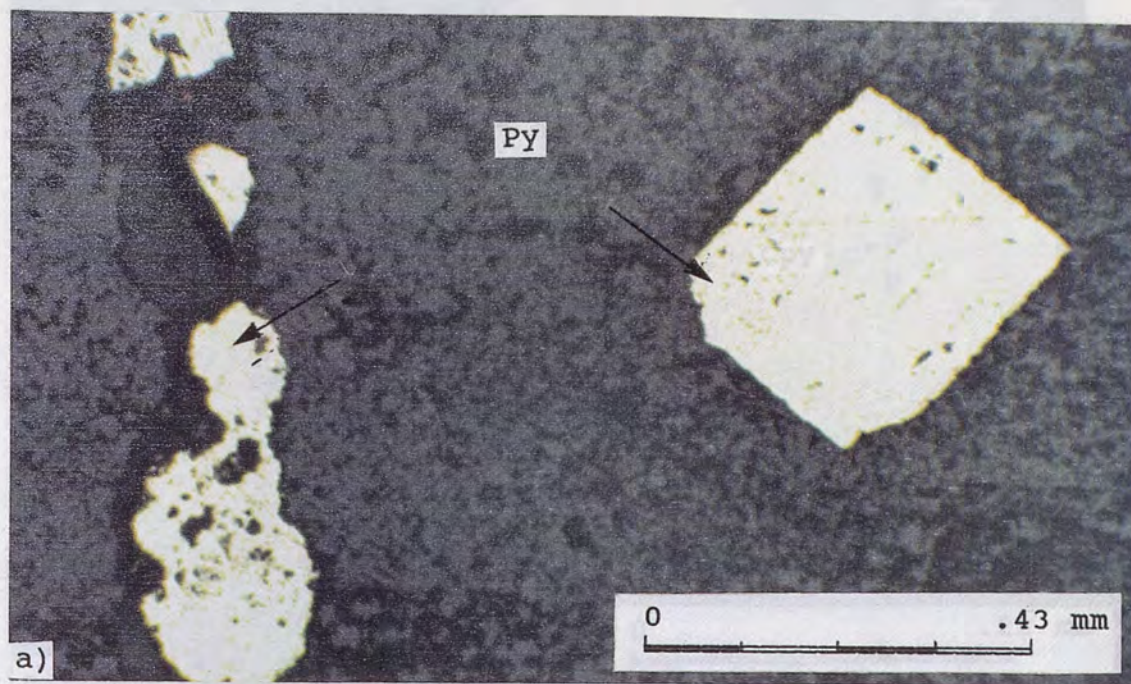


Figure 11. a) Idiomorphic, zoned, pyrite cube in the groundmass along with allotriomorphic pyrite grains infilling a fracture (section 4-272). b) Fractured idiohypidiomorphic pyrite grain (section 1).

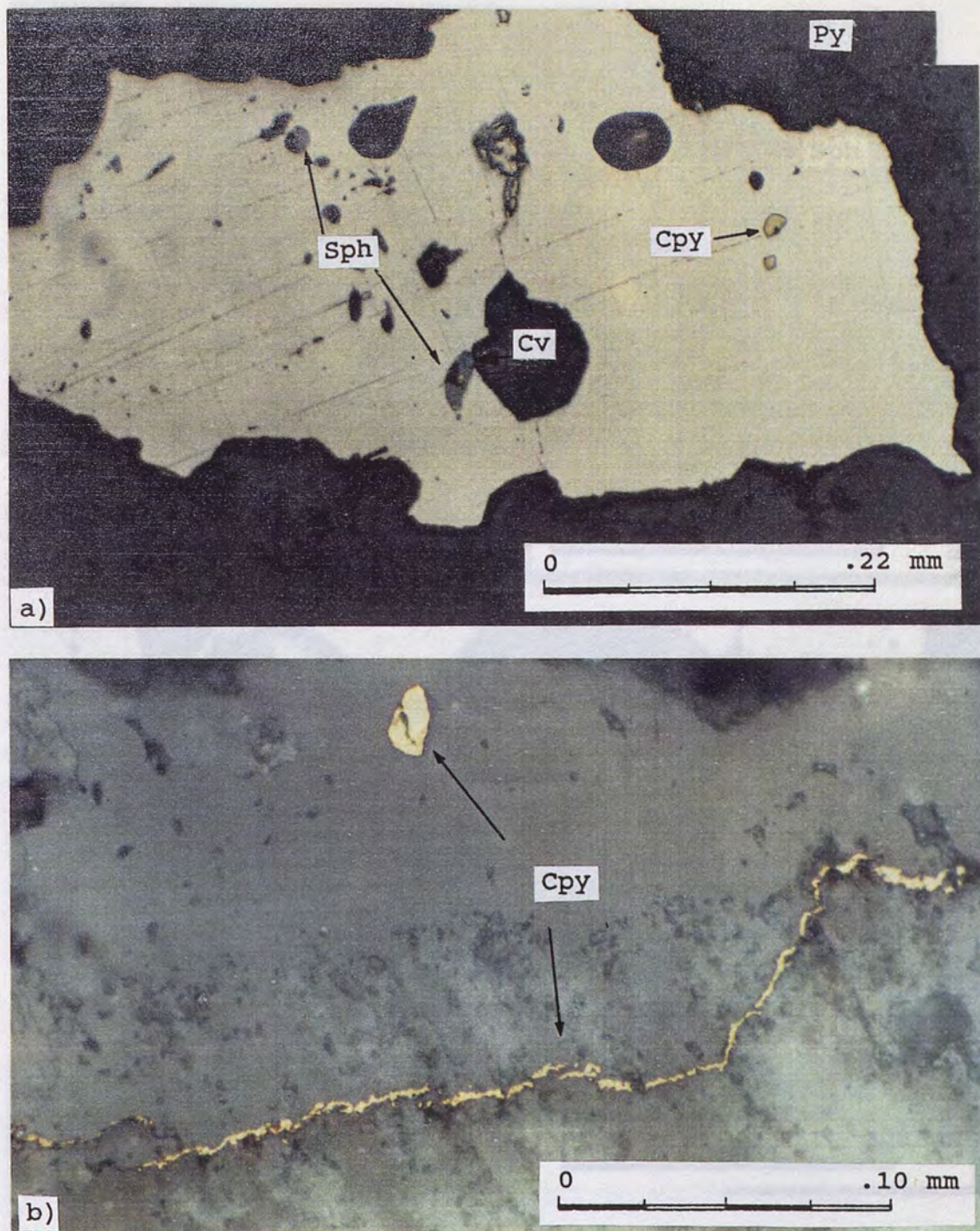


Figure 12. a) Allotriomorphic pyrite grain with inclusions of chalcopyrite, sphalerite, and covellite (section A-1). b) Allotriomorphic chalcopyrite grain in the groundmass along with chalcopyrite infilling a fracture (section Cr-286).

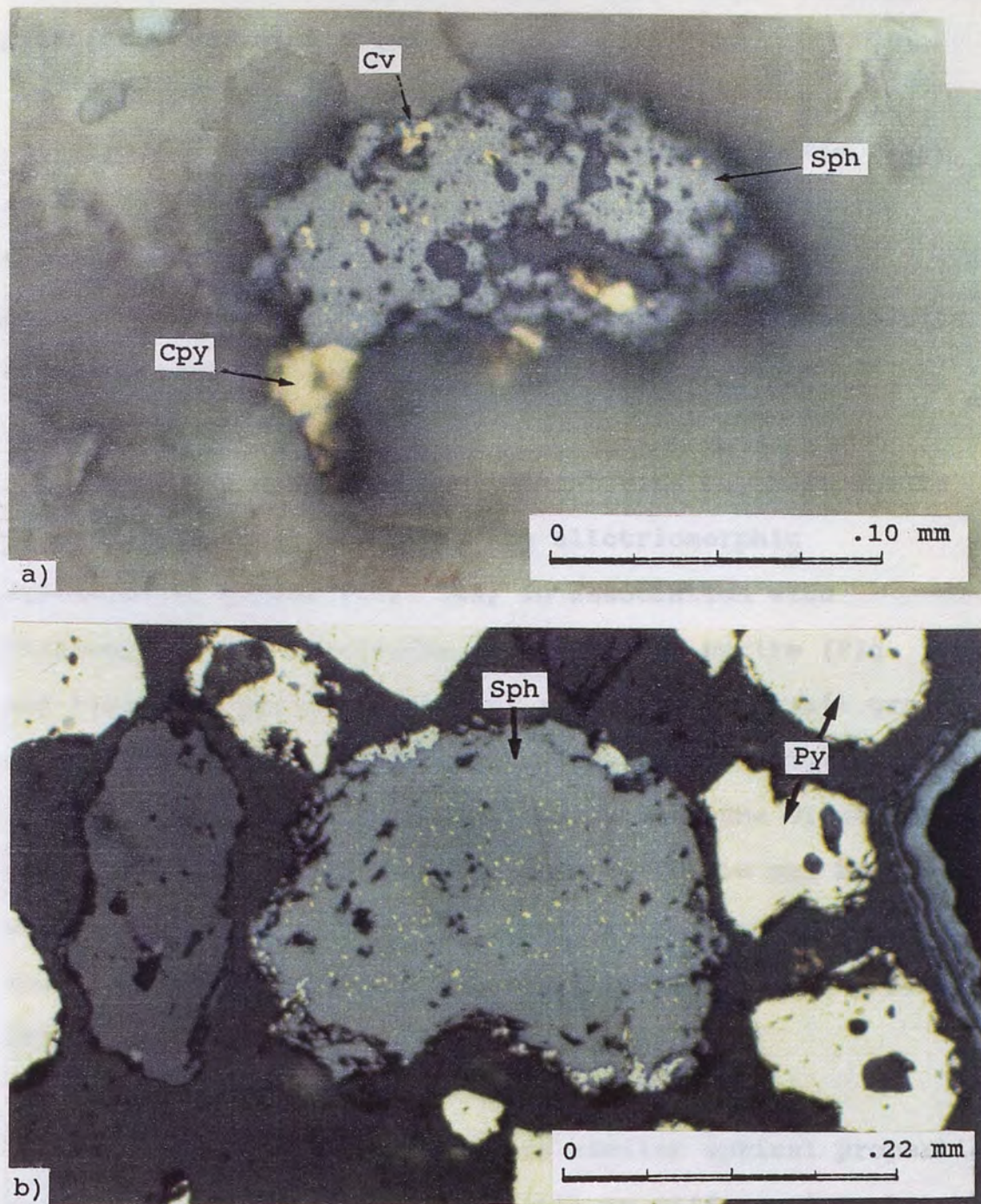


Figure 13. a) "Chalcopyrite disease" in sphalerite. The presence of larger chalcopyrite grains favors replacement of sphalerite by chalcopyrite (section Cr-286). b) "Chalcopyrite disease" in sphalerite. Random orientation of chalcopyrite blebs favors exsolution origin for the chalcopyrite (section Cr-1-90).

associated with chalcopyrite (Fig. 14a). Minor disseminated pyrrhotite was also noted.

Sphalerite - $(\text{Zn,Fe})\text{S}$

Sphalerite occurs as inclusions in pyrite (Fig. 14a), as allotriomorphic disseminated grains, and in-filling fractures with chalcopyrite and pyrite (Fig. 14b). Sphalerite, in association with chalcopyrite also exhibits "chalcopyrite disease" (Fig. 13a, 13b).

Covellite - CuS

Covellite occurs as replacement rims on chalcopyrite (Fig. 15a), as hypidiomorphic to allotriomorphic disseminated grains (Fig. 14a) in association with chalcopyrite and sphalerite inclusions in pyrite (Fig. 12a), and replacing pyrite (Fig. 15b) and bornite. Small grains of covellite, associated with chalcopyrite and sphalerite inclusions in pyrite (Fig. 12a) along with the disseminated covellite (Fig. 14a), indicate that covellite may have been early as well as late in the paragenetic sequence. Most of the covellite observed is replacing chalcopyrite and pyrite (Fig. 15a).

Chalcocite/Digenite - Cu_2S

Chalcocite and digenite have similar optical properties and chemistries making it difficult to differentiate between the two phases. Vickers microhardness estimations on the chalcocite (digenite) grains favors digenite as the correct mineral name. Chalcocite/digenite occurs as hypidiomorphic

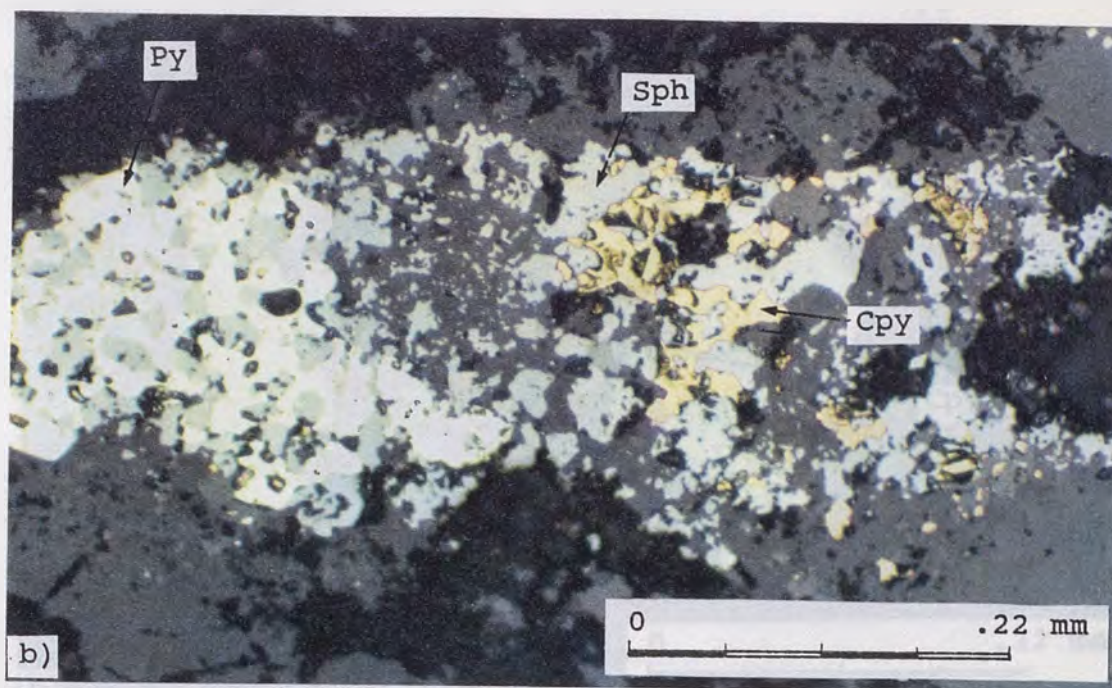
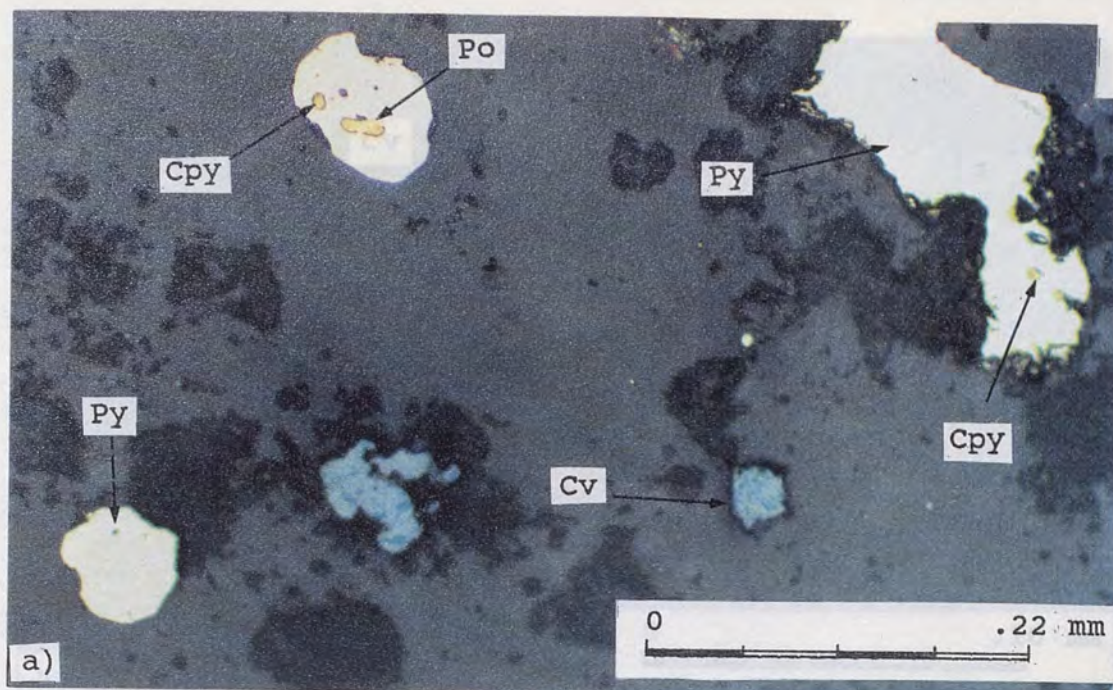


Figure 14. a) Allotriomorphic to hypidiomorphic pyrite grains with inclusions of chalcopyrite and pyrrhotite, and disseminated covellite (section 2). b) Chalcopyrite, pyrite, sphalerite, and gangue infilling a fracture with mutual boundaries (section 4-1395).

to idiomorphic grains disseminated along fractures (Fig.

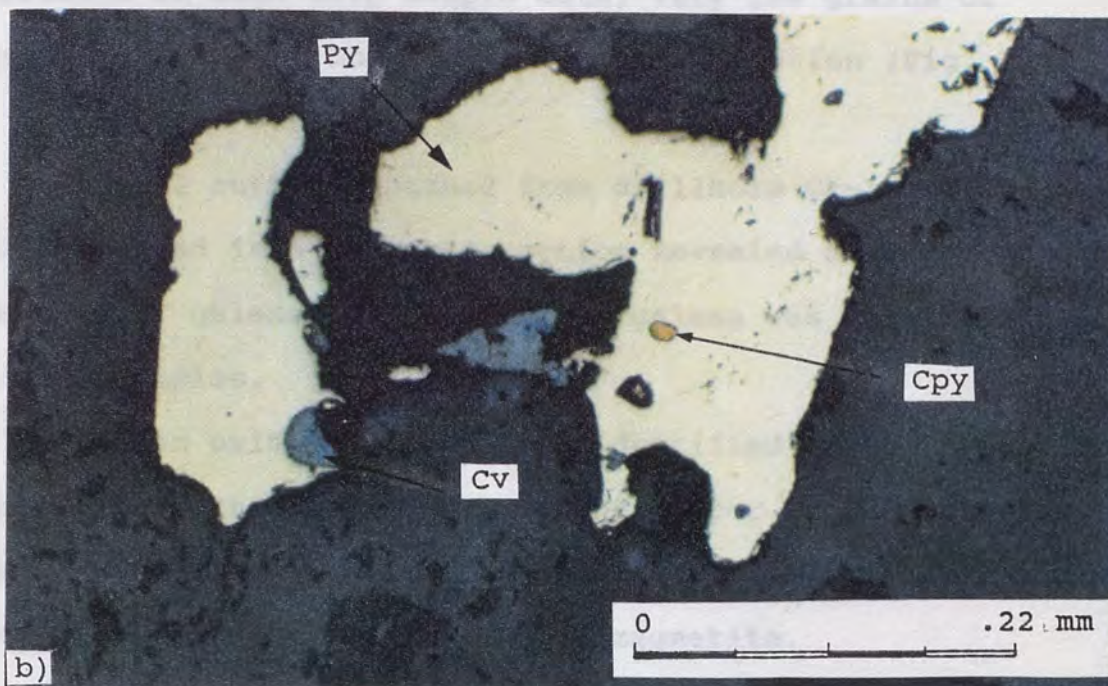
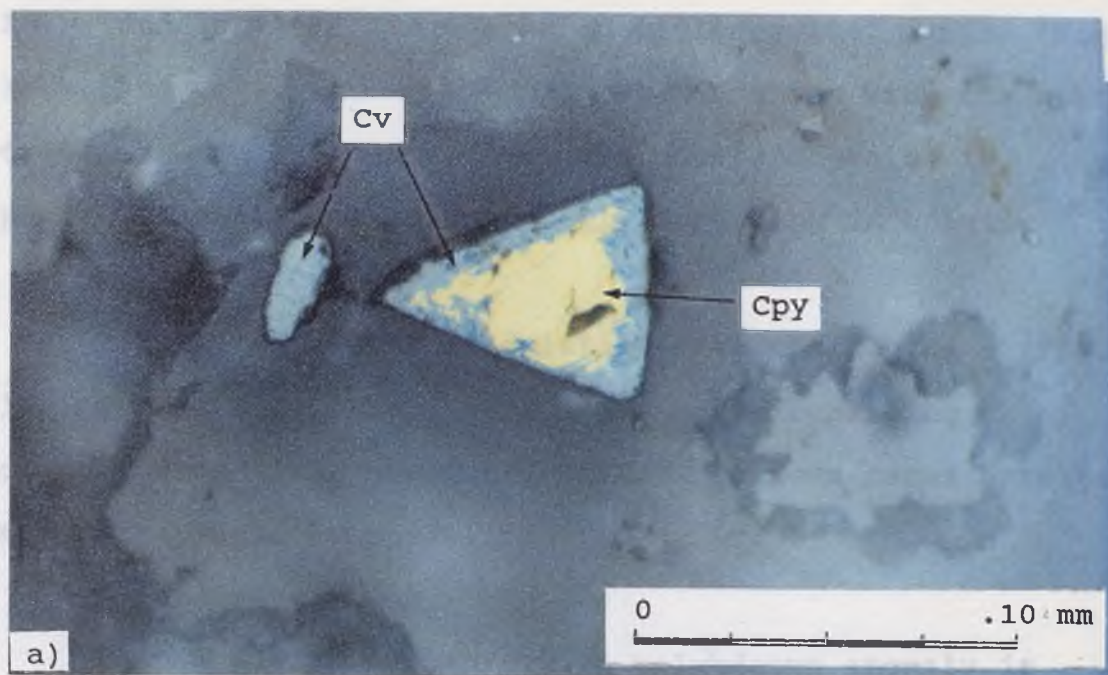


Figure 15. a) Replacement of idio-hypidiomorphic chalcopyrite grain by covellite; and disseminated covellite grain (section 7). b) Pyrite with chalcopyrite inclusion, and replacement of pyrite by covellite (section 3).

to allotriomorphic grains disseminated along fractures (Fig. 16a), and as replacement rims on chalcopyrite, pyrite (Fig. 16b), and covellite. Textural relationships with the other opaque minerals indicate that chalcocite/digenite is paragenetically late and probably supergene in origin.

Bornite - Cu_5FeS_4

Bornite occurs in association with chalcopyrite (Fig. 17a) and is rare. Bornite appears to be replacing chalcopyrite along small fractures. In some cases bornite may be replaced by covellite.

Molybdenite - MoS_2

Though a fairly significant molybdenum anomaly is present in rock chip sample data, very few grains of molybdenite were observed in polished section (Fig. 17b).

Galena - PbS

Drill cuttings panned from drillhole Cr-1-90 (Fig. 39) and mounted in a polished section revealed a few scattered grains of galena (Fig. 18a). No galena was observed in any other samples.

Seven oxide minerals were identified in the prepared polished sections and include the copper oxides: azurite, malachite, chrysocolla, and melanochalcite; and the iron oxides: goethite, hematite, and magnetite.

Copper Oxides

Azurite (Fig. 18b), malachite (Fig. 19a, 19b), and chrysocolla in-fill along small shear and brecciated zones,

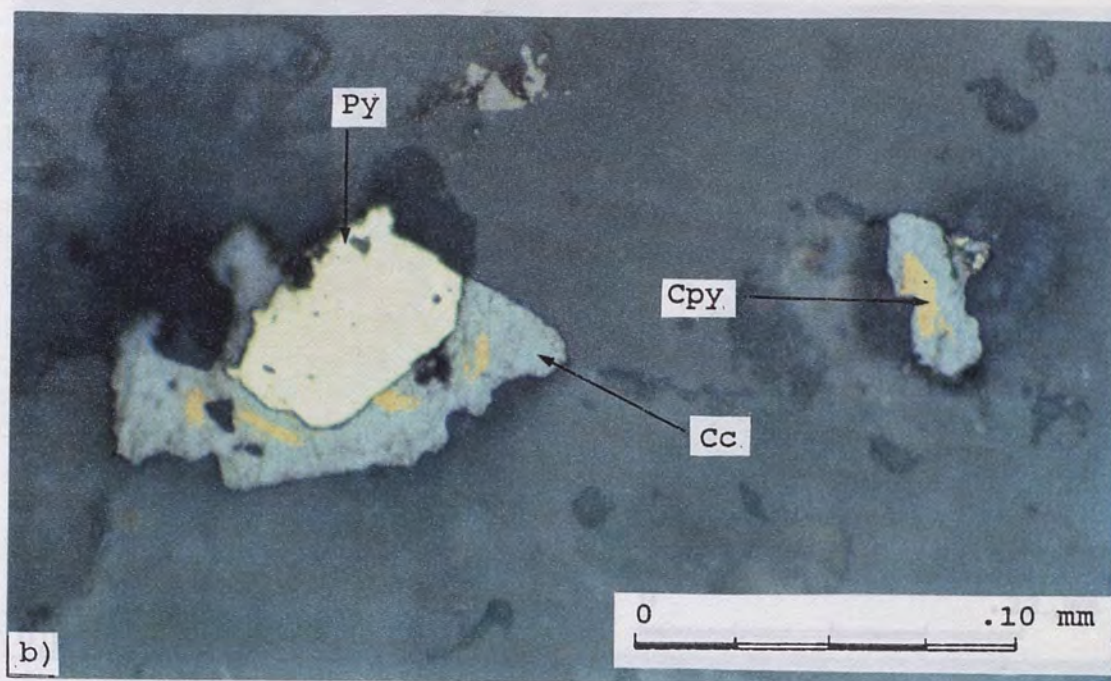
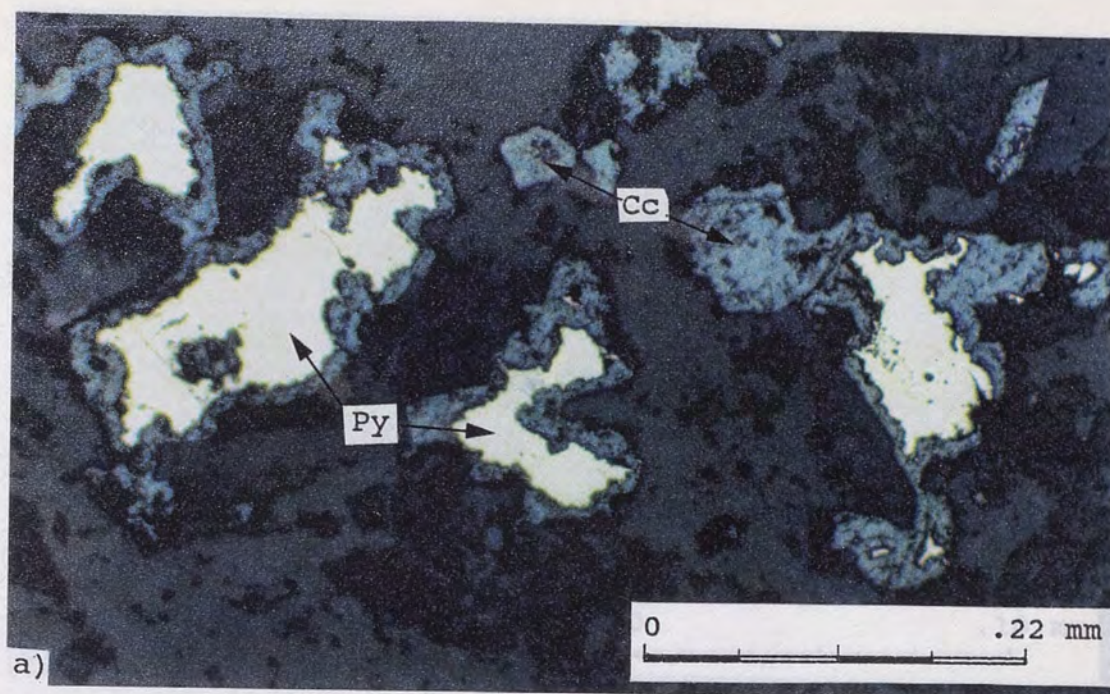


Figure 16. a) Chalcopyrite and bornite. Textural relations
 Figure 16. a) Disseminated chalcocite/digenite grains along
 a fracture with pyrite (section 2). b) Chalcocite/digenite
 replacing chalcopyrite and rimming pyrite (section 7).

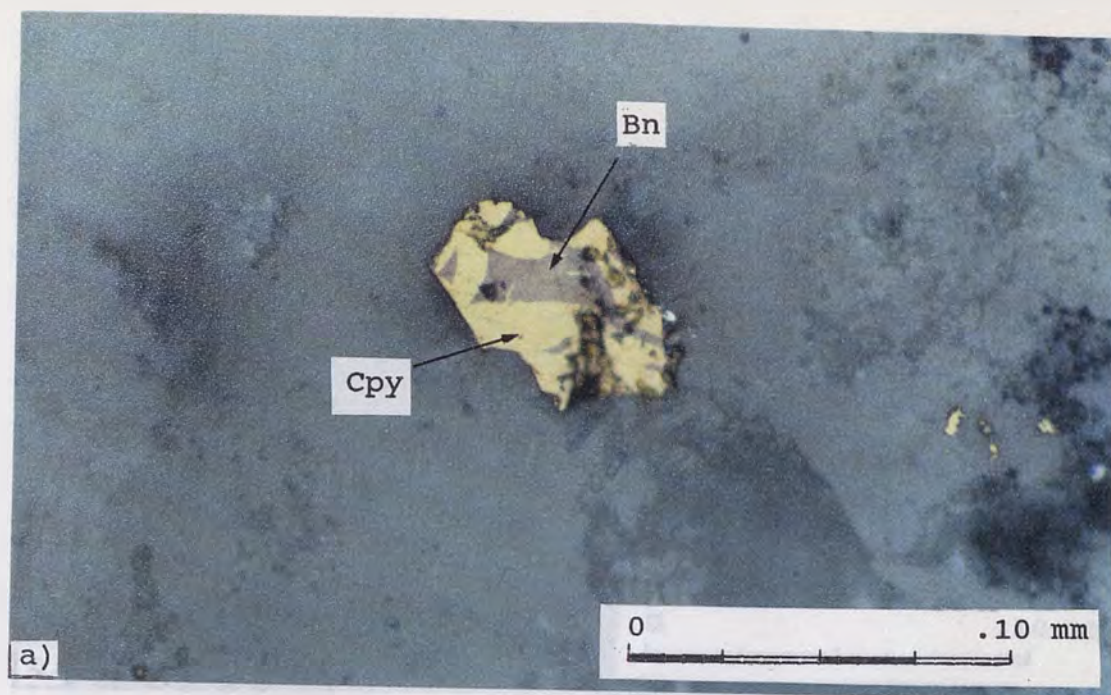


Figure 17. a) Chalcopyrite and bornite. Textural relations are unclear, but bornite appears to be replacing chalcopyrite along fractures (section Cr-286a). b) Disseminated molybdenite grain (section 7).

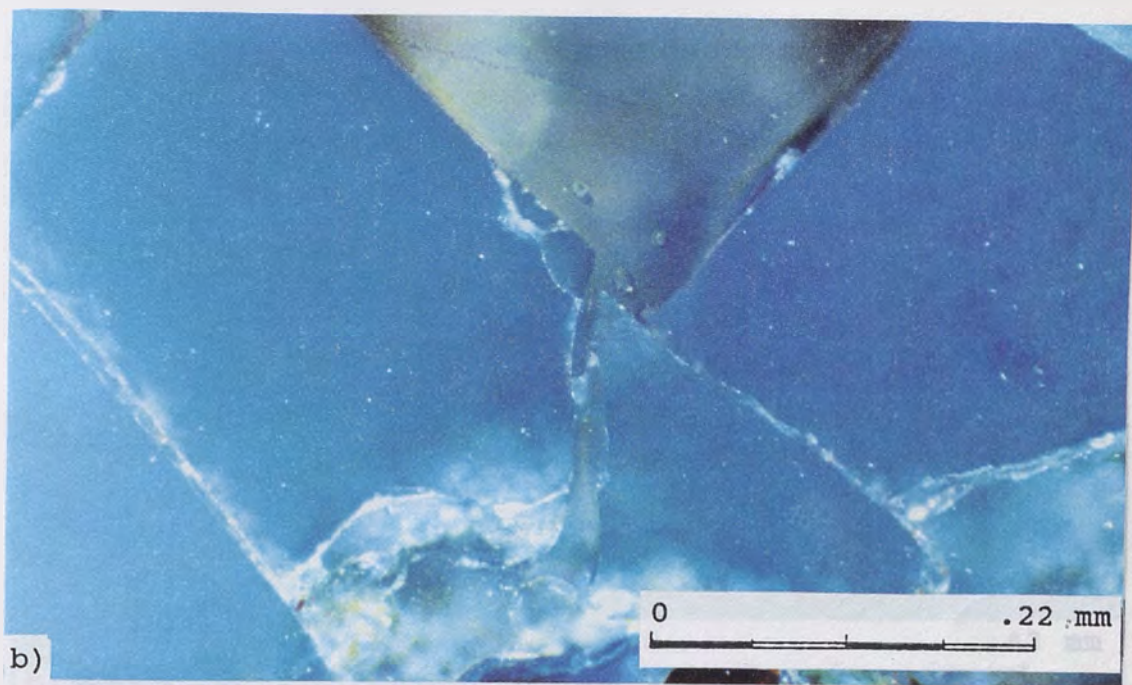
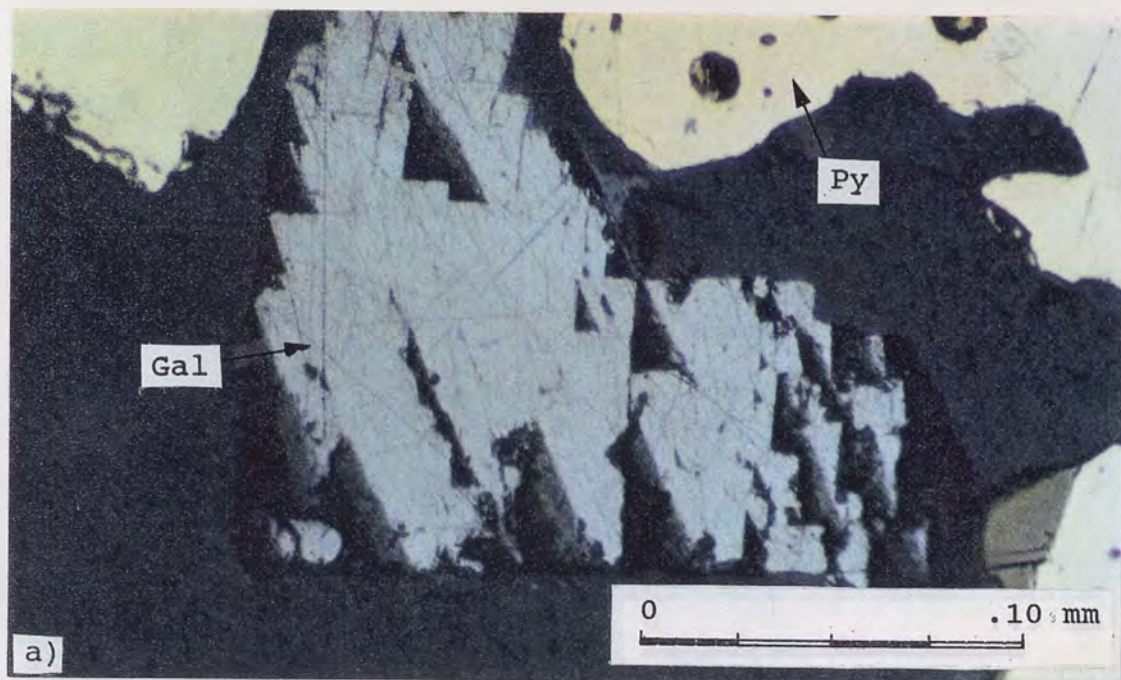
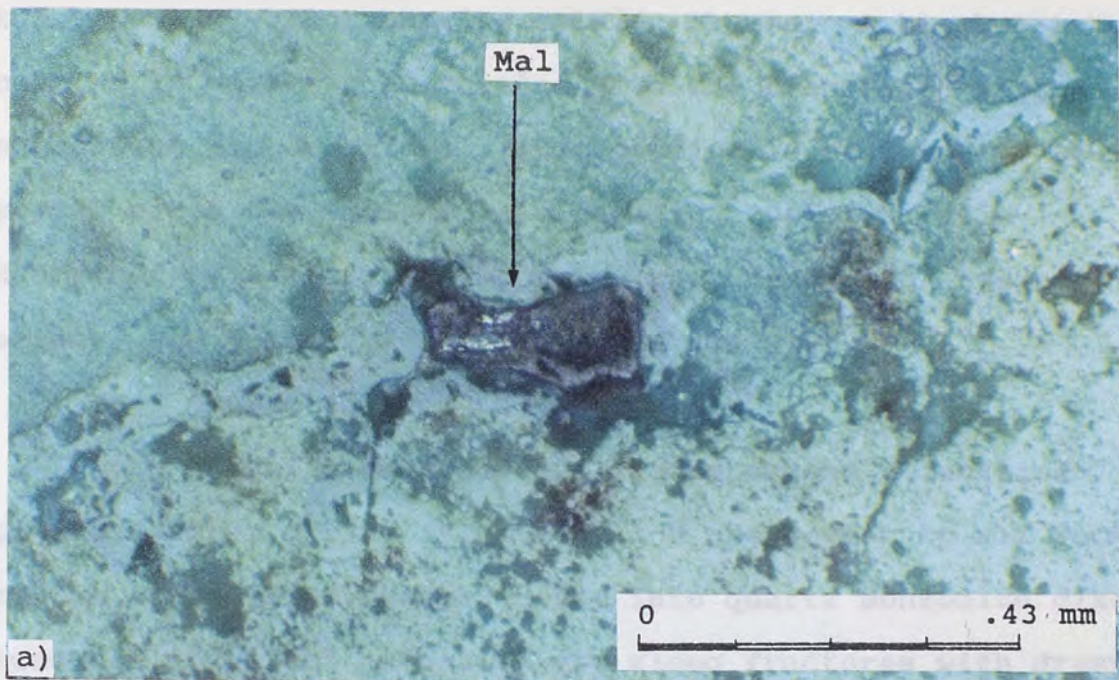
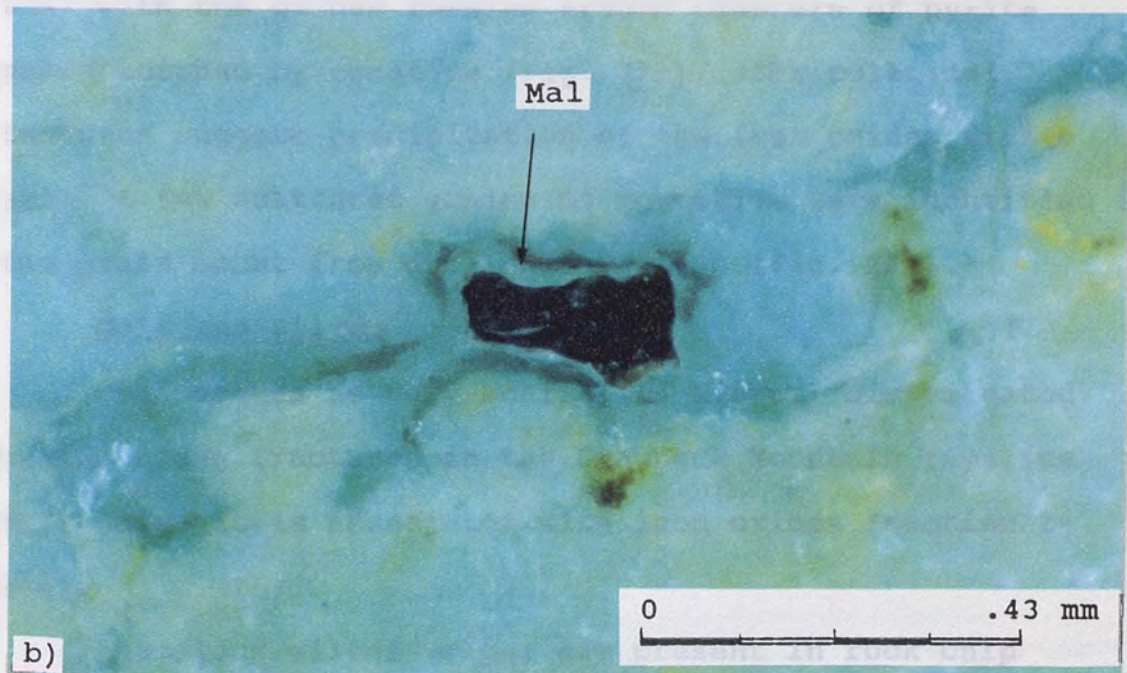


Figure 18. a) Triangular plucks in galena (section Cr-1-90). b) Azurite (crossed nicols) in sample from brecciated zone (section 775).

and along fractures. They clearly are supergene products of



malachite. These veins show excellent colloidal banding (Fig.



malachite, however no other malachite veins were observed in

Figure 19. a) Malachite infilling fracture (section 20158), b) same as 19a under crossed nicols.

and along fractures. They clearly are supergene products of the hypogene copper bearing sulfide phases. A black pitchy coating is commonly associated with the brecciated zones containing copper oxides. This coating is believed to be copper pitch ore, melanochalcite (Fig. 20a), which is described as a mixture of copper, manganese, iron hydrous oxides, and colloidal silica (Guild, 1929).

Iron Oxides

Both goethite and hematite are supergene alteration products after pyrite (Fig. 20b) and are common to all rocks of the area. Iron oxides in the late quartz monzonite dikes occur as gossanous accumulations along fractures with drusy quartz. These zones show excellent colloidal banding (Fig. 21a) with the oxides forming around clusters of pyrite pseudomorphed by hematite (Fig. 21b). The colloidal textures suggest precipitation of the iron oxides from a gel. A few scattered grains of magnetite were identified in the grain mount from drillhole Cr-1-90 (Fig. 22a).

Gold and Silver

Gold occurs as very small (1-5 micron) disseminated grains along fractures in the Grayback Mountain rhyolite tuff where it is associated with iron oxides (section 1-244).

Anomalous silver values are present in rock chip samples, however no silver bearing phases were observed in polished section. The silver telluride, hessite, associated

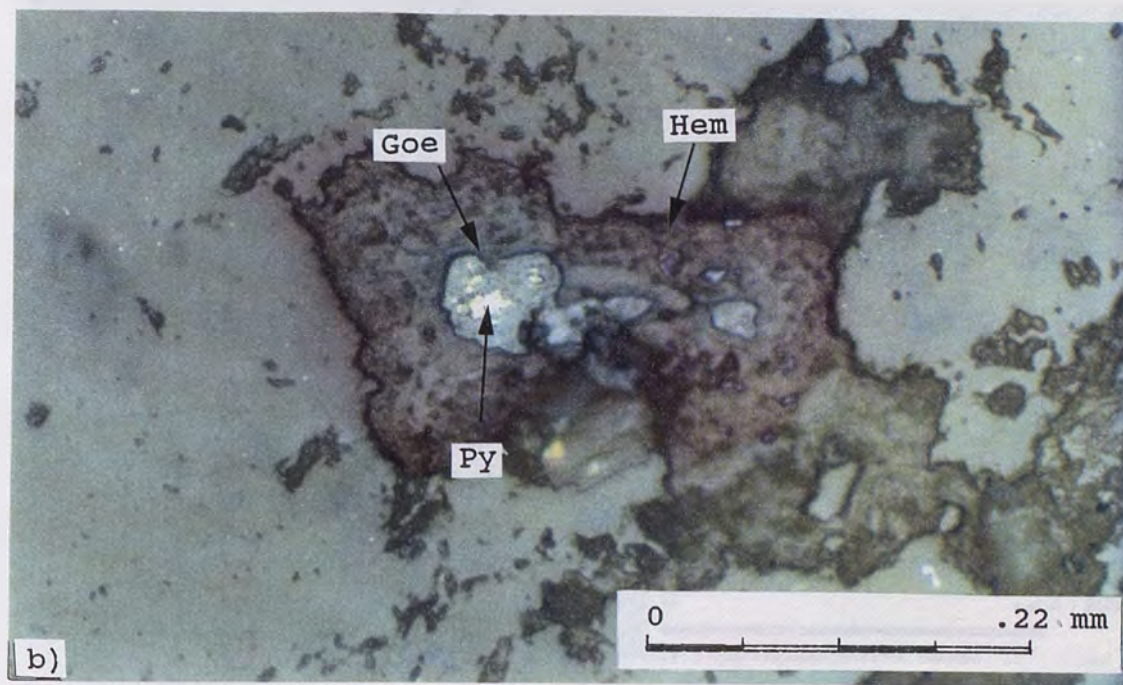
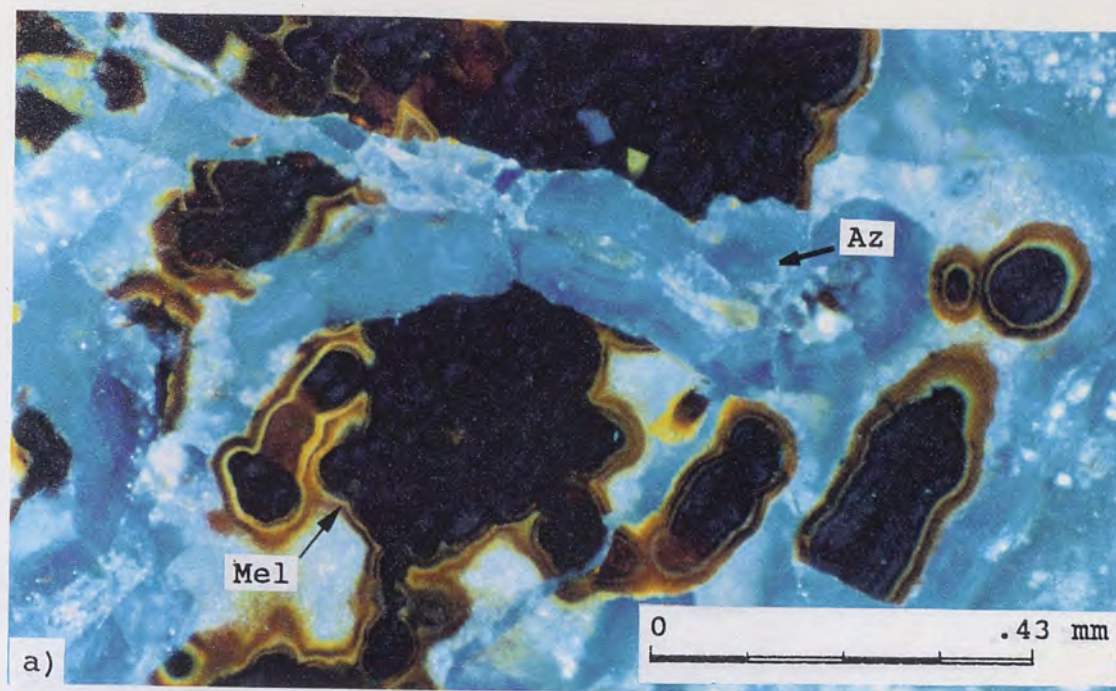


Figure 20. a) Copper pitch ore, melanochalcite, with azurite from brecciated zone (section 775). b) Goethite and hematite after pyrite (section A-4).

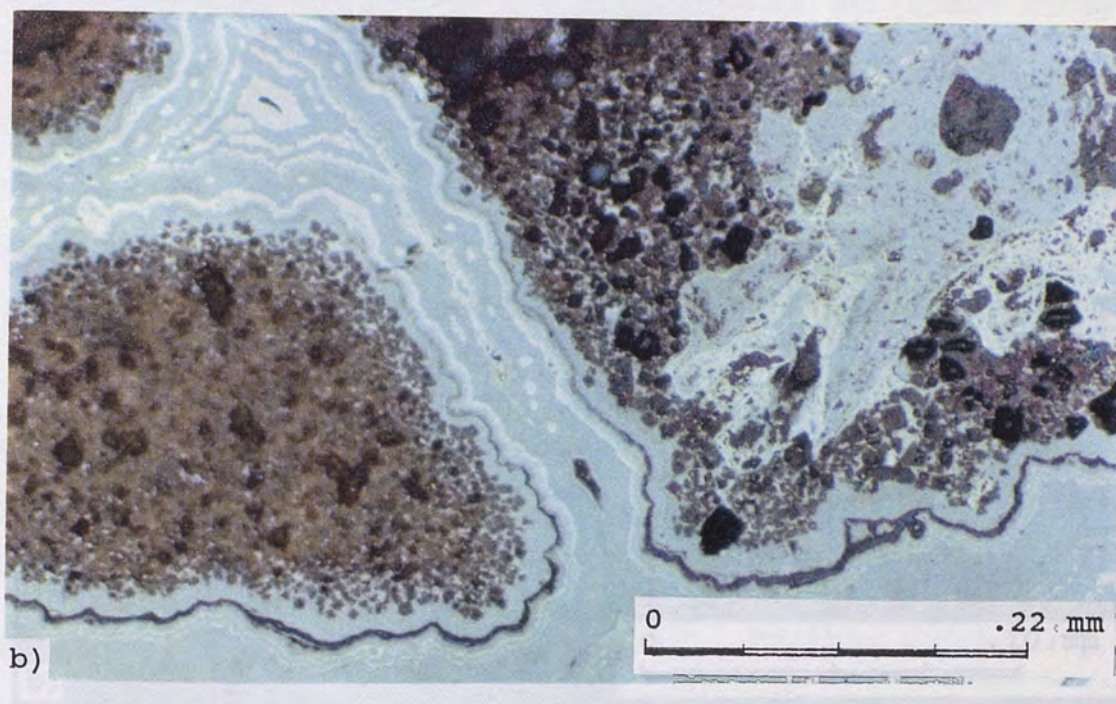
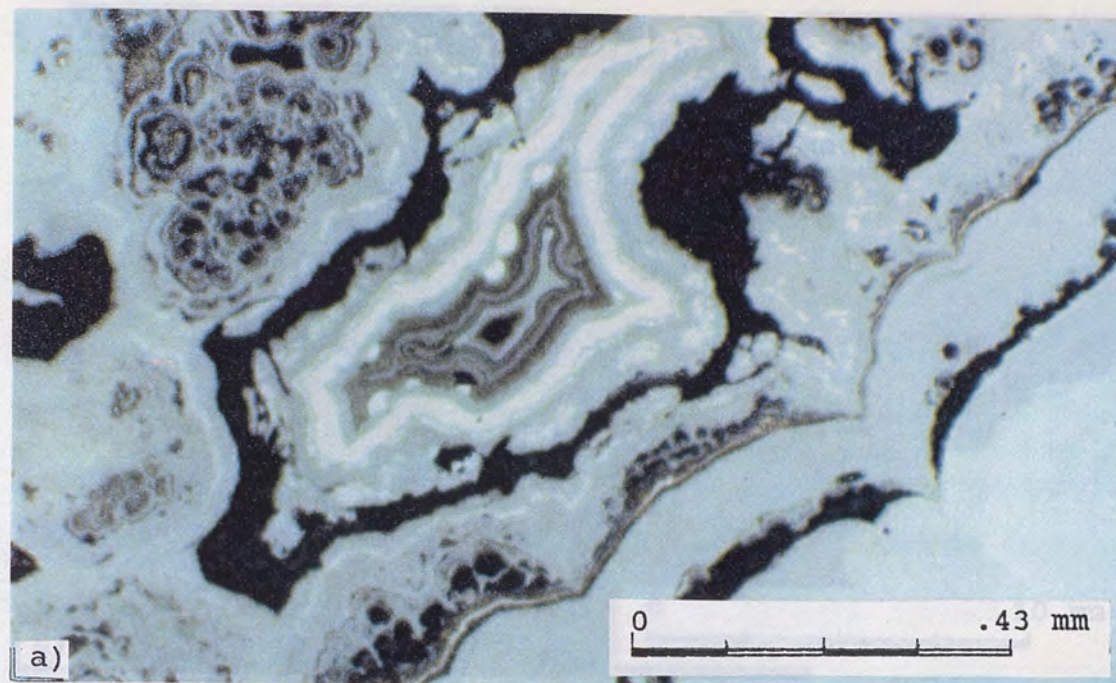


Figure 21. a) Colloidal banding of iron oxides (section 20160). b) Pseudomorphs of hematite after pyrite with colloidal banding of iron oxides around pseudomorphed aggregates (section 20160a).

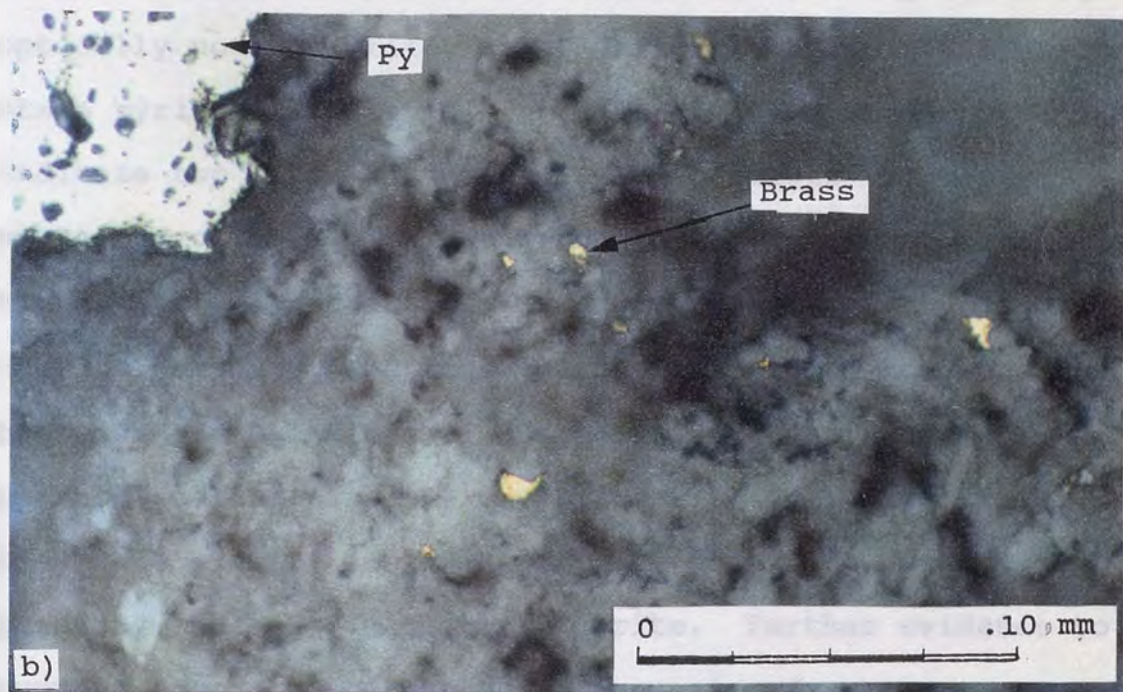
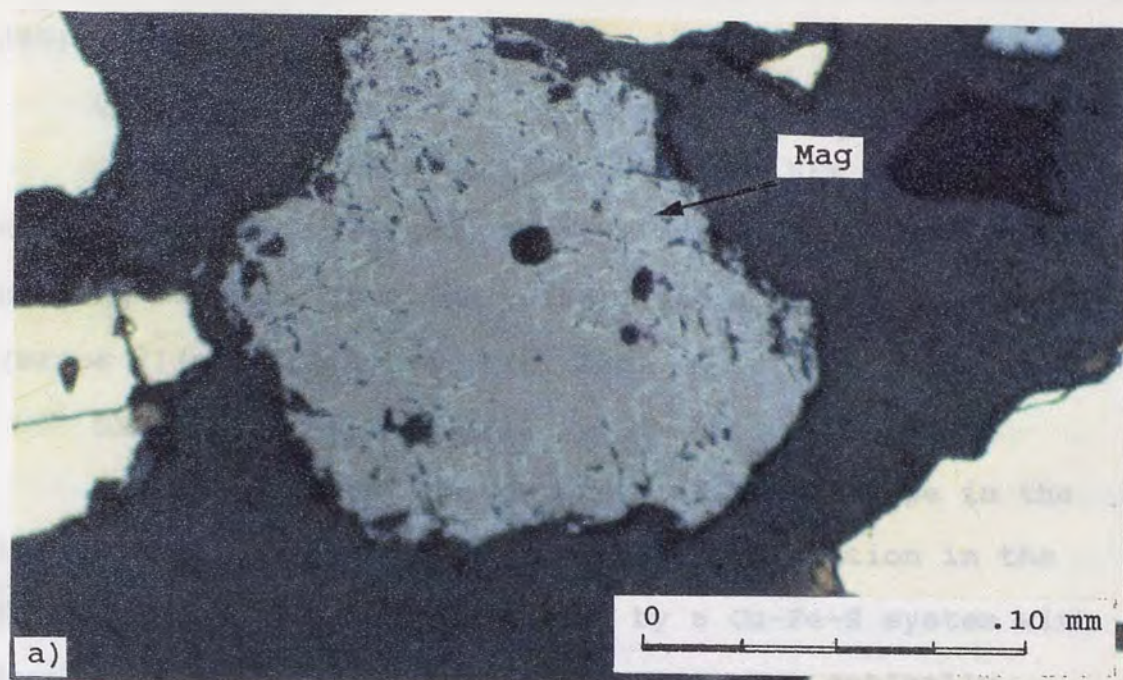


Figure 22. a) Magnetite grain from section Cr-1-90.
 b) Disseminated Cu-Zn compound (brass ?) with iron oxides
 and pyrite (section 1-244).

with chalcopyrite, was identified using the SEM (section Cr-286).

Other Minerals

Other minerals identified using the SEM include: the thorium-uranium silicate, thorite (section Cr-286), Cerium bearing monazite (section 20160), and a copper-zinc compound (brass ?) (section 1-244, Fig. 22b).

Summary and Paragenesis

The mineralization common to each rock type in the thesis area is shown in table 1. Mineralization in the Grayback Mountains was dominated by a Cu-Fe-S system with pyrite as the dominant sulfide phase. Two optically distinctive pyrite phases are observed: 1) early-mid stage optically normal pyrite, and 2) slightly anisotropic, late stage pyrite. The two distinctive pyrite phases may indicate two different mineralization stages: 1) early-stage: associated with the granodiorite to quartz monzonite stocks and; 2) late-stage: associated with the rhyolite, diorite porphyry, and late quartz monzonite dikes. The presence of inclusions of chalcopyrite, sphalerite, pyrrhotite, and possibly covellite (?), in pyrite indicates they were present early in the mineralization history, probably contemporaneous with pyrite. Further evidence to support the contemporaneous paragenesis of pyrite, chalcopyrite, and sphalerite is the presence of disseminated chalcopyrite and sphalerite, "chalcopyrite disease" in

sphalerite (Fig. 13a, 13b), and fracture fillings of sphalerite and chalcopyrite with pyrite (Fig. 14b). Covellite as inclusions (?) in association with chalcopyrite and sphalerite (Fig. 12a) suggests that it may have been early, as well as late, in the paragenetic sequence. Bornite is associated with, and appears to be replacing chalcopyrite. Bornite, in turn, may be replaced by covellite. Bornite is therefore placed later than chalcopyrite and prior to late stage(?) supergene covellite

Key:

X = Present - = Not identified
 ? = Not positively identified

Rock Types

Kgbrt = Grayback Rhyolite Tuff
 Kgds = Granodiorite Stock
 Kqmp = Quartz Monzonite Porphyry
 Trd = Rhyolite Dike
 Tdpd = Diorite Porphyry
 Trt = Copper Ridge Tuff
 Tlqmd = Late Quartz Monzonite Dike

Common Occurrence

D = Disseminations
 F = Fracture filling
 V = Veins or veinlets

Minerals

Py = Pyrite Mo = Molybdenite
 Cpy = Chalcopyrite Sph = Sphalerite
 Po = Pyrrhotite Gal = Galena
 Cc = Chalcocite/Digenite IO = Iron Oxides
 Bn = Bornite CO = Copper Oxides
 Cv = Covellite Au = Gold
 Ag = Hessite

Rock type	Common Occurrence	Py	Cpy	Po	Cc	Bn	Cv	Mo	Sph	Gal	IO	CO	Au	Ag
Kgbrt	D/F	X	X	X	X	X	X	X	X	-	X	X	X	X
Kgds	D/F	X	X	X	-	-	X	-	X	X	X	-	-	-
Kqmp	D/F/V	X	X	-	-	-	-	X	-	-	X	X	?	-
Trd	D/F	X	X	X	-	-	X	-	X	X	X	X	X	-
Tdpd	D/F	X	X	X	-	-	-	-	-	-	X	X	-	-
Tcrt	D	X	-	-	-	-	-	-	-	-	-	-	-	-
Tlqmd	F/V	X	-	-	-	-	-	-	-	-	X	-	?	-

Table 1. Rock type mineralization summary.

in the paragenetic sequence. Galena was observed in the grain mount from a drillhole Cr-1-90 and, for lack of more conclusive evidence, was placed in the middle of the paragenetic sequence. Paragenetic evidence for the deposition of molybdenite was also limited, however, rock chip sampling shows a close geochemical correlation of molybdenum with copper. Molybdenite is therefore placed near, but slightly later than, chalcopyrite in the paragenetic sequence.

Supergene mineralization in the area is characterized by copper oxides and sulfides, and iron oxides. Azurite, malachite, chrysocolla, and melanochalcite occur along fractures primarily within the shear zone. A supergene origin for covellite and chalcocite/digenite is supported by the replacement of chalcopyrite by both phases (Fig. 15a and 16b), the rimming of pyrite by chalcocite/digenite (Fig. 16b), and replacement of covellite by chalcocite/digenite. Oxidation of pyrite is characterized by goethite and hematite. Both iron oxides occur as rims on pyrite (Fig. 20b), complete replacement after pyrite (Fig. 21b), or in fractures as colloidal bands around completely replaced pyrite (Fig. 21a). Magnetites' relationship to overall mineralization is unclear.

Gold was identified (SEM determination) in at least one polished section (section 1-244) where it occurs as fine (1-5 micron) disseminated grains in association with iron

oxides. Both gold and the slightly anisotropic variety of pyrite appear to be intimately associated with the rhyolite, diorite porphyry, and late quartz monzonite dikes. For this reason both minerals are inferred to be relatively late in the overall paragenetic sequence.

The silver telluride, hessite, was found in association with chalcopyrite (section Cr-286) and is tentatively placed late in the paragenetic sequence with the late stage chalcopyrite.

The postulated paragenetic sequence for mineralization in the Grayback Mountains is shown in table 2. The opaque mineralogy for the forty polished sections studied can be found in Appendix 1.

Table 2. Paragenetic sequence for mineralization in the Grayback Mountain thesis area, based on forty polished cross-section rock types.

Mineral Paragenesis

Key: Early Stage = Post Grayback Mountain rhyolite tuff: associated with the Granodiorite-Quartz Monzonite intrusives

----- Possible Hiatus -----

Late Stage = Rhyolite to late quartz monzonite dikes

Oxidation = Post QM dikes to present

	Early Stage	Possible Hiatus ↓	Late Stage	Supergene and Oxidation
Pyrite	-----		-----	
Chalcopyrite	-----		-----	
Pyrrhotite	-----		-----	
Chal./Dig.				-----
Bornite		?---	---	
Covellite	?		-----	
Molybdenite	-----		-----	
Sphalerite	-----		-----	
Galena		?---	---	
Copper Oxides				-----
Iron Oxides				-----
Gold		---?---		
Silver		---?---		

Table 2. Paragenetic sequence for mineralization in the Grayback Mountain thesis area, based on forty samples from seven rock types.

Structure and Genesis of the Grayback Mountain Rhyolite Tuff

A major northeast-trending shear zone, paralleling the northeast Precambrian trend, extends through the Grayback Mountain thesis area (Fig. 6), and continues through the Bagdad porphyry deposit (Fig. 4). This northeast trending shear zone not only provided a zone of weakness which aided the venting of the Grayback Mountain rhyolite tuff but continued to be a zone of weakness for the intrusion of the later stocks and dikes (Fig. 5, 6, and Plate 1). Evidence to support a northeast trending shear zone includes: 1) air photo lineaments; 2) geophysical data; 3) northeast trending breccia, gouge, and silicified zones; 4) elongation of the intrusive stocks, including the Bagdad stock (oral comm. J. Hawley, Cyprus Bagdad, 1991), in a northeasterly direction; 5) northeast trending rhyolite, diorite porphyry, and quartz monzonite dikes, which intrude and in-fill the shear zone (Fig. 4); 5) elongation of the alteration halo (Fig. 10) and the Cu/Mo mineralization trends in the thesis area (Figs. 27 and 28); and 6) data reported by Anderson et al. (1956).

Very little direct evidence for faulting within the Grayback Mountain rhyolite tuff was found during mapping. Linear silicified and brecciated zones were mapped as possible faults. Marginal fault structures are inferred where rhyolite dikes parallel the Grayback Mountain-Precambrian contact, and late quartz monzonite and rhyolite dikes parallel the Copper Ridge tuff-Grayback Mountain tuff

contact. A large east-west trending structure occurs along the southern margin and dips 60-75° to the north (Fig. 6 and Plate 1) bringing Grayback Mountain rhyolite tuff in contact with both Precambrian Lawler Peak granite and alaskite porphyry. It is unclear whether this structure represents a bounding fault or a vent margin structure. If the structure represents a bounding fault then the concurrence of fault and pumice compaction foliation orientation, and the lack of gouge or brecciation in the Grayback Mountain rhyolite tuff support movement along the structure prior to complete cooling of the tuff. However, along this structure the Precambrian country rock is highly brecciated, the Grayback Mountain rhyolite tuff compaction foliation dips steeply to the north (+70°) with strong lineation of pumice in the plane of foliation, and the structure disappears under the Grayback Mountain rhyolite tuff outcrop on the eastern end; these features favor the structure as a vent margin.

Multiple working hypotheses for the origin of the Grayback Mountain rhyolite tuff that were reviewed include: 1) a flat lying or tilted remnant ash-flow sheet that filled a paleovalley, 2) a tufaceous vent eruption, and 3) a caldera.

A valley-fill hypothesis appears unlikely when one compares features seen in the Grayback Mountain rhyolite tuff to a known valley-fill ash-flow tuff sequence. A valley-fill ashflow tuff which shows both primary and

secondary flow structures is the Wall Mountain tuff which was deposited in the Gribbles Run paleovalley, central Colorado. Pumice compaction foliation in the Wall Mountain tuff is commonly steep with many exceeding 40° . Geologic evidence indicates that tectonic tilting could not be responsible for most of the steeper dips. Chapin and Lowell (1979) found that static postemplacement (secondary) compaction could not produce foliation dipping steeper than the valley walls, and steeper than 22° along cliffy areas (Fig. 23a/b). Near vertical dips were observed in the Wall Mountain tuff, however, pumice compaction foliation dip decreases as you move down into the paleovalley; yielding a nearly U-shaped cross-sectional profile (Fig. 23c). Postemplacement compaction, as seen above (Fig. 23a/b), could not yield such steep dips, so it is believed that the steeply dipping foliation is due to primary compaction. Deposition of the Wall Mountain tuff occurred more rapidly along the sides of the Gribbles Run paleovalley than along its axis. The difference in deposition rates caused inward accretion of welded tuff with steep primary flow foliation, forming a U-shaped channel profile (Chapin et al., 1979).

The pumice compaction foliation in the Grayback Mountain rhyolite tuff, though steep in many localities, does not coincide with that observed in the Wall Mountain tuff. In general, pumice compaction foliations on the outer margins of the outcrop dip very shallow ($0-20^\circ$) both toward

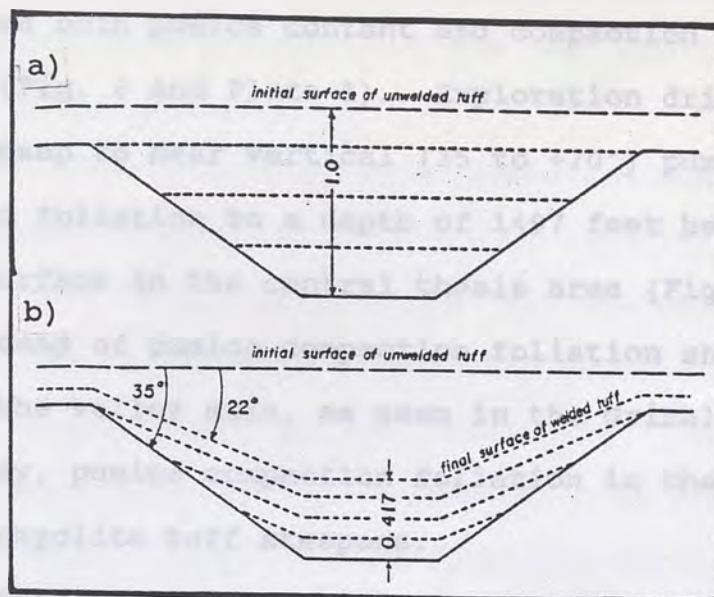


Figure 23. a and b) Graphic derivation of the maximum compaction dip that can be formed by static, postemplacement compaction. a) Valley at the moment of ashflow emplacement filled overfull with uncompacted ash of specific gravity 1.0. Maximum thickness of tuff equals 1.0 unit. b) Valley after compaction and dense welding to a final specific gravity of 2.4. Maximum thickness of compacted tuff equals 0.417 unit. The valley walls slope at the angle of repose (35°), and dense welding is achieved throughout the tuff. A linear relationship between specific gravity of the tuff and its compacted thickness is assumed. Under these conditions the maximum compaction dip is approximately 22° (Chapin and Lowell, 1979).

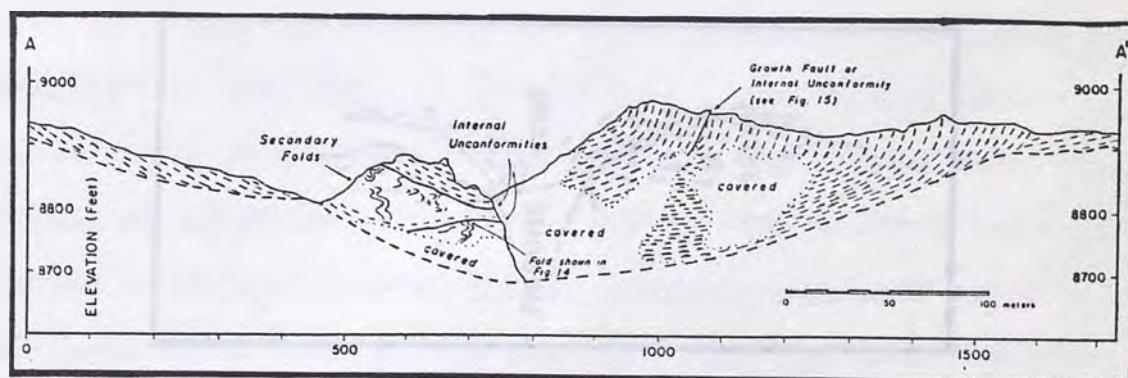


Figure 23c. Cross section through the Gribbles Run paleovalley. Dashed lines show the attitude of the pumice compaction foliation (Chapin and Lowell, 1979).

and away from the valley center. Toward the center of the thesis area both pumice content and compaction foliation dip increase (Fig. 6 and Plate 1). Exploration drillcore reveals steep to near vertical (35 to +70°) pumice compaction foliation to a depth of 1497 feet below the present surface in the central thesis area (Fig. 36, 37, and 38). Instead of pumice compaction foliation shallowing as you near the valley axis, as seen in the Gribbles Run paleovalley, pumice compaction foliation in the Grayback Mountain rhyolite tuff steepens.

A tufaceous vent eruption constitutes a second working hypothesis for the origin of the Grayback Mountain rhyolite tuff. Features seen in the Grayback Mountains were compared to a few known tufaceous vent occurrences. Work done by Fridrich et al. (1991) in the Grizzley Peak caldera, Sawatch Range, Colorado, provides a cross-section through a tufaceous vent within the caldera (Fig. 24). Important to

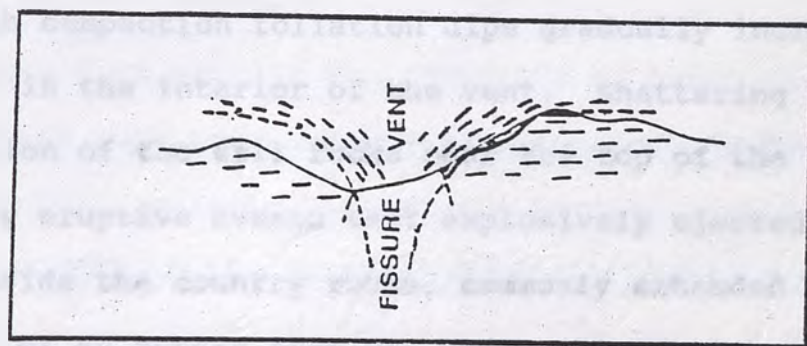


Figure 24. Cross-section through the tufaceous vent within the Grizzley Peak Caldera, Sawatch Range, Colo. Dashes indicate the attitude of compaction foliation in the tuff (Fridrich et al., 1991).

note is that the dip of pumice compaction foliation in the tuff increases with proximity to the vent and is near vertical in the vent proper.

The near vertical compaction foliation seen in the Grayback Mountain rhyolite tuff can be explained by one of two mechanisms. One, the erupting tuff agglutinated against the side walls of the vent forming the vertical compaction as accretion progressed or; two, horizontal and shear stresses were applied prior to cooling, with the horizontal stress and shear resulting from displacement along the crude ring fracture system during collapse events. The near vertical compaction foliation observed in diamond drillcore from the inner canyon areas is believed to have formed by agglutination of the tuff along vent sidewalls as accretion progressed (mechanism one).

Ekren and Beyers (1976) described an ash-flow fissure vent in west-central Nevada. Compaction foliation in the upper vent area dipped gently (less than 30°) toward the vent with compaction foliation dips gradually increasing to over 70° in the interior of the vent. Shattering and brecciation of the wall rocks near the top of the vent, caused by eruptive events that explosively ejected and shoved aside the country rocks, commonly extended for a distance of 90 meters from the vent wall (Ekren and Beyers, 1976). Figure 25 is a sketched cross section through the west-central Nevada fissure vent.

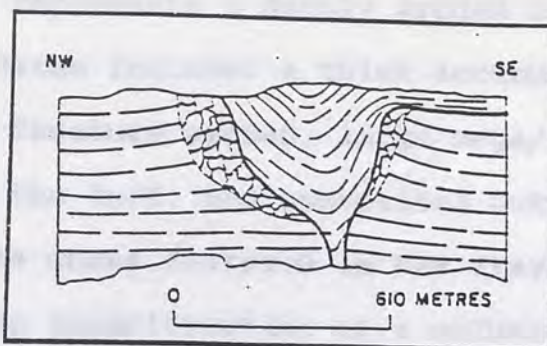


Figure 25. Cross section through the west-central Nevada fissure vent showing the relationships between fissure and wall rock, and showing the general attitude of foliation within fissure and adjacent wall rock. Shattered wall rock shown in broken pattern (Ekren and Beyers, 1976).

The pumice compaction foliation reported at both the tuffaceous vent within the Grizzley Peak caldera (Fridrich et al., 1991) and the west-central Nevada fissure vent (Ekren and Beyers, 1976) is nearly identical to that seen in the Grayback Mountain rhyolite tuff. Also, the wall rock shattering and brecciation seen near the top and extending outward (up to 90 meters) from the vent in west-central Nevada may help explain the abundance of brecciated Precambrian rock near the Precambrian-Grayback Mountain rhyolite tuff contact. Hence, the pumice compaction foliation seen in the Grayback Mountain rhyolite tuff along with the brecciation of the Precambrian rocks along the contact with the tuff suggests that a tuffaceous vent within the Grayback Mountains played a part in the generation and

accumulation of the Grayback Mountain rhyolite tuff.

The third working hypothesis is that the Grayback Mountain area represents a deeply eroded caldera. Features common to calderas include: a thick accumulation of tuff, a bounding ring fracture system, large mega/collapse breccia blocks within the tuff, and associated outflow sheets. The presence of the above features in the Grayback Mountains would be key to identification of a caldera within the area.

A thick (+1500 feet) pile of rhyolite tuff with near vertical pumice compaction foliation was intersected in two exploration drillholes in the inner canyon area (Fig. 36, 37, and 38).

Possible fault relationships at the Precambrian-Grayback Mountain rhyolite tuff contact (southern and northwestern flank) favor subsidence concurrent with vent activity. Near vertical compaction foliation (70-85°), lineation of pumice in the plane of foliation, lack of fault gouge, and concurrence of fault and pumice compaction foliation dip could be interpreted as having formed by horizontal and shear stress applied prior to cooling of the tuff, associated with collapse along the crude ring fracture system (mechanism two from above). Flow banded rhyolite dikes in-filling along the Precambrian-Grayback Mountain rhyolite tuff contact are interpreted as in-filling along part of the fracture system.

Medium to large (15 to 400 feet) mega-breccia/collapse

breccia or lithic blocks are present in the Grayback Mountain rhyolite tuff. Medium size lithics (5 to 15 feet in diameter) include: Precambrian diabase and Lawler Peak granite. Two outcrops of Precambrian rock, which may represent lithic/ mega-breccia blocks, are near the main access road going into the inner canyon area (see Plate 1). The largest block (approx. 400 by 300 feet) is Precambrian schist with the smaller block (approx. 150 by 200 feet) composed of Precambrian alaskite porphyry breccia. It is unclear whether the three outcrops of Alaskite porphyry in the northeastern thesis area represent erosional windows of Alaskite porphyry breccia-vent margin breccia showing through the Grayback Mountain rhyolite tuff or lithic/mega-breccia blocks within the tuff, however, based on their topographic position and close proximity to the rhyolite contact the first option seems more likely.

No extensive outflow sheets associated with the eruption of the Grayback Mountain rhyolite tuff were found in mapping. Several topographic highs to the south-southwest of the main rhyolite outcrop (Fig. 5 and Plate 1) are capped by Grayback Mountain rhyolite tuff, however, the lack of clear contact relationships in these areas leaves some question as to whether they truly represent outflow sheet fragments. If the outcrops represent remnant outflow sheets they would add evidence to support asymmetrical subsidence and outflow to the southwest of the Grayback

Mountains.

Features favoring the presence of a caldera include: large collapse breccia/megabreccia blocks found within the tuff, possible structural (fault) relationships and dike infilling observed at the Grayback Mountain rhyolite tuff-Precambrian contact, a considerable (+1500 feet) thickness of tuff, late stage intrusive activity, and possible late stage extrusive activity along the structural margin ("venting" of the Copper Ridge tuff).

Evidence negating the presence of a caldera are: 1) the overall size and extent of outcrop (being unusually small for a caldera); 2) no apparent shallowing of pumice compaction with depth; 3) the fact that the tufaceous vent hypothesis could explain a +1500 feet thickness of tuff, with near vertical compaction foliation; 4) the possibility that the Precambrian lithics were emplaced by the tufaceous vent eruption; and 5) the lack of large outflow sheets commonly associated with caldera forming eruption.

The above comparisons, along with the information provided by geologic mapping and exploration drilling, suggest that the most reasonable alternative for the genesis of the Grayback Mountain rhyolite tuff, is a localized tufaceous vent eruption. Collapse or sagging, due to the evacuation of the magma chamber at depth, was likely asymmetrical with respect to the total outcrop and occurred along the southwestern vent margin with possible outflow to

the southwest. The lack of voluminous outflow sheets suggests that the eruption was fairly small scale, though the outflow sheets could have been complete removed by weathering and erosion.

Exploration up until the mid-1970's focused on base metal targets similar to the typical porphyry deposits that might be present in the intrusive rocks of the Coast Range Mountains. Previous work included: the Geological Survey maps (1959; Phelps Dodge, 1970; Cyprus Mines); several maps of copper and molybdenum in rock chip samples, drillhole logs and assays for west of the post-1970 drillhole, T.P./Geological survey data specific to the Copper Ridge claim, and detailed exploration reports (Cyprus Mines reports and maps, 1970-1974).

From the mid-1970's to the present, exploration has focused on precious metal targets in both the intrusive and extrusive units of the Coast Range Mountains. While most available data in the early-1970's were not available for many but precious metal assays were available from some of the post-1970's exploration drilling (composite assays). Drilling, primarily done for yearly assessment work, yielded limited intervals of anomalous gold mineralization (two, one hundred foot intervals of 0.011 gpt. Au in drillhole Cr-2-66, see Fig. 74).

Exploration Program and Data

An exploration program designed to fit the thesis

Mineral Exploration

Previous Exploration

Mineral exploration began with an in-depth look at previous exploration programs and their results.

Exploration up until the mid-1970's focused on base metal targets similar to the Bagdad porphyry deposit that might be present in the intrusive rocks of the Grayback Mountains.

Previous work included: two incomplete geologic maps (1969: Phelps Dodge, and 1976: Cyprus Bagdad), contour maps of copper and molybdenum in rock chip samples, drillhole logs and assays for most of the post-1971 drillholes, I.P./Resistivity survey data specific to the Copper Ridge claims, and interim exploration reports (Cyprus Bagdad reports and maps, 1972-1974).

From the mid-1970's to the present, exploration has focused on precious metal targets in both the intrusive and extrusive units of the Grayback Mountains. Pulps from sampling done in the early-1970's were not available for assay but precious metal assays were available from some of the post 1970's exploration drilling (composite assays). Drilling, primarily done for yearly assessment work, yielded limited intervals of anomalous gold mineralization (two, one hundred foot intervals of 0.013 opt. Au in drillhole Cr-2-86, see Fig. 38).

Exploration Program and Data

An exploration program designed to fit the thesis

budget and time-frame, was aimed primarily at the delineation of areas with anomalous precious metal values. The exploration program is outlined in table 3.

(Appendix 7, Table A). The ICP package was changed for

- Phase 1. Evaluation of previous exploration data.
- Phase 2. Drainage sampling to delineate areas of anomalous precious metal mineralization.
- Phase 3. Follow-up drainage sampling of anomalous areas from Phase 2.
- Phase 4. Rock chip sampling of prominent alteration and possible mineralizing structures.
- Phase 5. Delineation of a drill target based upon the data gathered in the previous phases.

elements, the range and width of the assay for all the samples. Table 3. Grayback Mountain thesis area exploration program outline.

Drainages exiting major canyons, in the highly altered inner canyon area, were sampled and sieved (nylon sieves) to -80 mesh in the field (Appendix 2, Fig.39). Nine samples were assayed for gold using standard fire assay techniques (Appendix 2, Table 7). A 15 element ICP assay package was added to supplement the fire assay analysis.

Stream sediments from several drainages had gold values of 6 to 18 ppb, with one assaying 49 ppb Au.

Phase three exploration began with the resampling of the drainage which assayed 49 ppb Au. The original sampling site was resampled with three additional samples taken upstream.

Rocks were sampled (phase 4) concurrent with geologic mapping. Areas anomalous for gold, in drainage samples,

were sampled more heavily to try and locate the source area (Appendix 2, Fig. 40). Rock chip samples were assayed for gold using the same techniques as the drainage samples (Appendix 2, Table 8). The ICP package was changed for financial and logistical reasons with the last 25 samples run for 30 elements (thirteen of which were common to the previous package). Figure 26 displays the elements common to both rock chip sampling packages (excluding those at or below detection limits). The data includes: selected elements, the range and arithmetic mean for all the samples, and the arithmetic mean for each rock type sampled. The complete geochemical assay data can be found in Appendix 2.

Previous, (Cyprus Bagdad, 1972-1974) copper and molybdenum rock chip data pertaining to the area was added to the current geochemical contour diagrams. The compiled contour maps of copper and molybdenum in rock chips are shown in figures 27 and 28. Gold in rock chip samples was not contoured due to the limited number of samples taken. The uncounted data for gold in rock chip samples (fire assay) is shown in figure 29.

Correspondence Analysis of Trace Element Geochemistry

Statistical analysis of rock chip sample data was accomplished using a form of multivariate analysis called correspondence analysis. The program used was CORMISS, written by Dr. James Carr, Mackay School of Mines, University of Nevada, Reno. Sample assay data for each

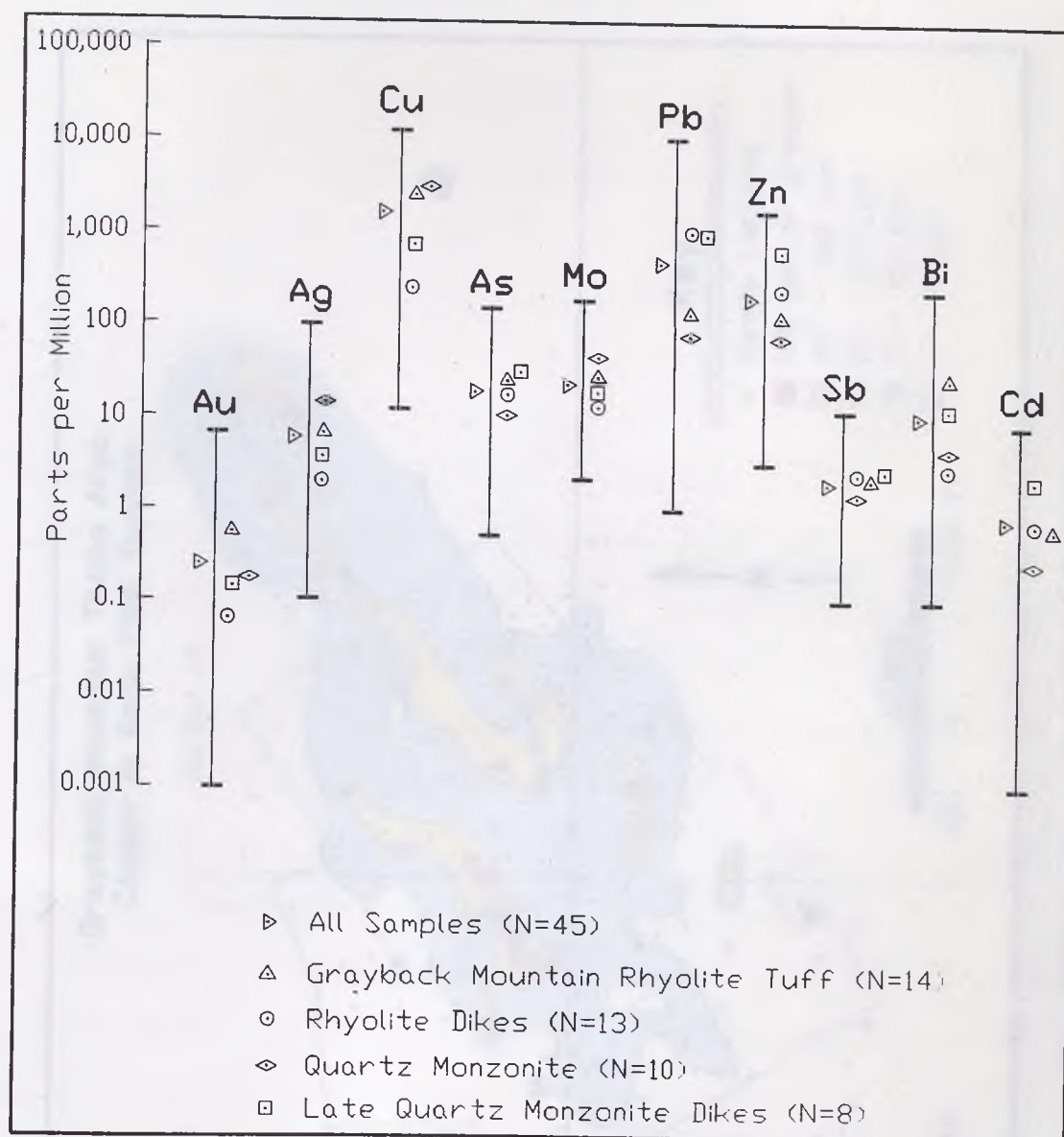


Figure 26. Selected elements from rock chip samples within the Grayback Mountain area as determined by ICP analysis (gold by fire assay). The plot includes: the range and arithmetic mean for all samples, and the arithmetic mean for each separate rock type.

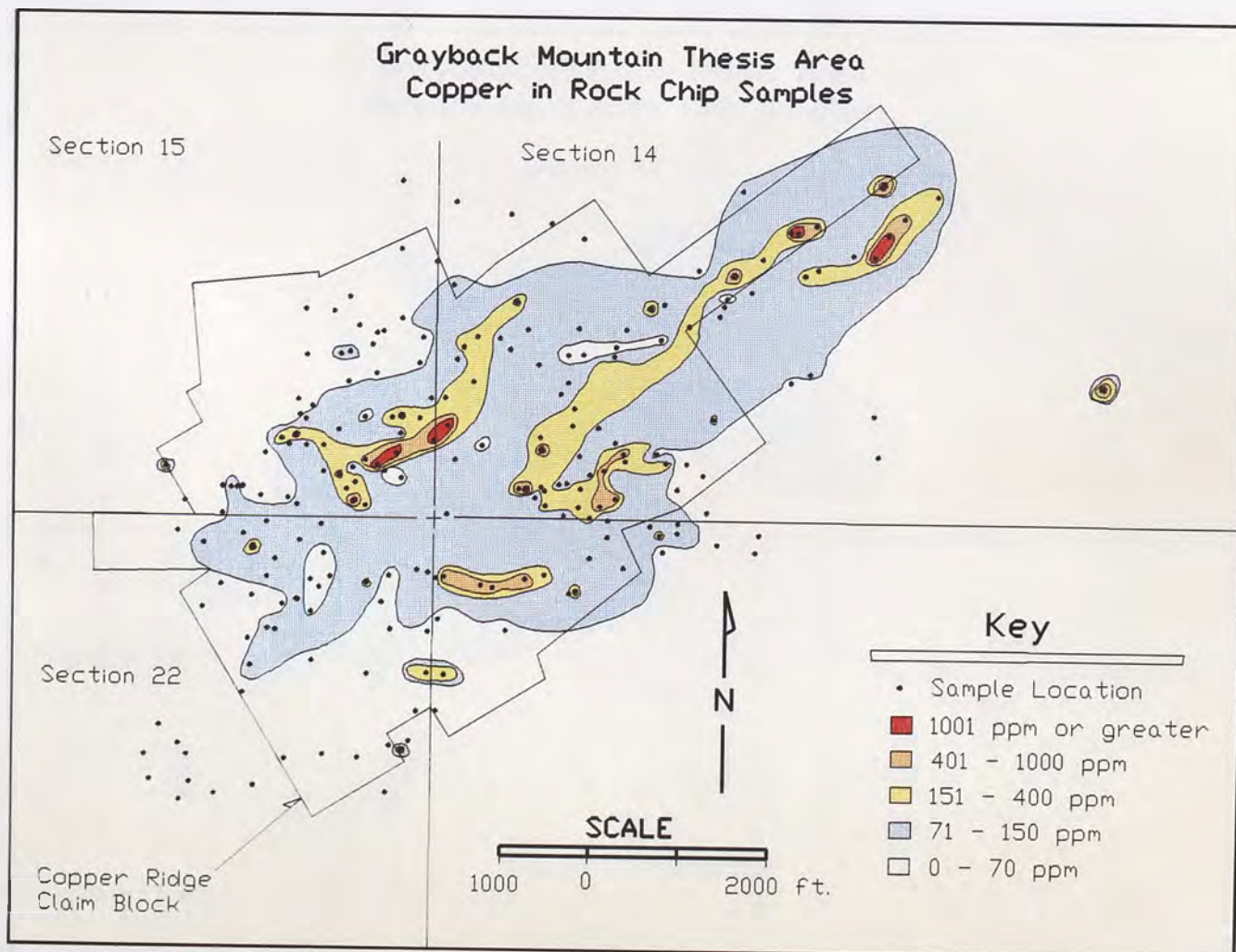


Figure 27. Geochemical contour map of copper in rock chip samples.

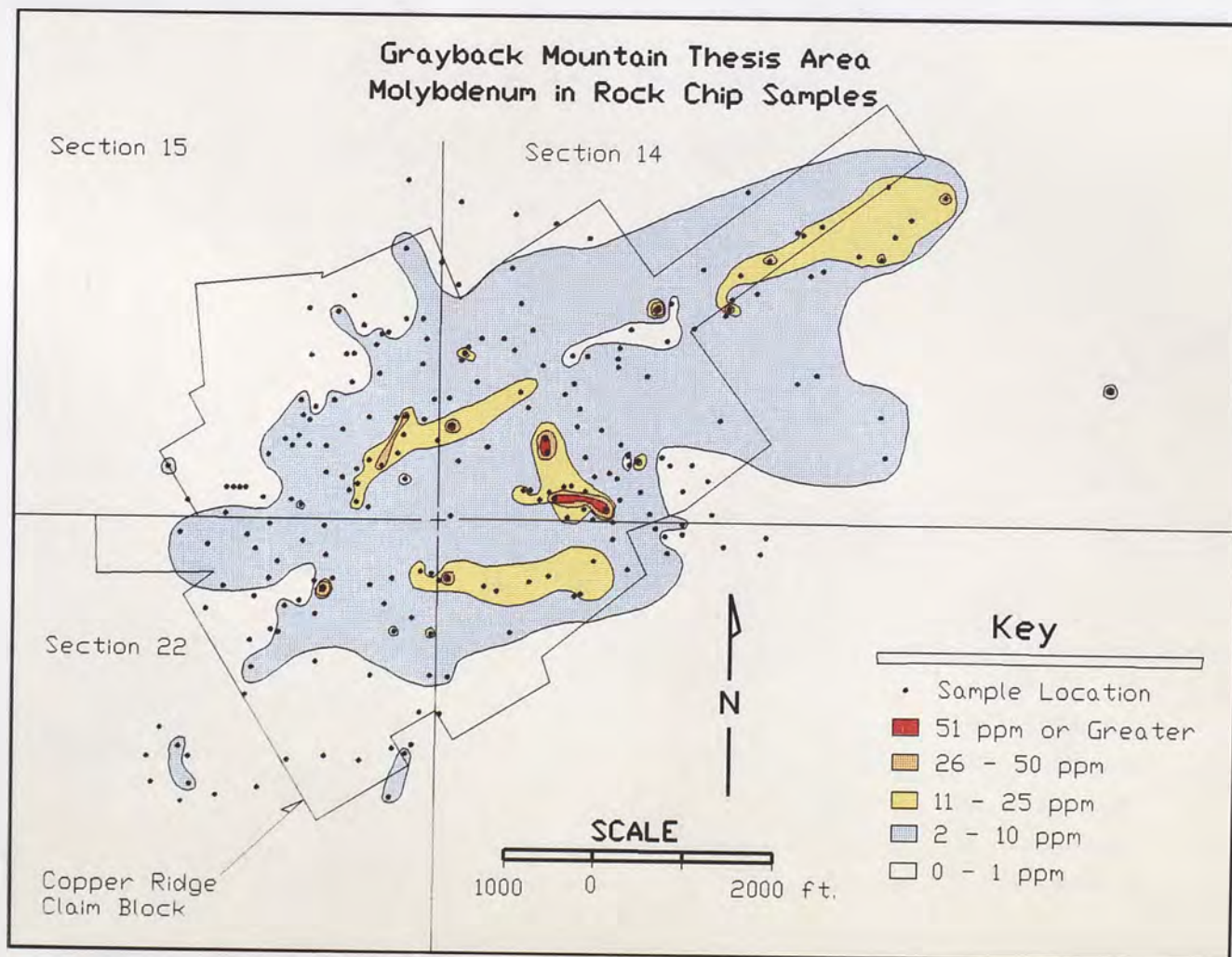


Figure 28. Geochemical contour map of molybdenum in rock chip samples.

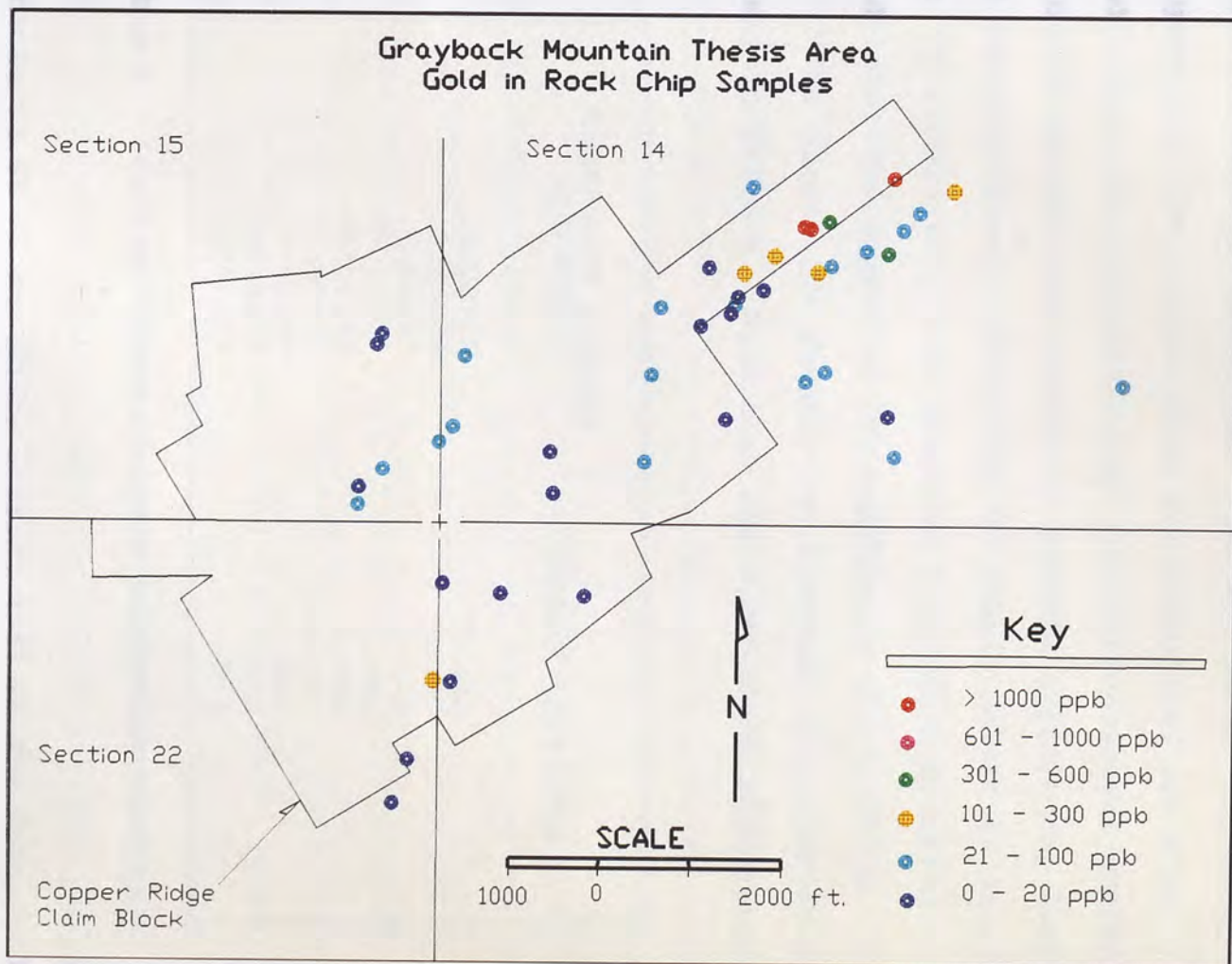


Figure 29. Geochemical map of gold in rock chip samples (uncontoured).

sample was input and saved as an ASCII file and then loaded into the CORMISS program. The data are displayed in rows and columns known as a contingency table. The resultant geometry, produced from the contingency table, relates columns (attributes) to rows (individual samples) and a correspondence is developed. Through matrix algebra, eigenvalues and eigenvectors are calculated for each individual and its attributes. The eigenvectors are then plotted against one another to produce a graphical display of correspondence. Proximity of sample points or attributes to one other along with consistent quadrant location indicates the degree of correspondence (Carr, 1990).

The eigenvalue summary for the rock chip samples is shown in Table 4. Note that the first three eigenvalues

EIGENVALUE SUMMARY	
EIGENVALUE	PERCENT VARIATION
.6662725	75.682
.0924569	10.502
.0484387	5.502
.0313556	3.562
.0254640	2.892
.0108056	1.227
.0049280	.560
.0005245	.060
.0001116	.013

Table 4. Correspondence analysis eigenvalue summary.

contain 91.6% of the data, leaving 8.4% of the data excluded

from the analysis. Correspondence analysis results are shown in figures 30-32. The graphical plots show the relationship of individuals (samples) to attributes (trace elements). All three plots were interpreted since each contained a significant percentage of eigenvalues. Associations were determined by proximity of attributes to one another and consistency of correspondence from one plot to another. Ten attributes were used in the correspondence analysis and include the elements: Au, Ag, As, Sb, Cu, Mo, Pb, Zn, Cd, Bi.

The elements Au, Cu, Mo, Ag, and Bi show a consistent correspondence in each of the graphical plots. Subdividing slightly further, the best correspondence relationships are seen between gold and copper, and silver and bismuth. Molybdenum appears to share correspondence with the Au-Cu association as well as the Ag-Bi association. Zinc in 75% of the samples corresponds with arsenic and cadmium, but this correspondence does not hold for the rest of the data. No good correspondence relationship was observed for lead.

The samples which assayed highest in gold (1-6 ppm Au) were taken along the northeastern end of the shear zone trend (Fig. 29) in or near small prospects with visible supergene copper oxide mineralization (ie. malachite, azurite, and chrysocolla). Samples with 100-600 ppb Au were taken in the same general area but lacked visible copper sulfides or oxides. This area contains an abundance of

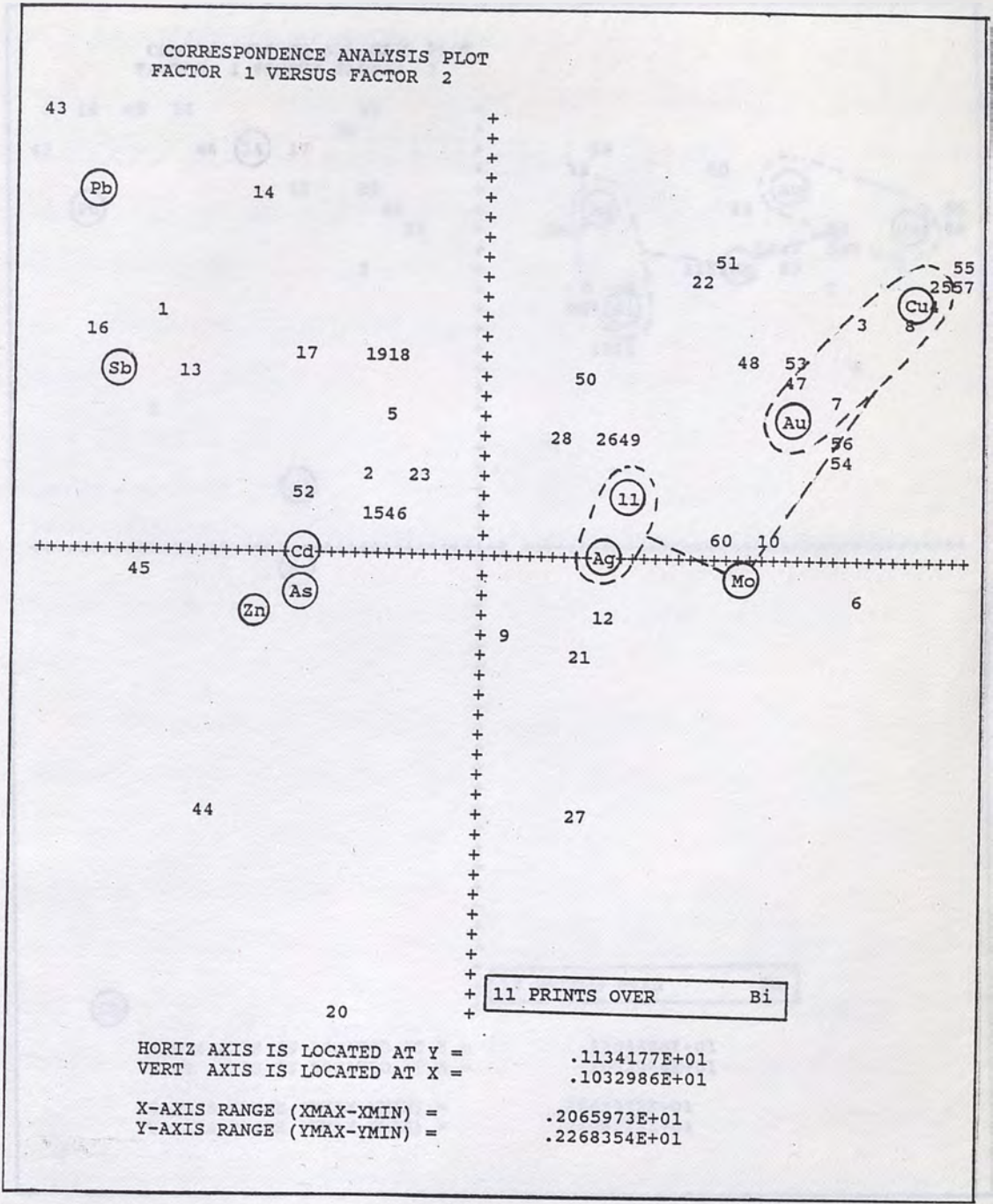


Figure 30. Correspondence analysis eigenvector plot, representing 75.6% of the data (factor 1 vs. factor 2).

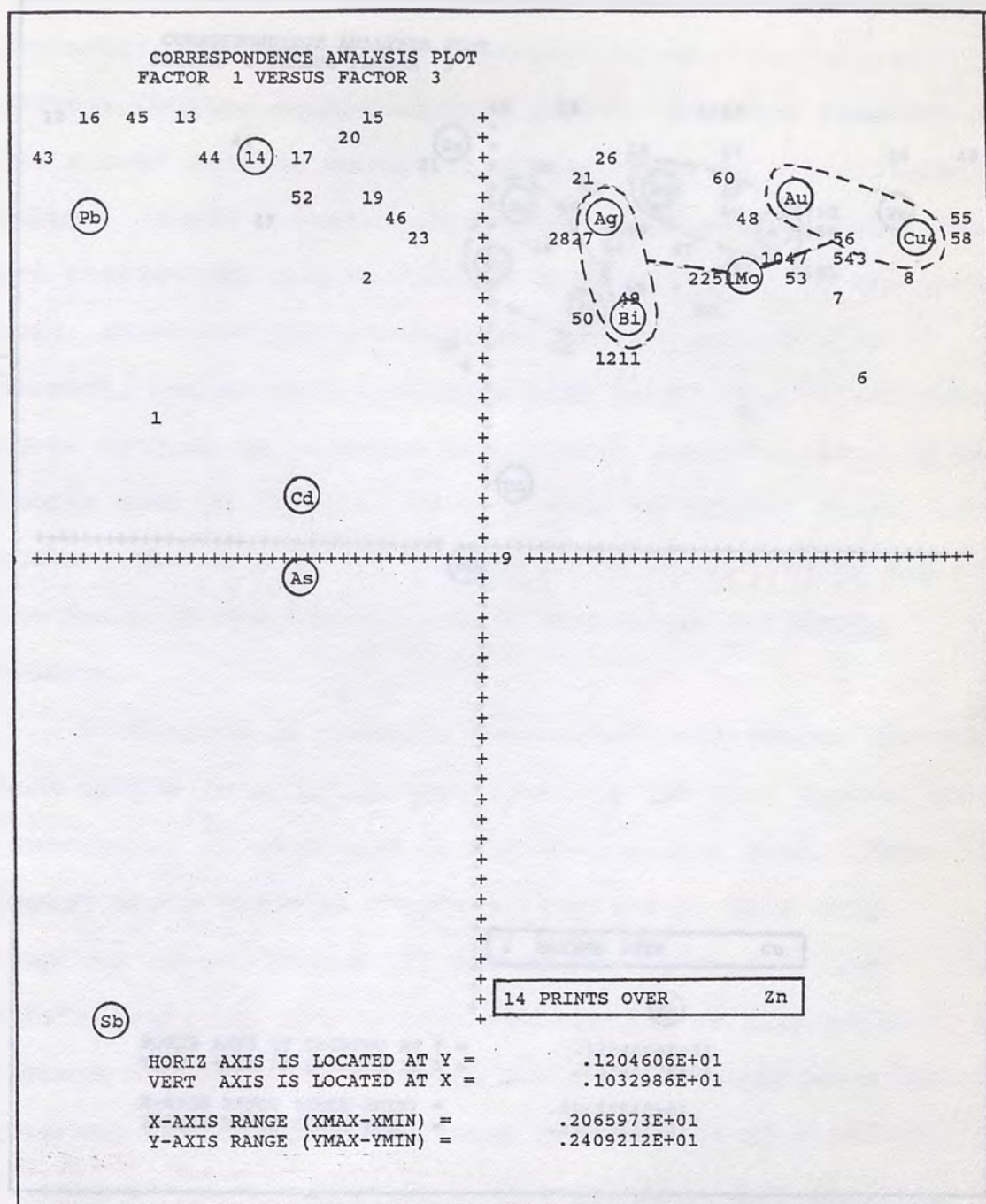


Figure 31. Correspondence analysis eigenvector plot, representing 10.5% of the data (factor 1 vs. factor 3).

rhyolite, diorite porphyry, and late quartz monzonite dikes which crosscut the Grayback Mountain rhyolite tuff.

The abundant lead/silver deposits of Central Yavapai County typically occur where fissure veins intersect Precambrian igneous and metamorphic rocks. Silver, in Yavapai County, occurs as free silver, but more commonly as the silver sulfide acanthite/argentite or in argentiferous galena. Known geologic occurrence therefore substantiates the statistical association Ag-Bi-Pb. Silver, in the thesis area, shows extremely consistent correspondence with bismuth, but no correspondence with lead. The relationship Ag-Bi without Pb suggests that silver mineralization in the thesis area is atypical to that seen in Yavapai County as a whole. The only silver bearing phase recognized by SEM in the rocks of the thesis area is the silver telluride, hessite.

Molybdenum is commonly associated with copper and other base metals in porphyry type settings and this typical Cu-Mo association is also seen in the thesis area data. Major copper and molybdenum trends delineated by rock chip sampling (Figs. 27 and 28) are nearly coincident and substantiate the statistical association as determined through correspondence analysis. The correspondence between gold and molybdenum is somewhat unusual and at first was thought to be coincidental. However, rock chip sampling data shows the higher gold coincident with higher

molybdenum, substantiating the statistical Au-Mo association.

A summary of the best pathfinders for precious metal/base metal mineralization, as indicated by correspondence analysis performed on rock chip sample analyses, are shown in Table 5.

<u>Element</u>	<u>Corresponding Elements</u>
Copper	Gold, Molybdenum
Molybdenum	Copper, Gold, Silver, Bismuth
Gold	Copper, Molybdenum
Silver	Bismuth, Molybdenum

Table 5. Correspondence analysis pathfinder summary.

Geophysical Data

Three types of geophysical data related to the thesis area were available for interpretation. Aeromagnetics data covering the Bagdad area (1:62,500); gravity at the AMS scale (1:250,000); and I.P./Resistivity completed in 1974/75 on the central Copper Ridge property.

Aeromagnetics data covering the Bagdad area (Dempsey et al., 1963), shows a magnetic low centered over the Bagdad deposit (Fig. 33). The northeast trend of the magnetic low appears to be in response to alteration within the porphyry and along the northeast shear zone trend. The thesis area lies just off the map to the southwest.

The gravity data covering the thesis area shows a

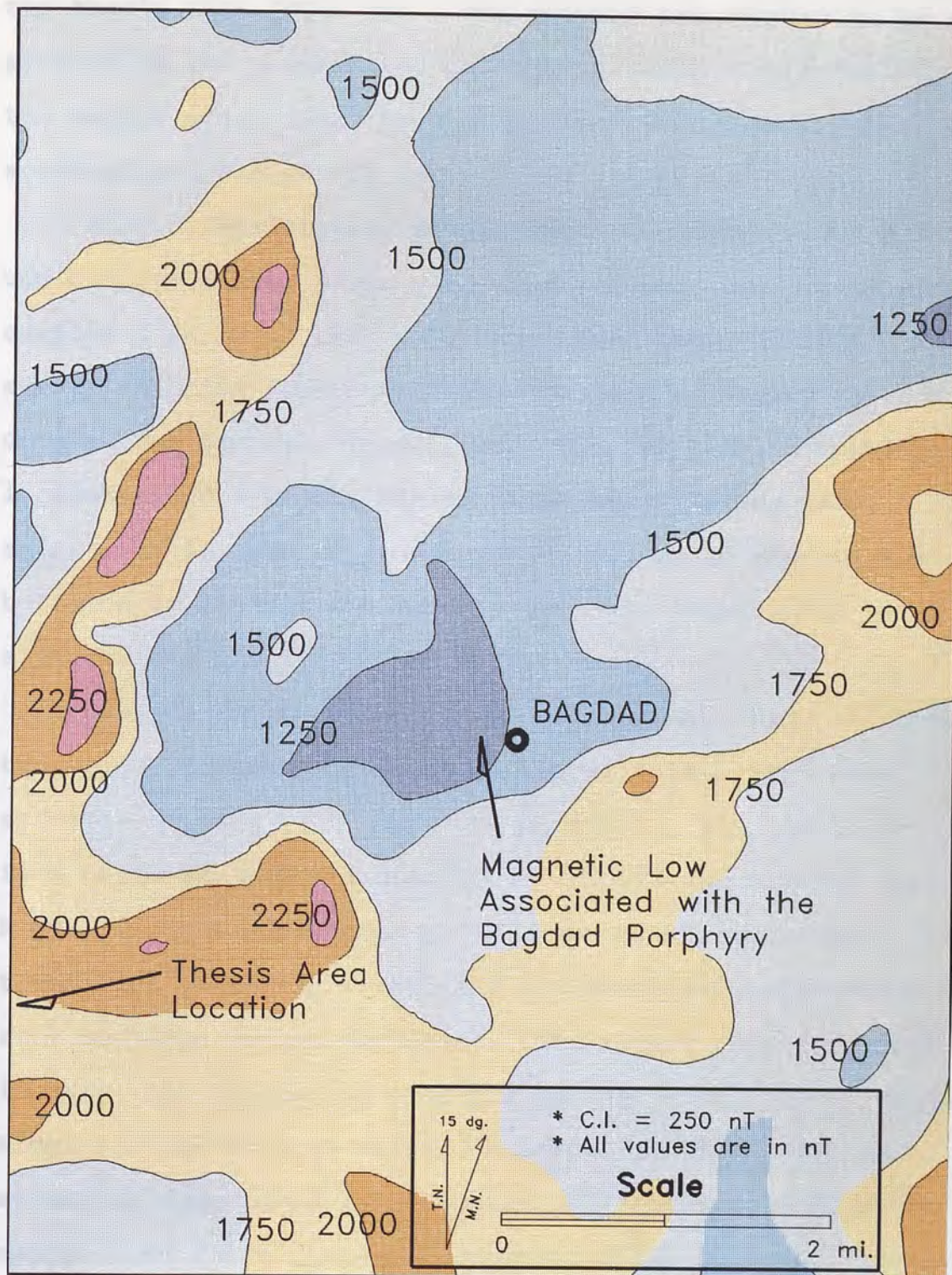


Figure 33. Aeromagnetics survey over the Bagdad area, Yavapai County, Arizona (Dempsey et. al., 1963).

moderate northeast gravity low which partially extends into the thesis area (Fig. 34). The gravity low appears to be a product of the northeast-southwest intrusive trend seen in the Bagdad area, with the thesis area intrusives on the southwestern end of the low.

An I.P./Resistivity survey over the Copper Ridge area was completed over a two year time period. Four lines were completed in 1974, with five more lines added in 1975. The survey and data interpretation were done by Mining Geophysical Surveys, Tucson, Az. The following information is summarized from the Mining Geophysical Survey final report, 1975. The resistivity data was quite complex and is believed to reflect the complex geology, topographic effects, and mineralization in the area.

The I.P./Resistivity survey contour map (Fig. 35) shows two major sulfide trends attributed to either shallower sulfides or more total sulfides at depth. The first trend is a north-south broad area located south and east of Copper Ridge, east of a proposed north-south fault structure. This trend lies primarily within the northeast-southwest shear zone and dips to the northeast. The higher response areas in this trend lie at or near the surface southeast of Copper Ridge and the central valley drainage (see Plate 1). The second sulfide trend is a tabular body located west of the north-south fault structure, dipping slightly to the north.

Several other structures were interpreted from the

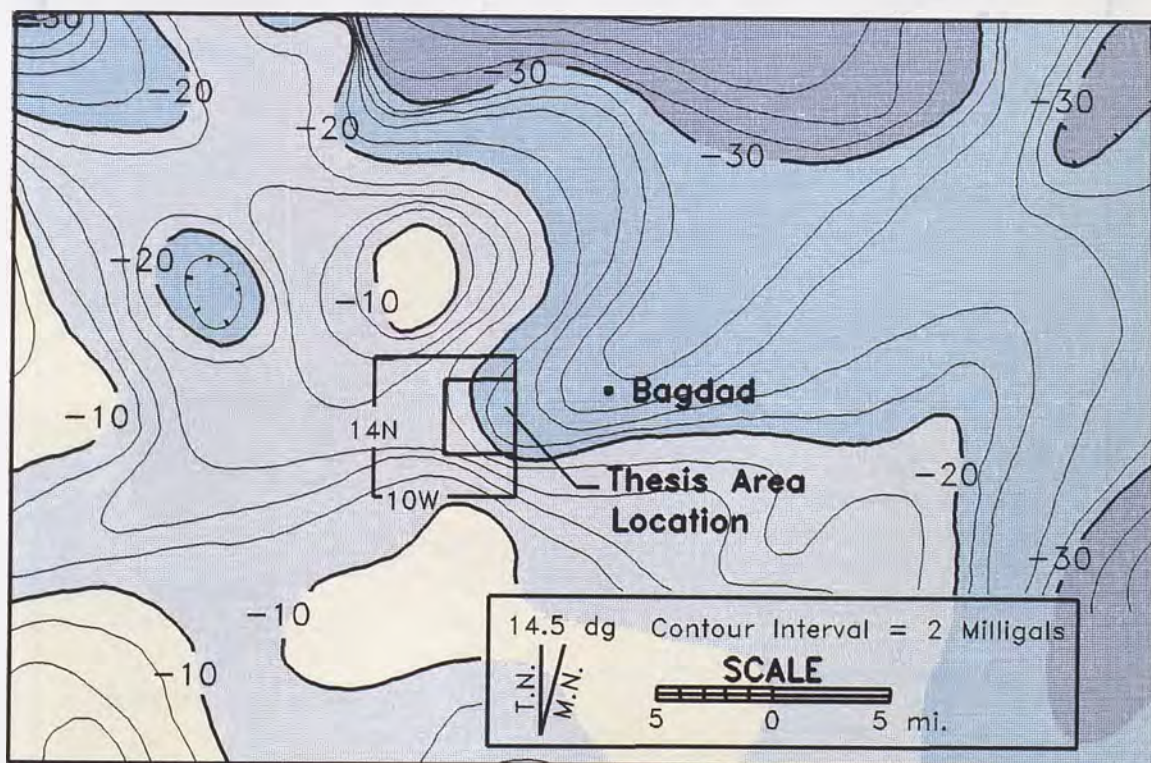


Figure 34. Residual Bouguer gravity anomaly map of the Bagdad area (Lysonski et. al., 1981).

data. Evidence to support a northwest-southeast shear zone is indicated by the westerly trending resistivity contacts. Field evidence supports the existence of this structural feature in every the area located on the survey. The major north-south trending structure delineated by the survey is not delineated by field mapping. Other structures interpreted from the geophysical data also lack field evidence for their existence.

Drilling history

Figure 34 locates the exploratory drillholes in the Grayback Mountains. Drill logs from two of these holes

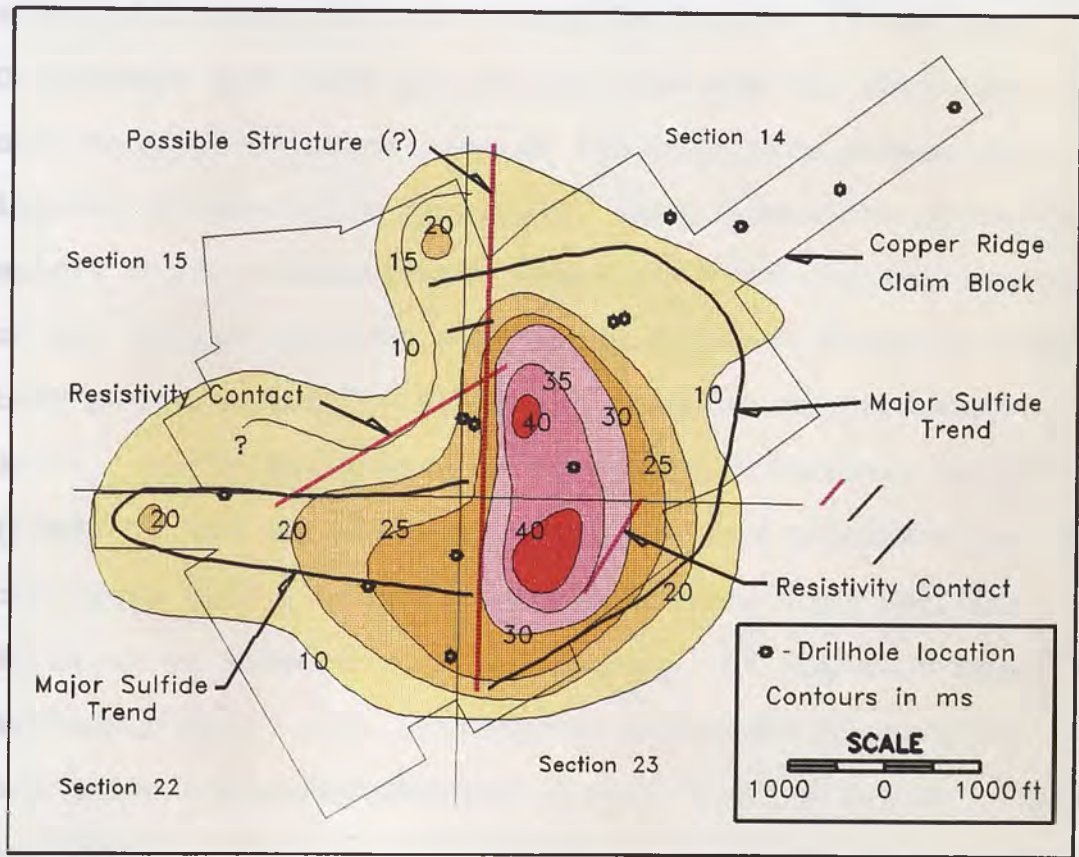


Figure 35. Results of the I.P./Resistivity survey over the Copper Ridge claim block (CBCC, 1974).

data. Evidence to support a northeast-southwest shear zone is indicated by the similarly trending resistivity contacts. Field evidence supports the existence of this structural feature in nearly the same location as the survey. The major north-south trending structure delineated by the survey is not indicated by field mapping. Other structures interpreted from the geophysical data also lack field evidence for their existence.

Drilling Summary

Figure 36 locates the exploration drillholes in the Grayback Mountains. Drill-logs from nine of these holes along with assay data are shown in figures 37 and 38. Drill-logs from core now unavailable did not show the crosscutting relationships of the intrusive dikes, and logging of available drillcore, shows intrusive contacts at nearly every orientation. Therefore, the contact relations of the intrusive rocks within the Grayback Mountain rhyolite tuff and granodiorite stock are shown as horizontal at depth. Areas designated as "possible structural zones" (Figs. 37 and 38) represent possible fault/gouge zones which correlate with a high percentage of core loss during drilling or intense clay alteration. Of the nine holes with available data, four intercepted intervals of marginal to ore grade copper/molybdenum or gold mineralization (Figs. 37 and 38).

Drillhole Cr-1-72 was drilled prior to the geophysical

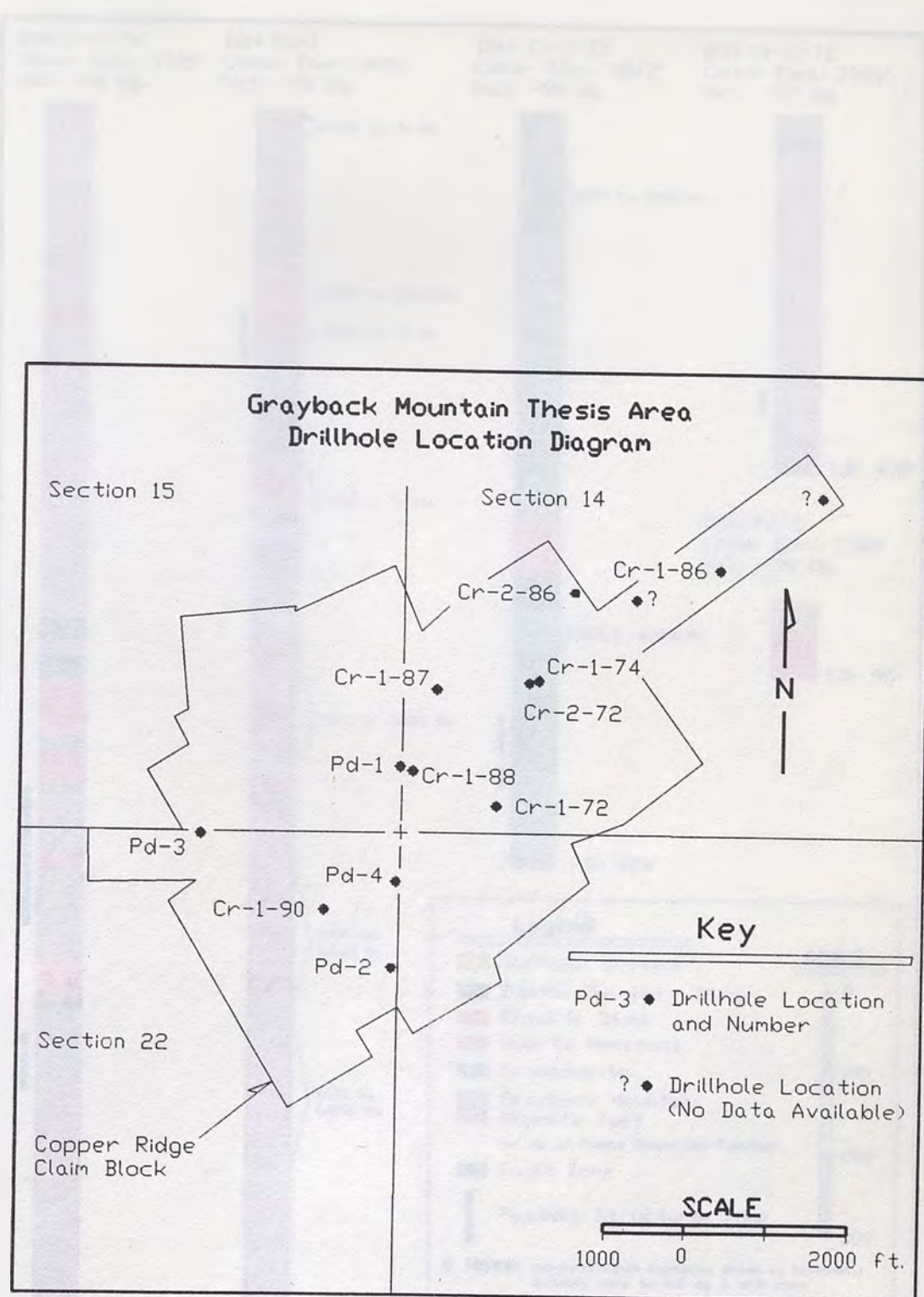


Figure 36. Grayback Mountain thesis area drillhole location diagram.

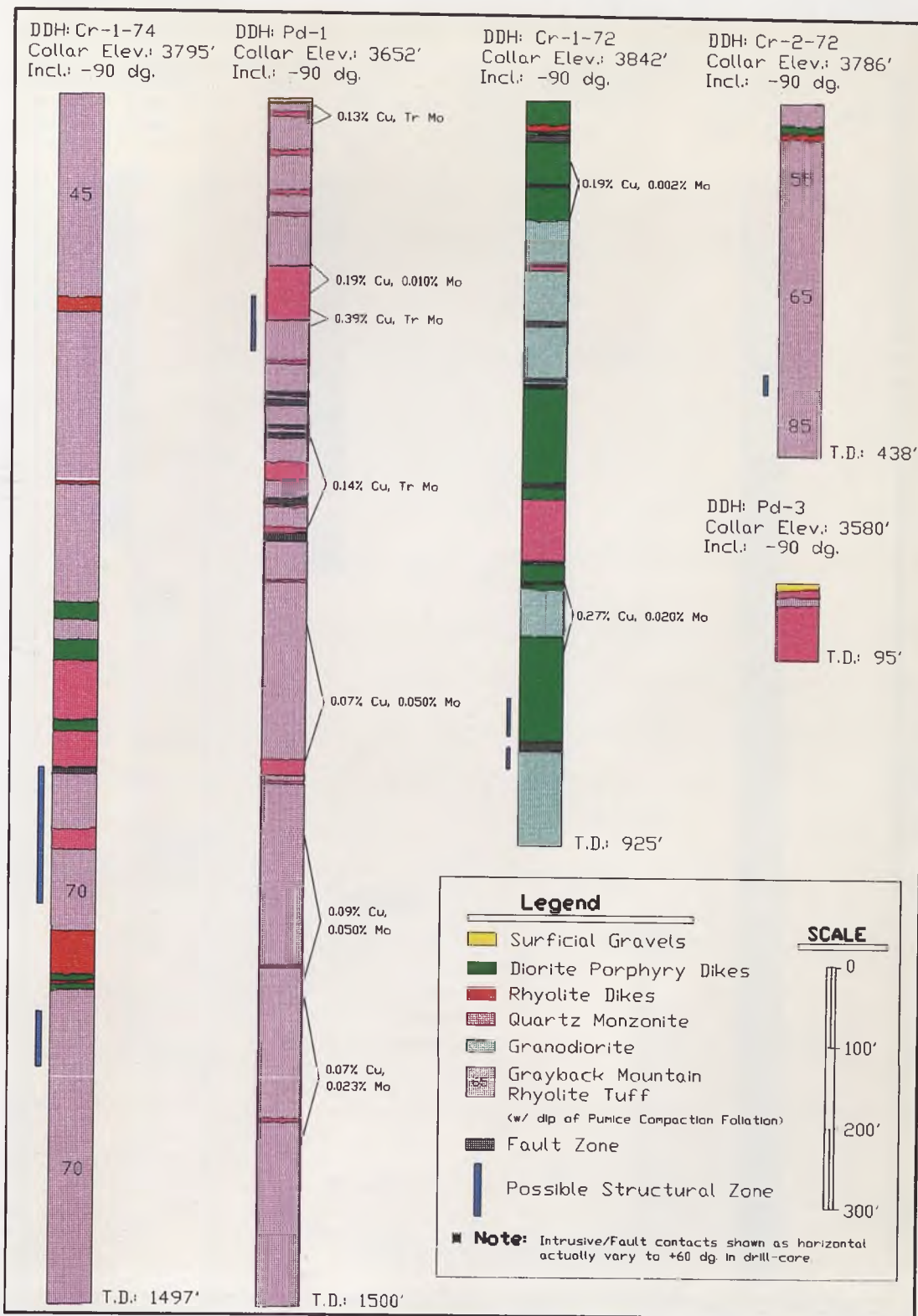


Figure 37. Exploration drillcore log summary.

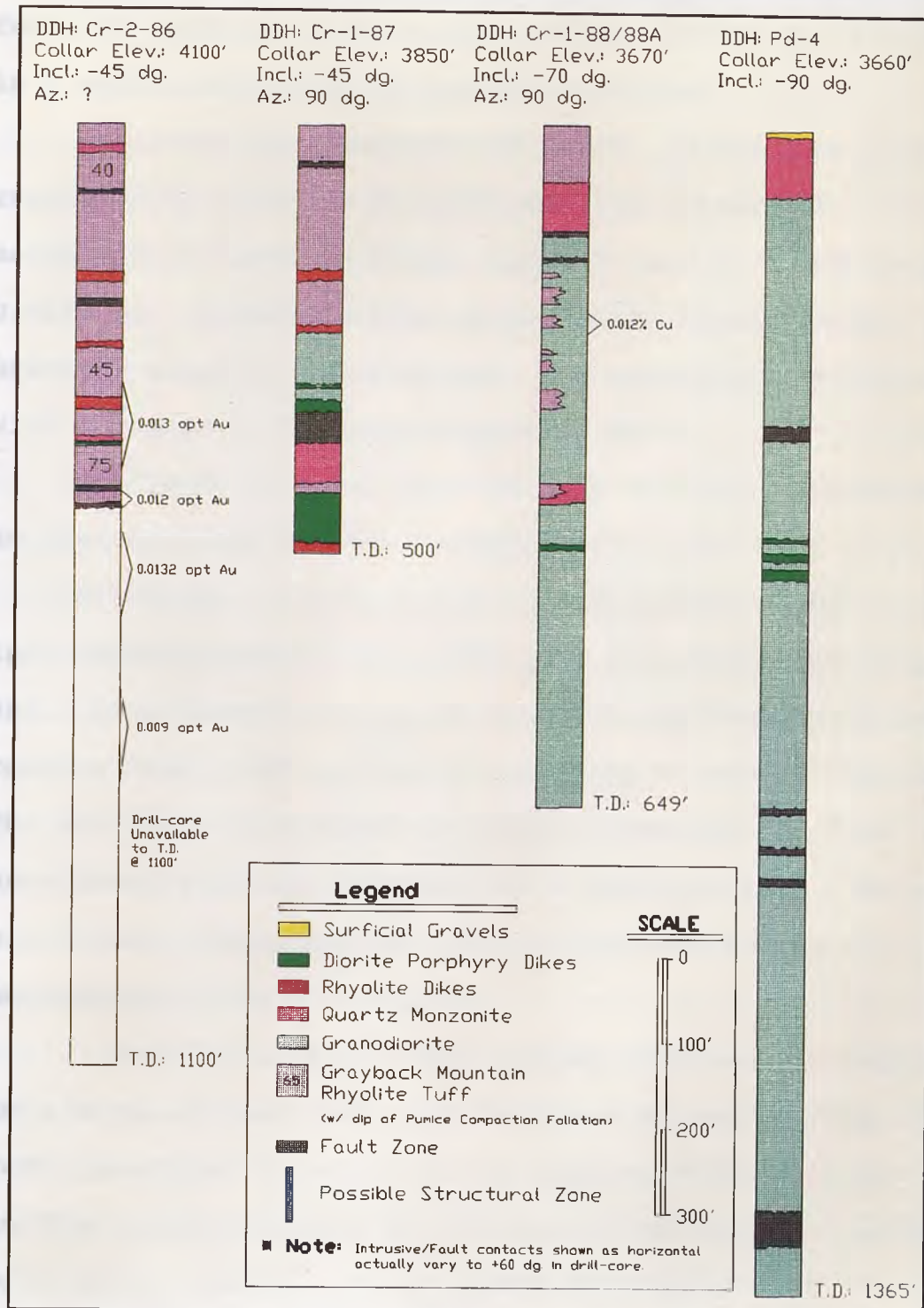


Figure 38. Exploration drillcore log summary continued.

survey and is on the east flank of the eastern sulfide trend. This drillhole had two intercepts, totaling 150 feet, of marginal Cu/Mo mineralization (0.23% Cu, 0.020% Mo) in a quartz monzonite to granodiorite host.

Drillhole Pd-1 encountered seven, 20-200 foot intervals ranging from 0.07% Cu to 0.39% Cu with a trace of molybdenum. Total thickness was 860 feet of 0.10% Cu and 0.027% Mo. Mineralization is primarily hosted in the Grayback Mountain rhyolite tuff and spatially associated with intrusions of quartz monzonite dikes.

Drillhole Cr-1-88, located near DDH Pd-1, intercepted 20 feet of 0.20% Cu, in a granodiorite host.

Drillhole Cr-2-86 is the only drillhole which intercepted marginal ore grade gold mineralization (Fig. 38). Four intervals varying from 100-120 feet thick and ranging from 0.009 opt Au to 0.013 opt Au were encountered. The available core shows the upper anomalous interval associated with the intrusion of a rhyolite dike. No significant intercepts of Cu/Mo mineralization were encountered in this drillhole.

Drillhole Cr-1-74 was drilled vertically, completed to a depth of 1497 feet, and designed to test a deep (+2000 feet) geophysical target in the eastern sulfide trend. Sulfide mineralization and alteration increased slightly with depth, however, no ore grade intercepts were encountered.

Drillhole Cr-2-72 is located approximately 100 feet southwest of Cr-1-74, and provides data similar to that of DDH Cr-1-74.

No Cu/Mo ore grade intercepts were encountered in drillholes: Pd-3, Pd-4, Cr-1-90, and Cr-1-87.

Exploration Summary and Suggestions for Further Exploration

Mineral exploration combined with geologic mapping reveals anomalous base and precious metals mineralization in the thesis area along the northeast shear zone trend.

The outcrops of intrusive stocks occur in the central thesis area (Fig. 6 and Plate 1) and correlate with anomalous Cu/Mo trends delineated by rock chip sampling (Figs. 27 & 28). Drilling data (Figs. 38 & 39) confirms that base metal mineralization occurs in the quartz monzonite porphyry/granodiorite stocks, and the Grayback Mountain rhyolite tuff; with mineralization occurring along fractures, in veinlets, and as disseminations.

The highest gold values occur in the Grayback Mountain rhyolite tuff with slightly lower values in the quartz monzonite porphyry, rhyolite dikes and late quartz monzonite dikes (Fig. 26). Drilling data (Fig. 38), ore microscopy, and field relations (Fig. 6) indicate that gold is associated with the intrusion of the rhyolite/diorite porphyry and late quartz monzonite dikes. It is possible that gold mineralization was also associated with the late stages of the quartz monzonite porphyry intrusive and

persisted with the later intrusive dikes. A structural intersection which may have focused gold mineralization (Fig. 29) is indicated by: 1) the coalescing of the dike swarms in the northeast thesis area (Fig. 6); and 2) the structural convergence seen by projection of the resistivity contacts, from the I.P./resistivity survey, to the northeast (Fig. 35).

Recommendations for further exploration and drilling, based upon the compiled geologic and exploration data, are summarized below.

Base Metals

A Cu/Mo porphyry target is probable in the vicinity of the resistivity highs west of drillhole Cr-1-72 and east of drillhole Pd-1, both to the north and south. This is evidenced by: 1) diamond drillhole Cr-1-72 having two marginal intercepts totalling 150 feet of 0.23% Cu, 0.020% Mo in a quartz monzonite to granodiorite host; 2) drillhole Pd-1 having a total of 860 feet of 0.10% Cu, 0.027% Mo; 3) the presence of the eastern sulfide trend delineated by the I.P./Resistivity survey (which has not been fully tested by exploration drilling; 4) drillholes (Pd-1 and Cr-1-72) lying within the northeast/southwest structural trend indicated by mapping, geochemistry, and I.P.; and 5) the coincident areas of anomalous copper and molybdenum mineralization delineated by rock chip sampling.

Access to the above area is good (via old prospect

roads) and would require a minimum of site preparation prior to drilling.

Precious Metals

A precious metals target is indicated in the northeastern portion of the thesis area where rock chip samples contain from 100 ppb to 6 ppm Au (Fig. 29 - NE $\frac{1}{4}$, Sec. 14).

Sample density was insufficient to tightly delineate a drill site. Further sampling is recommended using either a rock chip or soil sampling grid, oriented perpendicular to the northeast shear zone trend. Drilling targets could then be premised upon sampling results.

Space-Time Relationships to the Bagdad Porphyry

General Description of the Bagdad Porphyry

The Bagdad porphyry deposit is situated within a 12 mile-long belt of N 60-70°E trending, compositionally and texturally similar Laramide intrusive stocks and plugs. Potassium-Argon dates from two of the stocks in the district average approximately 77 Ma (Hawley and Blacet, 1990). Potassium-argon age dates on secondary biotite from within the Bagdad porphyry show main stage mineralization at approximately 70.9 ± 2.3 Ma. (Titley and Anthony, 1989).

The Bagdad porphyry is a multiphase intrusive with at least three, possibly four, intrusive events. Mine geologists have divided the intrusives into the following groups: the QM series, the KPQM, the KDP(?), and the KGRP.

The QM series includes intrusives of granodiorite to quartz monzonite composition. The earlier granodiorite facies (QM1) is characterized by chlorite after hornblende and biotite. The late QM (QM2) facies contains less biotite and hornblende, and has abundant K-feldspar intergrown with quartz in a fine to medium grained matrix (Hawley and Blacet, 1990).

The KPQM is a distinctly porphyritic quartz monzonite characterized by euhedral orthoclase phenocrysts (up to 15 mm), rounded quartz eyes (up to 6mm), and book biotite in a fine to medium groundmass of quartz and feldspar. A five to ten foot chill zone is present at the contact between the

KQM and the PKQM indicating that the KQM had cooled at the time of the KPQM emplacement (Hawley and Blacet, 1990).

The KDP is a diorite porphyry intrusive which is post KQM series and possibly post KPQM. Exposures of KDP are limited so a positive determination on the timing of the KDP intrusion is unclear.

The KGRP is an intensely clay and sericite altered granite porphyry intrusive and breccia dike. The KGRP is divided into two distinct facies: a rhyolite porphyry with euhedral orthoclase and quartz phenocrysts (KGRP), and a clast rich intrusive breccia (KGRP breccia) with mineralized clasts set in a clay/sericite matrix (Hawley and Blacet, 1990).

Rhyolite dikes, though not found in the active pit area, are found in close proximity to the mineralized stock. Diorite porphyry dikes, from the northeast trending dike swarm (Fig. 4), continue into the pit area (Hawley and Blacet, 1990).

Alteration within the porphyry generally follows the typical porphyry pattern of concentric alteration zones (oral comm., J. Hawley, Cyprus Bagdad, 1991) and depth of emplacement estimates, based upon fluid inclusion data, suggest emplacement of the stocks under about six thousand feet of cover (Nash and Cunningham, 1974).

Relations of the Bagdad Porphyry to the Grayback Mountain Thesis Area

Spatial Relationships

A close spatial relationship between the Bagdad porphyry and the thesis area is suggested by: 1) intrusive stocks of quartz monzonite to granodiorite composition in both areas lying within the 12 mile-long intrusive belt; 2) the close proximity of the thesis area to the porphyry (approx. five miles); 3) similarity of megascopic and microscopic features seen in the intrusives of each area, most notably in the stocks; 4) Crosscutting relationships of the diorite porphyry dikes in both areas; and 5) similarity in the style of mineralization, with both areas being dominated by a Cu-Fe-S system.

Time Relationships

Age dates, summarized in table 6, show a window of extrusive and intrusive related magmatic activity in the Bagdad area beginning approximately 84 (\pm 14) million years ago.

The tufaceous vent eruption which caused the accumulation of the Grayback Mountain rhyolite tuff appears to represent the initial stage of high level magmatic activity associated with the onset of the Laramide Orogeny and subsequent intrusion of the, calc-alkaline, QM series rocks. The granodiorite and quartz monzonite stocks, rhyolite and diorite porphyry dikes, along with the Copper Ridge tuff and the late quartz monzonite dikes are

progressive magmatic stages and all share a close spatial and temporal relationship with the Bagdad porphyry system.

Rock Unit	Age Dates	Method	Source
Grayback Mountain Rhyolite Tuff	84.0 ± 14 Ma. 71.2 ± 12 Ma.	Ft - Zircon Ft - Apatite	Oral Comm. Bruce Bryant
Bagdad Qm Series 12 mile-long intrusive belt	Approx. 77 Ma.	Not Known	Hawley and Blacet, 1990
Alteration and Mineralization Bagdad	70.9 ± 2.3 Ma.	Hydrothermal Biotite	Titley, 1981
Rhyolite Dikes	66.7 ± 8.1 Ma	Ft - Zircon	Oral Comm. Bruce Bryant
Diorite Porphyry Dikes	65.5 ± 11 Ma	Ft - Zircon	Oral Comm. Bruce Bryant
	Approx. 75 Ma.	K/Ar	Hawley and Blacet, 1990

Table 6. Age dating summary.

Conclusions

Extrusive and intrusive rocks exposed in the Grayback Mountain thesis area document magmatic activity and evolution from the late Cretaceous through the early Tertiary in the Bagdad area. The most extensive unit in the area, the Grayback Mountain rhyolite tuff, was erupted from a tuffaceous vent within the thesis area, with the vent lying along the major northeast shear zone trend. The Grayback Mountain rhyolite tuff rests unconformably on the Precambrian basement rocks. Along the southern flank, the Grayback Mountain rhyolite tuff is in structural contact with the Precambrian Lawler Peak Granite and alaskite porphyry. This southern structure is believed to represent the tuffaceous vent margin. Evidences supporting this interpretation include: concurrence of pumice compaction foliation with structural dip ($65-85^\circ$), the lack of gouge and brecciation of the Grayback Mountain rhyolite tuff, the intense brecciation of the Precambrian country rock along the structure, and the disappearance of the structure under Grayback Mountain rhyolite tuff outcrop on the east end. Fault contact relationships are observed along the northern margin of the thesis area and are inferred where rhyolite dikes are intruded at the Grayback Mountain-Precambrian contact. The tuffaceous vent eruption was most likely small and localized given the lack of both voluminous outflow sheets and abundant lithic/mega-breccia blocks within the

tuff. The shear zone remained a zone of weakness aiding the intrusion of the granodiorite to quartz monzonite stocks, rhyolite and diorite porphyry dikes, venting of the Copper Ridge tuff (?), and intrusion of the late quartz monzonite dikes.

Alteration in the area is complex and overlapping due to the multiplicity of intrusive activity but can best be characterized by the mineral assemblage quartz-sericite-pyrite \pm kaolinite. Other, more localized, alteration types recognized include: adularization, propylitization, silicification, and argillization.

Mineralization, dominated by a Cu-Fe-S system, is directly related to the intrusion of the stocks and dikes. All the rocks mapped in the area have been mineralized to some extent. Mineralization occurs along small fractures and shear surfaces, and as disseminations. The hypogene phases present include: pyrite, chalcopyrite, molybdenite, sphalerite, galena, pyrrhotite, and bornite. Supergene mineralization is represented by: chalcocite/digenite, covellite, malachite, azurite, chrysocolla, and iron oxides.

Correspondence analysis, performed on rock chip analytical data, shows the associations Ag-Bi-Mo and Cu-Au-Mo, to be dominant pathfinder element groups.

A base metal Cu/Mo target is revealed by several areas of anomalous copper/molybdenum mineralization that correspond with two broad I.P./resistivity sulfide trends

within the central thesis area. Drilling data shows intercepts of marginal Cu/Mo mineralization in three drillholes with alteration and mineralization increasing with depth. Drilling for a Cu/Mo target is recommended in the eastern sulfide trend, west of drillhole Cr-1-72 and east of drillhole Pd-1, both to the north and the south.

Gold mineralization appears to be related to the intrusion of the later dikes within the northeast trending shear zone. Sample density was not great enough to closely delineate a target but did reveal an area within which rock chip samples contain anomalous gold mineralization (100 ppb-6 ppm). Further sampling in the northeastern anomalous area is recommended to more tightly define the gold mineralization and perhaps a drill target.

The close proximity of the thesis area to the Bagdad porphyry, crosscutting relationships seen in the dikes, similarities in intrusive composition and style of mineralization, concurrence of both areas within the N60-70°E shear zone and intrusive trend, and age dating data, all suggest a close spacial and temporal relationship between the thesis area and the porphyry copper deposit at Bagdad.

Bibliography

- Anderson, C.A., 1950, Alteration and metallization in the Bagdad porphyry copper deposit, Arizona: *Econ. Geology*, v. 45, p. 609-628.
- Anderson, C.A., Scholz, E.A., and Strobell J.D. Jr., 1956, Geology and ore deposits of the Bagdad area, Yavapai County, Arizona. U.S. Geol. Survey Prof. Paper #278, 103 p.
- Bryant, Bruce, 1988, Geologic Map (preliminary) of the Poachie Range, Yavapai and Mohave Counties, Arizona, U.S. Geol. Survey Open File Report, p. 88-390.
- Butler, B.S., and Wilson, E.D., 1938, Bagdad Mine, Eureka District: Arizona Bur. Mines Bull. 145, p. 98-103.
- Carr, James R., 1990, Corspod: A portable Fortran 77 Program for Correspondence Analysis, *Computers and Geosciences*, v. 16, no. 3, pp. 289-307.
- Damon, P.E., and Giletti, B.J., 1961, The age of basement rocks of the Colorado Plateau and adjacent areas: *New York Acad. Sci., Annal.* no. 91, art. 2, p. 443-453.
- Damon, P.E., Shafiqullah, M., and Clark, K.F., 1981, Age trends of igneous activity in relation to metallogenesis in the southern Cordillera, in Dickinson, W.R., and Payne, W.D., eds., *Relations of tectonics to ore deposits of the southern Cordillera: Arizona Geological Society Digest*, v. 14, p. 137-154.
- Damon, P.E., Shafiqullah, M., and Clark, K.F., 1983, Geochronology of the porphyry copper deposits and related mineralization of Mexico: *Canadian Journal of Earth Science*, v. 20, p. 1052-1071.
- Dempsey, W.J., Fackler, W.D., and others, 1963, Aeromagnetics map of the Bagdad area, Yavapai County, Arizona, U.S. Geol. Survey, Map Gp-411.
- Dickenson, William R., in Jenny, J.P. and Reynolds, S.J., 1989, Geologic Evolution of Arizona, *Arizona Geological Society Digest*, v. 17, p. 1-16.
- Dickenson, William R., 1981, Plate tectonic evolution of the southern Cordillera, in Dickinson, W.R. and Payne, W.D., eds., *Relations of tectonics to ore deposits in the southern Cordillera: Arizona Geological Society Digest*, v. 14, p. 113-135.

- Ekren, E.B., 1981, Van Horn Peak - a Welded Tuff Vent in Central Idaho, Montana Geol. Soc. Field Conf. Southwest Montana, p. 311-315.
- Ekren, E.B., and Beyers, F.M. Jr., 1976, Ashflow fissure vent in west-central Nevada, *Geology*, v. 4 no. 4, p. 247-251.
- Guild, F. N., 1929, Copper Pitch Ore, *Am. Mineralogist*, v. 14, p. 313-318.
- Hawley, John W., and Blacet, Phil M., 1990, Geology and Mine Planning at the Cyprus Bagdad Mine, AIME Presentation, May 1990.
- Haxel, Gordon, Tosdal, R.M., May, D.J., and Wright, J.E., 1984, Latest Cretaceous and early Tertiary orogenesis in south-central Arizona; thrust faulting, regional metamorphism, and granitic plutonism: *Geological Society of America Bulletin*, v. 95, p. 631-653.
- Keith, Jeffrey D., and Shanks, Wayne C. III, 1985, Chemical evolution and volatile fugacities of the Pine Grove porphyry molybdenum and ash-flow tuff system, south-western Utah, *Canadian Inst. Mining and Metallurgy Spec. Vol.*, "Recent Advances in the Geology of Granite Related Mineral Deposits", p. 402-423.
- Keith, S.B., 1978, Paleosubduction geometries inferred from Cretaceous and Tertiary magmatic patterns in south-western North America: *Geology*, v. 6, p. 516-521.
- Keith, S.B., 1984, Map of outcrops of Laramide (Cretaceous to Tertiary) rocks in Arizona and adjacent regions: Arizona Bureau of Geology and Mineral Technology, 1:1,000,000.
- Lipman, Peter W., 1984, The roots of ashflow calderas in western North America: Windows into the tops of granitic batholiths, *Journal of Geophysical Research*, v. 89, no. B10, p. 8801-8841.
- Lipman, Peter W., and Sawyer, David A., 1985, Mesozoic ashflow caldera fragments in southeastern Arizona and their relation to porphyry copper deposits, *Geology*, v. 13, p. 652-656.
- Lyonski, Joseph C., Aiken, C.L.V., and Sumner, John S., 1981, The Complete Residual Bouguer Gravity Anomaly Map - Prescott AMS Sheet, Arizona Geological Survey, OFR - 81-24 : #17.

- Nash, Thomas J., and Cunningham, Charles G. Jr., 1974, Fluid Inclusion Studies of the Porphyry Copper Deposit at Bagdad, Arizona, U.S. Geol. Survey Journal of Research, v. 2, no. 1, p. 31-34.
- Pierce, H.W., 1984, The Mogollon escarpment: Arizona Bureau of Geology and Mineral Technology, v. 14, no. 2., p. 8-11.
- Pierce, H.W., 1985, Arizona's backbone - The Transition Zone: Arizona Bureau of Geology and Mineral Technology, v. 15, no. 3. p. 1-6.
- Reynolds, Stephen J., 1988, Geologic Map of Arizona - Map # 26, 1:1,000,000, Arizona Geological Survey.
- Reynolds, Stephen J., and Keith, S.B., 1982, Geochemistry and mineral potential of peraluminous granitoids: Arizona Bureau of Geology and Mineral Technology Field Notes, v. 12, no. 4, p. 4-6.
- Shafiqullah, M., Damon, P.E., Lynch, D.J., Reynolds, S.J., Rehring, W.A., and Raymond, R.H., 1980, K-Ar geochronology and geologic history of southwestern Arizona and adjacent areas, in Gen, J.P., and Stone, Claudia, eds., Studies in Western Arizona: Arizona Geological Society Digest, v. 12, p. 201-260.
- Silver, L.T., 1966, U-Pb isotope relations and their historical implications in Precambrian zircons from Bagdad, Arizona, (abs) Geol. Soc. Amer. Spec. Paper #101. p. 420.
- Silver, L.T., Williams, I.S., and Woodhead, J.A., 1980, Uranium in granites from the southwestern United States: Actinide parent-daughter systems, sites and mobilization, U.S. D.O.E. Open File Report GJBX-45, 380 p.
- Titley, S.R., and Anthony, E.Y., in Jenny, J.P., and Reynolds, S.J., 1989, Geologic evolution of Arizona. Tucson, Arizona, Geol. Soc. Dig. #17, p. 485-514.
- Titley, S.R., 1981, Geologic and geotectonic setting of porphyry copper deposits in the southern Cordillera, in Dickinson, W.R., and Payne, W.D.. eds., Relations of tectonics to ore deposits in the southern Cordillera: Arizona Geological Society digest, v. 14, p. 79-97.

Appendix 1

Opaque Mineralogy

Key: X = Present in section - = Absent in section
 ? = Not positively identified

Rock Types

Gbrt = Grayback Rhyolite Tuff Gds = Granodiorite Stock
 Dpd = Diorite Porphyry Rd = Rhyolite Dike
 Qms = Quartz Monzonite Stock Crt = Copper Ridge Tuff
 Lpg = Precambrian Granite Qmd = Quartz Monz. Dike

Minerals

Py = Pyrite Mo = Molybdenite
 Cpy = Chalcopyrite Sph = Sphalerite
 Po = Pyrrhotite Gal = Galena
 Cc = Chalcocite/Digenite IO = Iron Oxides
 Bn = Bornite CO = Copper Oxides
 Cv = Covellite Au = Gold

Section number	Rock type	Py	Cpy	Po	Cc	Bn	Cv	Mo	Sph	Gal	IO	CO	Au
1	Gbrt	X	X	X	-	-	-	-	X	-	X	-	-
2	Gbrt	X	X	X	X	-	X	-	X	-	X	X	-
3	Gbrt	X	X	X	X	-	X	-	X	-	X	-	-
4	Gbrt	X	X	X	X	-	X	-	X	-	X	-	-
5	Gbrt	X	X	X	X	X	X	-	X	-	X	-	-
6	Gbrt	X	X	X	X	-	X	-	X	-	X	X	-
7	Gbrt	X	X	X	X	-	X	X	X	-	X	-	-
8	Dpd	X	X	X	-	-	-	-	X	-	X	-	-
A-1	Gbrt	X	X	-	-	-	X	-	X	-	X	-	?
A-2	Gbrt	X	X	X	X	-	-	-	?	-	X	-	-
A-3	Gbrt	-	-	-	-	-	-	-	-	-	X	-	-
A-4	Gbrt	X	-	-	-	-	-	-	-	-	X	-	-
A-5	Gds	X	X	-	-	-	-	-	-	-	X	-	-
4-272	Rd	X	-	-	-	-	X	-	-	-	X	-	-
1A-530	Qmd	X	X	X	-	-	X	-	X	-	X	-	-
4-1395	Lpg	X	X	X	-	-	-	-	X	-	X	-	?
4-1265	Gbrt	X	X	-	-	-	-	-	-	-	-	-	-
Cr-286	Gbrt	X	X	-	-	-	X	-	X	-	X	-	?
Cr-286A	Gbrt	X	X	X	-	X	-	-	-	-	X	-	-
1-264	Qm	X	X	X	-	X	X	-	-	-	X	-	-
4-1493	Gbrt	X	-	-	-	-	-	-	-	-	-	-	-
2-260	Rd	X	X	-	-	-	-	-	X	-	X	-	-
20155	Qms	-	-	-	-	-	-	-	-	-	X	X	-
20157	Qms	-	-	-	-	-	-	-	-	-	X	X	-
20158	Qms	-	-	-	-	-	-	-	-	-	X	X	-
20159	Qms	-	-	-	-	-	-	-	-	-	X	X	-
20160	Qmd	-	-	-	-	-	-	-	-	-	X	-	?
20160A	Qmd	-	-	-	-	-	-	-	-	-	X	-	-

Opaque Mineralogy - Continued

Section number	Rock type	Py	Cpy	Po	Cc	Bn	Cv	Mo	Sph	Gal	IO	CO	Au
Crt-1	Crt	-	-	-	-	-	-	-	-	-	X	-	-
4-1047	Rd	X	X	-	-	-	-	-	X	-	-	-	-
1-244	Rd	X	X	X	-	-	-	-	X	-	X	-	X
G-1	Qms	-	-	-	-	-	-	-	-	-	X	-	-
Dp-2	Dpd	-	-	-	-	-	-	-	-	-	X	-	-
755	Gbrt	X	X	-	X	-	X	X	X	-	X	-	-
761	Gbrt	-	-	-	-	-	-	-	-	-	X	-	-
762	Rd	-	-	-	-	-	-	-	-	-	X	-	-
763	Rd	-	-	-	-	-	-	-	-	-	X	-	-
775	Qms	-	-	-	-	-	-	-	-	-	X	X	-
Cr-1-90	Gds	X	X	X	-	-	X	-	X	X	X	-	-
Qm-rd	Qms	-	-	-	-	-	-	-	-	-	X	-	-

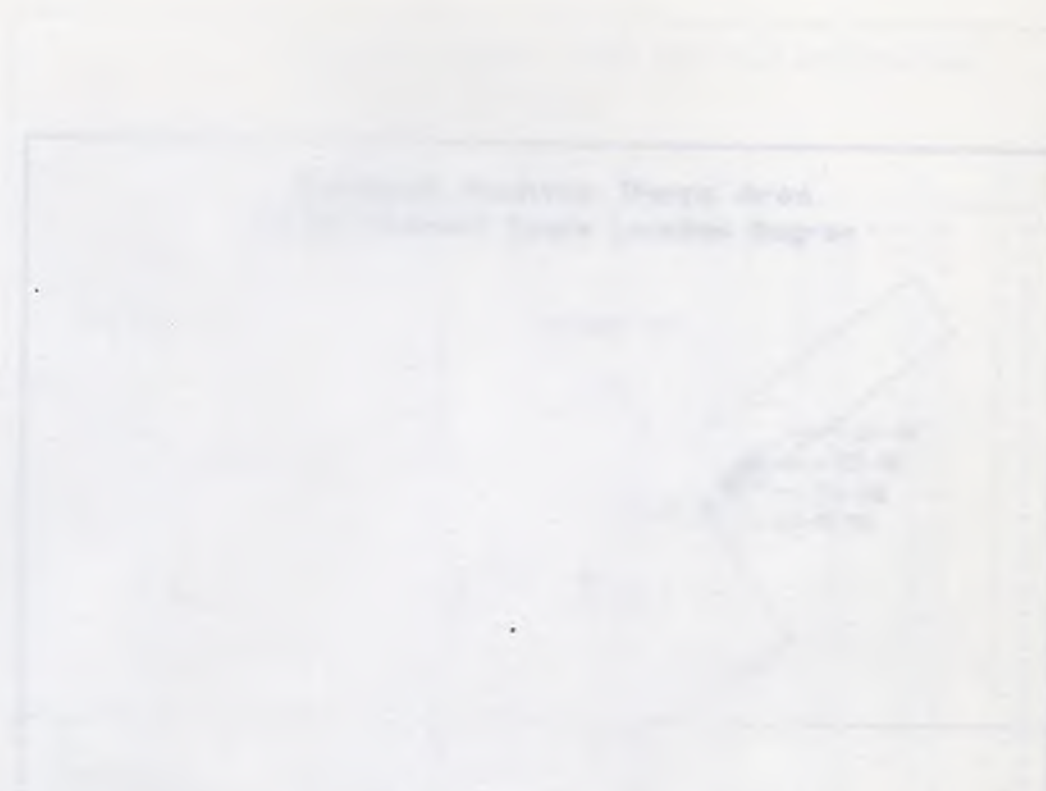
Strain gradient mapping data

Sample	W	W ₂	W ₃	W ₄	W ₅	W ₆	W ₇	W ₈	W ₉	W ₁₀
10-1	1.000	1.000	0.914	0.8	2.18	21.5	1.32	28.0	0.25	0.10
10-2	1.000	1.000	0.914	0.8	2.18	21.5	1.32	28.0	0.25	0.10
10-3	1.000	1.000	0.914	0.8	2.18	21.5	1.32	28.0	0.25	0.10
10-4	1.000	1.000	0.914	0.8	2.18	21.5	1.32	28.0	0.25	0.10
10-5	1.000	1.000	0.914	0.8	2.18	21.5	1.32	28.0	0.25	0.10
10-6	1.000	1.000	0.914	0.8	2.18	21.5	1.32	28.0	0.25	0.10
10-7	1.000	1.000	0.914	0.8	2.18	21.5	1.32	28.0	0.25	0.10
10-8	1.000	1.000	0.914	0.8	2.18	21.5	1.32	28.0	0.25	0.10
10-9	1.000	1.000	0.914	0.8	2.18	21.5	1.32	28.0	0.25	0.10
10-10	1.000	1.000	0.914	0.8	2.18	21.5	1.32	28.0	0.25	0.10
10-11	1.000	1.000	0.914	0.8	2.18	21.5	1.32	28.0	0.25	0.10
10-12	1.000	1.000	0.914	0.8	2.18	21.5	1.32	28.0	0.25	0.10
10-13	1.000	1.000	0.914	0.8	2.18	21.5	1.32	28.0	0.25	0.10
10-14	1.000	1.000	0.914	0.8	2.18	21.5	1.32	28.0	0.25	0.10
10-15	1.000	1.000	0.914	0.8	2.18	21.5	1.32	28.0	0.25	0.10
10-16	1.000	1.000	0.914	0.8	2.18	21.5	1.32	28.0	0.25	0.10
10-17	1.000	1.000	0.914	0.8	2.18	21.5	1.32	28.0	0.25	0.10
10-18	1.000	1.000	0.914	0.8	2.18	21.5	1.32	28.0	0.25	0.10
10-19	1.000	1.000	0.914	0.8	2.18	21.5	1.32	28.0	0.25	0.10
10-20	1.000	1.000	0.914	0.8	2.18	21.5	1.32	28.0	0.25	0.10

Table 7. Strain gradient mapping data.

Appendix Two

Geochemical Data



Grayback Mountain Thesis Area Stream Sediment Samples n = 13 All values are in ppm										
Sample	Ag	As	Au	Cu	Mo	Pb	Sb	Zn	Bi	Cd
SS-1	0.095	7.83	0.012	58.6	2.15	26.5	1.12	56.5	0.75	0.69
SS-2	0.106	6.93	0.016	50.8	2.38	35.5	0.56	72.9	0.92	0.85
SS-3	0.026	2.67	0.008	25.4	0.73	6.6	0.31	21.8	1.16	0.10
SS-4	0.033	2.71	0.019	0.6	2.10	5.1	0.36	14.6	0.98	0.10
SS-5	0.052	3.67	0.015	170.0	3.06	6.2	0.42	25.2	0.31	0.15
SS-6	0.126	6.86	0.006	138.0	8.33	18.4	0.71	52.8	1.11	0.69
SS-7	0.265	8.64	0.015	131.0	2.50	57.0	1.14	130.0	1.92	2.68
SS-8	0.172	11.10	0.014	53.1	1.82	131.0	0.81	209.0	0.82	3.13
SS-9	0.186	32.30	0.049	37.2	1.90	193.0	0.64	220.0	1.02	2.44
SS-9A	0.242	21.10	0.218	46.3	2.19	178.0	0.75	307.0	1.18	2.72
SS-9B	0.217	22.80	0.105	37.9	2.00	166.0	0.67	258.0	1.11	2.35
SS-9C	0.234	22.00	0.226	40.0	2.15	176.0	0.67	273.0	1.13	2.55
SS-9E	0.217	12.80	0.179	28.8	1.51	122.0	0.49	167.0	0.72	1.94

Table 7. Stream sediment sampling data.

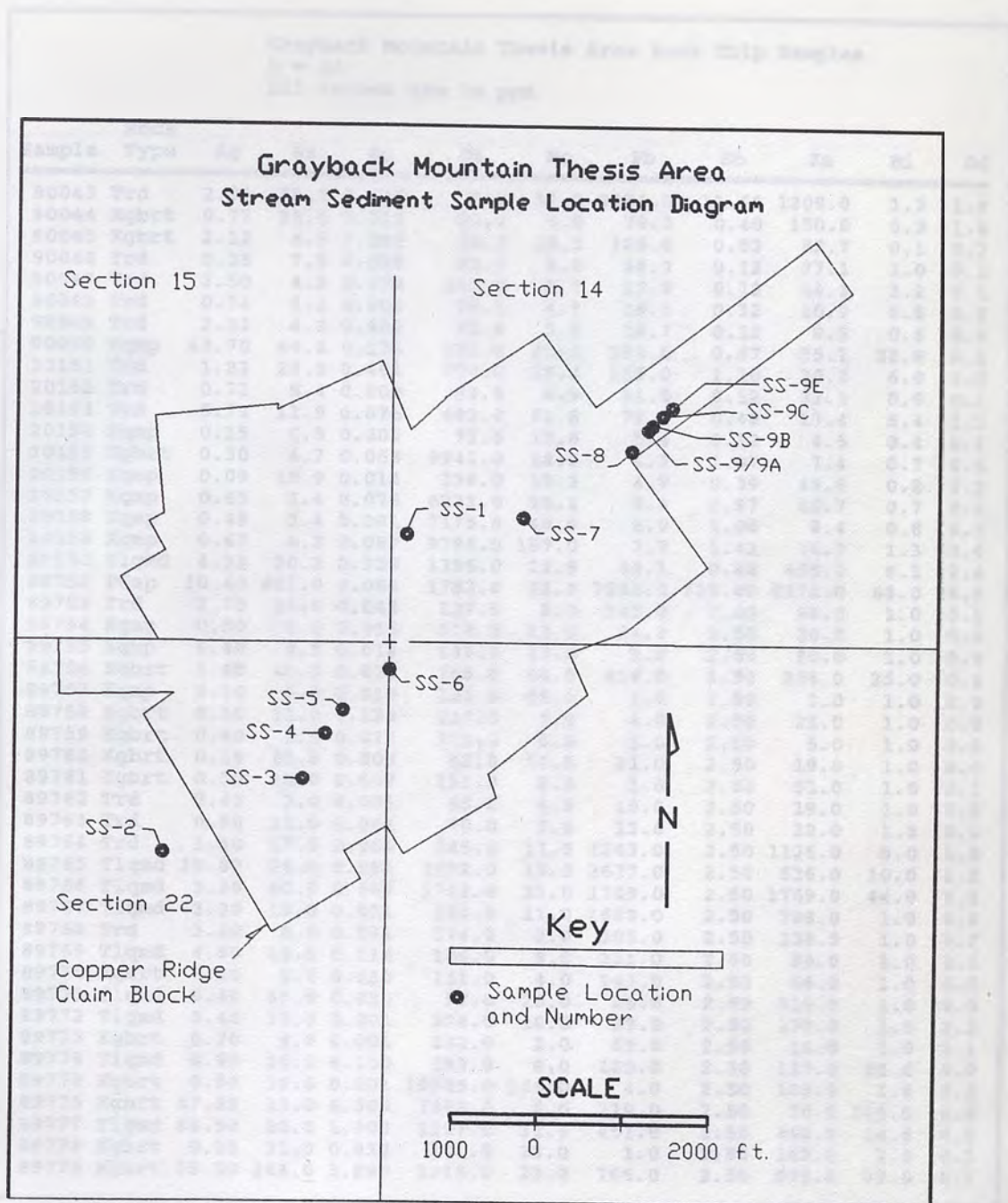


Figure 39. Stream sediment sample location diagram.

Grayback Mountain Thesis Area Rock Chip Samples
 n = 46
 All values are in ppm

Sample	Rock Type	Ag	As	Au	Cu	Mo	Pb	Sb	Zn	Bi	Cd
90043	Trd	2.99	75.5	0.105	2.0	33.8	9251.0	11.60	1208.0	1.2	1.5
90044	Kgbrrt	0.77	21.5	0.012	26.4	5.0	78.3	0.40	150.0	0.9	1.0
90045	Kgbrrt	2.12	4.9	0.093	10.4	10.0	106.0	0.53	82.7	0.1	0.2
90046	Trd	0.35	7.5	0.028	50.1	5.0	48.3	0.12	37.1	3.0	0.1
90047	Trd	2.50	4.8	0.079	143.0	5.7	15.3	0.12	14.3	3.2	0.1
90048	Trd	0.74	1.2	0.002	96.1	4.9	18.3	0.12	10.9	0.8	0.0
90049	Trd	2.33	6.0	0.003	52.4	5.5	18.7	0.12	9.5	0.6	0.0
90050	Kqmp	43.70	46.0	0.174	383.0	25.5	198.0	0.37	35.1	22.8	0.1
20151	Trd	1.23	29.0	0.464	703.0	15.4	195.0	1.10	20.0	6.0	1.5
20152	Trd	0.71	5.4	0.009	29.5	4.9	51.5	0.12	33.1	0.9	0.1
20153	Trd	5.71	11.9	0.076	483.0	51.8	72.3	0.48	13.4	5.4	3.1
20154	Kqmp	0.15	0.5	0.002	71.5	17.6	5.4	0.12	4.5	0.4	0.1
20155	Kgbrrt	0.30	4.7	0.068	9941.0	18.6	4.3	1.07	7.4	0.7	0.6
20156	Kqmp	0.09	10.9	0.014	339.0	19.3	4.9	0.39	49.6	0.8	0.2
20157	Kqmp	0.65	3.4	0.076	6231.0	26.1	5.4	0.97	60.7	0.7	0.4
20158	Kqmp	0.48	3.4	0.081	7175.0	49.9	6.9	1.06	8.4	0.8	0.3
20159	Kqmp	0.67	4.3	0.087	9794.0	157.0	7.7	1.42	14.7	1.3	0.6
20160	Tlqmd	4.33	30.2	0.229	1395.0	22.9	49.1	0.86	495.0	9.1	2.4
89752	PCap	10.40	607.0	0.068	1782.0	22.0	7285.0	729.00	2171.0	68.0	26.5
89753	Trd	2.70	24.0	0.042	127.0	5.0	145.0	7.00	96.0	1.0	0.1
89754	Kqmp	0.50	9.0	0.015	518.0	13.0	34.0	2.50	20.0	1.0	0.0
89755	Kqmp	0.40	2.5	0.018	625.0	13.0	9.0	2.50	20.0	1.0	0.6
89756	Kgbrrt	2.60	40.0	0.038	355.0	44.0	416.0	2.50	206.0	25.0	0.4
89757	Kqmp	0.10	6.0	0.019	122.0	58.0	1.0	2.50	3.0	1.0	0.0
89758	Kgbrrt	0.10	11.0	0.124	217.0	3.0	4.0	2.50	22.0	1.0	0.0
89759	Kgbrrt	0.40	2.5	0.015	214.0	8.0	3.0	2.50	5.0	1.0	0.0
89760	Kgbrrt	0.10	25.0	0.003	52.0	10.0	21.0	2.50	19.0	1.0	0.0
89761	Kgbrrt	0.30	10.0	0.007	191.0	8.0	1.0	2.50	51.0	1.0	0.1
89762	Trd	0.40	7.0	0.001	65.0	4.0	15.0	2.50	19.0	1.0	0.0
89763	Trd	0.50	11.0	0.001	70.0	7.0	13.0	2.50	32.0	1.0	0.0
89764	Trd	1.40	17.0	0.064	545.0	11.0	2243.0	2.50	1126.0	8.0	1.5
89765	Tlqmd	10.80	26.0	0.081	1092.0	15.0	2677.0	2.50	536.0	10.0	1.5
89766	Tlqmd	3.30	60.0	0.569	1743.0	31.0	1749.0	2.50	1769.0	44.0	8.2
89767	Tlqmd	3.30	15.0	0.051	124.0	11.0	1689.0	2.50	708.0	1.0	0.8
89768	Trd	3.40	8.0	0.031	174.0	2.0	305.0	2.50	138.0	1.0	0.2
89769	Tlqmd	4.50	15.0	0.112	186.0	8.0	221.0	2.50	89.0	1.0	0.3
89770	Kgbrrt	1.20	5.0	0.010	111.0	4.0	143.0	2.50	66.0	1.0	0.3
89771	Tlqmd	0.40	35.0	0.025	97.0	26.0	26.0	2.50	319.0	1.0	0.0
89772	Tlqmd	0.40	15.0	0.001	274.0	10.0	39.0	2.50	179.0	1.0	2.3
89773	Kgbrrt	0.70	9.0	0.001	232.0	2.0	65.0	2.50	14.0	1.0	0.1
89774	Tlqmd	0.90	24.0	0.100	193.0	8.0	185.0	2.50	123.0	25.0	0.0
89775	Kgbrrt	0.50	10.0	0.001	10535.0	156.0	4.0	2.50	106.0	1.0	0.3
89776	Kgbrrt	47.50	13.0	6.300	7863.0	5.0	219.0	2.50	76.0	226.0	0.0
89777	Tlqmd	88.50	20.0	1.300	1397.0	11.0	451.0	2.50	462.0	14.0	0.0
89778	Kgbrrt	0.10	31.0	0.032	201.0	38.0	1.0	2.50	168.0	1.0	0.1
89779	Kgbrrt	25.00	144.0	1.090	1773.0	23.0	766.0	2.50	573.0	93.0	5.1

Table 8. Rock chip sampling data. (see Grayback)

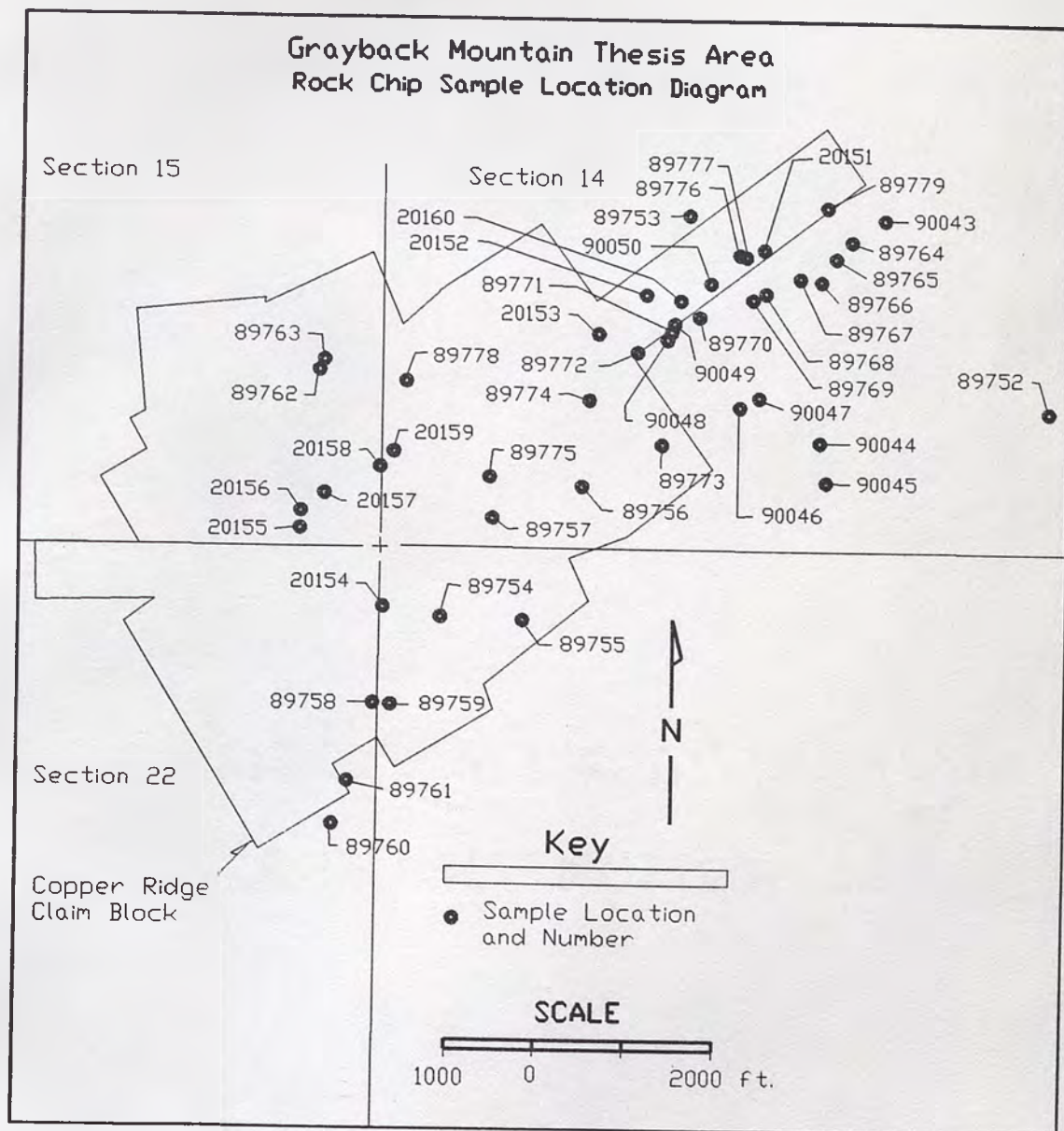


Figure 40. Rock chip sample location diagram.